PONTIFÍCIA UNIVERSIDADE CATÓLICA
DO RIO DE JANEIRO

Isabela Fernandes Soares

Interfacial rheology and properties of island-type asphaltenes

Tese de Doutorado

Thesis presented to the Programa de Pós–graduação em Engenharia Mecânica do Departamento de Engenharia Mecânica da PUC-Rio in partial fulfillment of the requirements for the degree of Doutor em Engenharia Mecânica.

Advisor : Prof. Mônica Feijó Naccache
Co-advisor: Dr. Eliana Paola Marín Castaño

Rio de Janeiro
Janeiro 2022

Isabela Fernandes Soares

Interfacial rheology and properties of island-type asphaltenes

Thesis presented to the Programa de Pós–graduação em Engenharia Mecânica do Departamento de Engenharia Mecânica da PUC-Rio in partial fulfillment of the requirements for the degree of Doutor em Engenharia Mecânica. Approved by Examination Committee.

Prof. Mônica Feijó Naccache
Advisor
Departamento de Engenharia Mecânica – PUC-Rio

Dr. Eliana Paola Marín Castaño
Co-advisor
Departamento de Engenharia Mecânica – PUC-Rio

Prof. Gerald Fuller
Departamento de Engenharia Química – Stanford University

Prof. Aurora Pérez Gramatges
Departamento de Química – PUC-Rio

Prof. Paulo Roberto de Souza Mendes
Departamento de Engenharia Mecânica – PUC-Rio

Dr. Márcia Khalil de Oilveira
Petróleo Brasileiro S.A – Petrobras

Rio de Janeiro, Janeiro the 25th, 2022

Isabela Fernandes Soares

Graduou-se em Engenharia Química pela Pontifícia Universidade Católica do Rio de Janeiro (PUC-Rio). Fez mestrado no programa de pós-graduação da Escola de Química da Universidade Federal do Rio de Janeiro (UFRJ), especializando-se na área de reologia interfacial dilatacional. Foi contemplada com uma bolsa de doutorado sanduíche pelo programa Fulbright em parceria com a Universidade de Stanford na Califórnia.

Acknowledgments

Firstly, I would like to thank our Lord Jesus Christ for giving me the inspiration to conduct this work, courage and faith to not give up during my Ph.D journey, and wisdom to make the right choices. I also thank Holy Mary, Our Lady, and Saint Jude Thaddeus for interceding for this work. I dedicate my thesis to my friend in heaven, the Servant of God Guido Schäffer, who has been guiding me since I was accepted in the Ph.D program in 2017.

I thank my wonderful mom, dad, sister, niece, nephew, uncle and grandparents for their love and support. I feel very grateful for everything that you have done and continue doing for me. I love you very much.

I thank my advisor, professor Mônica Naccache, for the wonderful mentoring and support during my doctorate studies. It has been a honor working with you for more than 10 years. Thank you for your knowledge, guidance, patience, and trust. I hope we can keep doing research together.

Special thanks to my co-mentor, Eliana Marín, for her marvelous guidance. This doctorate thesis would not be possible without you. Thank you so much for everything you taught me. I admire you greatly. You are tireless in helping people and sharing knowledge. I hope we will continue discovering exciting things in the amazing world of interfaces.

I am thankful to Priscilla Varges for teaching me rheology and also instructing me when I was using the rheometers. Thank you for your patience, mentoring and friendship. Thank you for giving me faith and not letting me give up during the real moments of "stress".

I thank Professor Gerry Fuller for receiving me as his visiting researcher in his laboratory. It was a honor working with your students and learning so much about interfacial rheology from our meetings. I admire you personally and professionally. I also thank Mariana Rodriguez for teaching me about the asphaltene science, dilatational rheology and spontaneous emulsification, and also for providing the asphaltenes. It was also a pleasure meeting and working with you. Special thanks to all Stanford friends from the Fuller Lab: Aad, Aadi, Chunzi Liu, Endre, John, Suzanne, Vinny, and Yogi. Thanks to the wonderful American and international friends that I met during my international experience, especially the "Good Cyclists" and the friends from the Catholic Community of Stanford for sharing with me wonderful moments of joy.

My gratitude to Professor Jones Limberger and his students for helping with the NMR experiments. I appreciate your patience, time and partnership with our team from the Departament of Mechanical Engineering. My special thanks to Rafaela Gomes Martins da Costa for performing the analyses. I thank

Abstract

Fernandes Soares, Isabela; Naccache, Mônica (Advisor); Marín, Eliana (Co-Advisor). **Interfacial rheology and properties of island-type asphaltenes**. Rio de Janeiro, 2022. 112p. Tese de doutorado – Departamento de Engenharia Mecânica, Pontifícia Universidade Católica do Rio de Janeiro.

Adsorption of asphaltene molecules at the oil-water interface induces the formation of a complex microstructure, which stabilizes emulsions and impairs the efficiency of crude oil refining. In this work, we design a set of new shear rheology protocols to assess the effect of polar and non-polar solvents on indigenous Brazilian (BR) asphaltene adsorption. Moreover, the asphaltene morphology upon addition of solvents with distinct aromaticities is investigated by SEM microscopy. Our findings indicate that asphaltenes are a polycondensate aromatic island-type structure that forms reversible films when polar solvents are placed on top of the adsorbed film. The interfacial study also reveals that non-polar solvents may lock up asphaltene nanoaggregates in mixture. These aggregates, upon the presence of weakly polar solvents, can consolidate into a more close-packed pattern, suggesting that network growth and asphaltene self-arrangement are directly related to the aromatic content. We explore the differences in asphaltene structuring and how it affects the extent of spontaneous emulsification. We find that the rate of emulsification is directly related to the chemical configuration of asphaltenes. Finally, we study the addition of stearic acid (SA) to asphaltene solutions in deionized water (DW) and synthetic water (SW) to better understand how surface and rheological properties are affected by competitive adsorption. We find that single SA are more prone to form liquid-like rather than solid-like films at the air-water interface. Furthermore, we show that the interfacial activity of our asphaltenes is enhanced in the presence of electrolytes and is dependent of the solvent aromaticity.

Keywords

Interfacial Rheology; Asphaltene adsorption; Solvent effect; Spontaneous emulsification; Emulsion stability; Coadsorption.

Resumo

Fernandes Soares, Isabela; Naccache, Mônica; Marín, Eliana. **Reologia interfacial e propriedades de asfaltenos do tipo "ilha"**. Rio de Janeiro, 2022. 112p. Tese de Doutorado – Departamento de Engenharia Mecânica, Pontifícia Universidade Católica do Rio de Janeiro.

A adsorção de moléculas de asfalteno na interface óleo-água induz a formação de uma microestrutura complexa, que estabiliza as emulsões e prejudica a eficiência dos processos de refino de petróleo. Neste trabalho, desenvolvemos um conjunto de novos protocolos de reologia de cisalhamento para avaliar o efeito de solventes polares e apolares na adsorção de genuínos asfaltenos brasileiros. Além disso, a morfologia do asfalteno, após a adição de solventes com aromaticidades distintas, é investigada por microscopia de varredura (MEV). Os resultados indicam que os asfaltenos estão organizados em uma estrutura do tipo ilha com unidades aromáticas e policondensadas, que formam filmes interfaciais reversíveis com a adição de solventes polares. O estudo interfacial também revela que solventes apolares podem "prender" os nanoagregados de asfalteno na mistura. Esses agregados, na presença de solventes fracamente polares, podem se consolidar em um padrão mais compactado, sugerindo que o crescimento do filme e o autoarranjo do asfalteno estão diretamente relacionados ao conteúdo aromático. Explora-se as diferenças na estruturação do asfalteno e como afetam a extensão da emulsificação espontânea. É proposto que a taxa de emulsificação está diretamente relacionada à configuração química dos asfaltenos. Finalmente, estuda-se a adição de ácido esteárico (AE) a soluções de asfalteno em conteúdo de água deionizada (AD) e água sintética (AS) para melhor compreender como as propriedades reológicas e superficiais são afetadas pela competição das coespécies. Verifica-se que interfaces formadas puramente por AEs originam filmes mais viscosos do que elásticos na interface ar-água. A atividade interfacial dos asfaltenos brasileiros é evidente e significativa na presença de eletrólitos e dependente da aromaticidade do solvente.

Palavras-chave

Reologia interfacial; Adsorção de asfaltenos; Efeito do solvente; Emulsificação espontânea; Estabilidade de emulsão; Coadsorção.

Table of contents

List of figures

List of tables

1
Motivation

If we could describe the interfacial world in two words, they would be "complex" and "dynamic". Fluid interfaces, the boundary layer of two liquids or liquid and a gas, are the scene for complicated interactions of active surface species, which are the protagonists of adsorption/desorption phenomena. Once these compounds populate those interfaces, significant microstructure arises, and its presence is attributed to the stability of water-in-crude oil emulsions. These emulsions are formed when oil blends with water during flow: the water may be originated from the subphase formation or sometimes intentionally from enhanced crude oil recovery (EOR) methods (see Fig. 1.1). The available water, used as smart water injection, is usually seawater, composed by distinct cations and ions [1]. It is injected into the reservoir to displace efficiently the remaining oil, which may lead to a higher recovery factor [2, 3]. The presence of asphaltenes has been pointed out as the main reason that hinders emulsion destabilisation due to its high interfacial activity, although other natural crude oil compounds, like naphthenic acids, are also known to be greatly associated and prone to adsorb onto fluid-fluid interfaces. Understanding the aggregation process of these structures is of great importance to the crude oil processing; besides, the comprehension of how the interfacial film behave upon distinct modes of deformation, still requires further investigation.

In the present work, we deepen knowledge on the interfacial/rheological properties of indigenous asphaltenes at distinct air-water and oil-water interfaces. We characterize adsorbed films of Brazilian (BR) asphaltenes with the main purpose of demonstrating the effect of polar and non-polar solvents in interfacial viscoelasticity by means of new shear experimental protocols. In a different way, we perform *in situ* additions of solvents onto asphaltene adsorbed layers to investigate the contribution of shear stresses to interfacial viscoelasticity. Asphaltene aggregation and morphology are assessed under the addition of solvents with distinct aromaticities. Scanning electron microscopy (SEM) and confocal microscopy are used in this investigation. The latter is also employed to explore the spontaneous emulsification of asphaltenes in polar solvents. We investigate the response of asphaltene layers upon planar compression by assessing pressure-area (Π - A) isotherms. Moreover, we

investigate the pseudoplastic behavior of the interface by disrupting asphaltene aggregates upon different shear rates. A comparative study of three asphaltenes from different sources is also conducted. Finally, we focus on evaluating the shear and compressional response of asphaltene-stearic acid mixtures. Deionized water (DW) and synthetic water (SW) are also used to compare the influence of deprotonated molecules in the microstructure buildup and surface energy.

The thesis is mainly organized as follows: initially, we present in Chapter 2 a background and literature review of the last published works about rheologically complex asphaltene laden interfaces, as well as the recent advances on the methods and simulations of the surface science field. In Chapter 3, the experimental methodology is described, and Chapters 4 and 5 present the experimental results and discussions. Chapter 4 discusses the rheology and self-assembly of asphaltene-only interfaces, besides showing a study of the effects of asphaltene structuring on viscoelasticity and spontaneous emulsification. In Chapter 5, it is explored the co-adsorption of asphaltenes and stearic acids employing some of the rheological protocols used in Chapter 4. Compression and interfacial dynamics of the adsorbed binary films are also assessed.
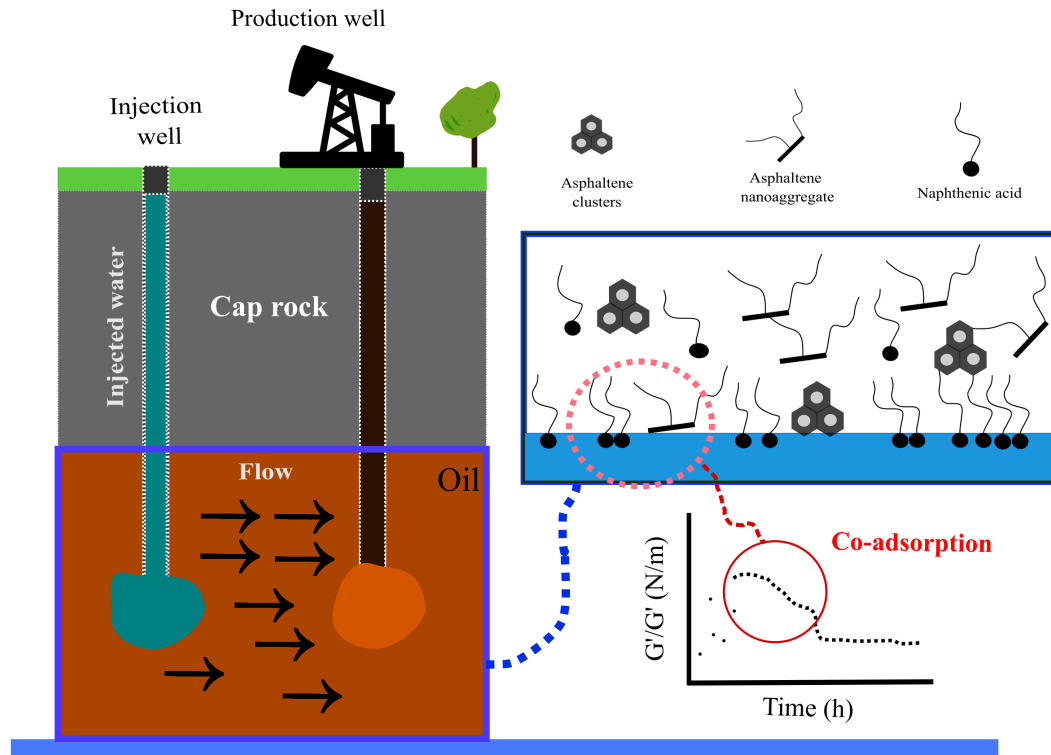
Figure 1.1: Schematic of an oil reservoir. Adsorption and molecular competition between asphaltenes and co-surfactants (i.e, naphthenic acids) occurs at the interface when oil and water streams flow together. This triggers the consolidation of a network capable of responding to deformation. Reservoir picture was drawn based on Ref. [4].

2
Background and Literature Review

In this chapter, we present a background on asphaltene molecular composition, interfacial activity and industrial applications. We also present the basic equations of the main stresses generated at interfaces, as well as the methods used to acquire rheological data. In the end, we review the most relevant and innovative work about asphaltene science, including the state-of-the-art research on molecular simulation.

2.1
Asphaltenes

Crude oil is a complex mixture of different compounds. It is constituted of hydrocarbons (mostly alkanes, cycloalkanes and aromatics), asphaltenes, resins, traces of metals, nitrogen, oxygen and sulfur [5]. Asphaltenes are the highest molecular-weight molecules found in crudes with a polar portion attached to a polycyclic aromatic chain containing other heteroatoms. The aromatic content in asphaltenes is around 50%, since the H/C ratio is lower due to the polycyclic structures [6, 7]. Mainly, these polyaromatic cores can be organized in two distinct configurations: the "island" type (also called "continental" or "pericondensed"), in which the asphaltene molecule comprises one planar aromatic center surrounded with aliphatic chains, or the "archipelago" type, in which two or more conjugated cores are interconnected by the aliphatic chains (see Fig. 2.2) [8–10]. The amount of asphaltenes in crudes varies considerably, from almost minimal in volatile oils to a high percent in heavy crude oils and bitumen, and their concentration affects the viscosity, transportation and quality of the petroleum [5]. The asphaltene behaviour changes considerably depending on the crude oil source, and maybe, even the fractionation procedure, which results in several distinct molecular architectures [9]. For this reason, their chemical properties are mostly defined as "average features", e.g, "average molecular weight" of asphaltenes, as presented by some authors [11,12]. Asphaltenes are defined as a solubility class; a portion of crude oil that is insoluble in n-alkanes (as heptane and pentane, considered "poor" solvents) yet soluble in aromatic solvents, as benzene and toluene (known as "good" solvents). Fig 2.1 represents a typical asphaltene

molecule and its heteatoms attached to the main aromatic core.
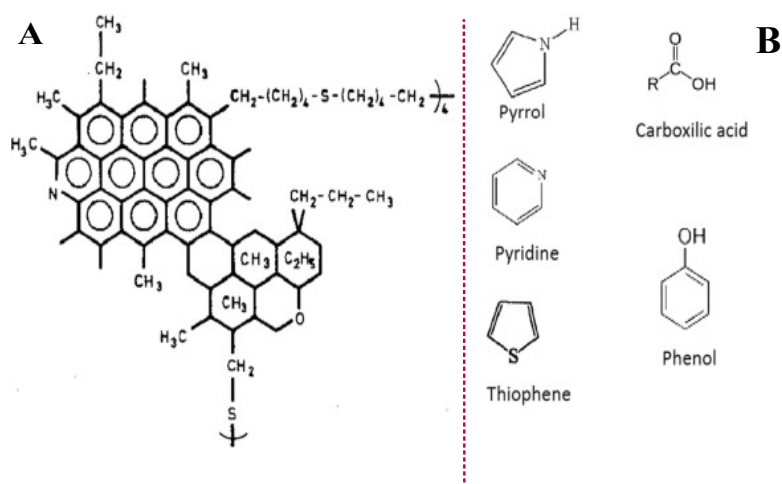
Figure 2.1: A. Representation of a typical asphaltene molecule. B. Examples of typical asphaltene heteroatoms. Image adapted from Ref. [6].
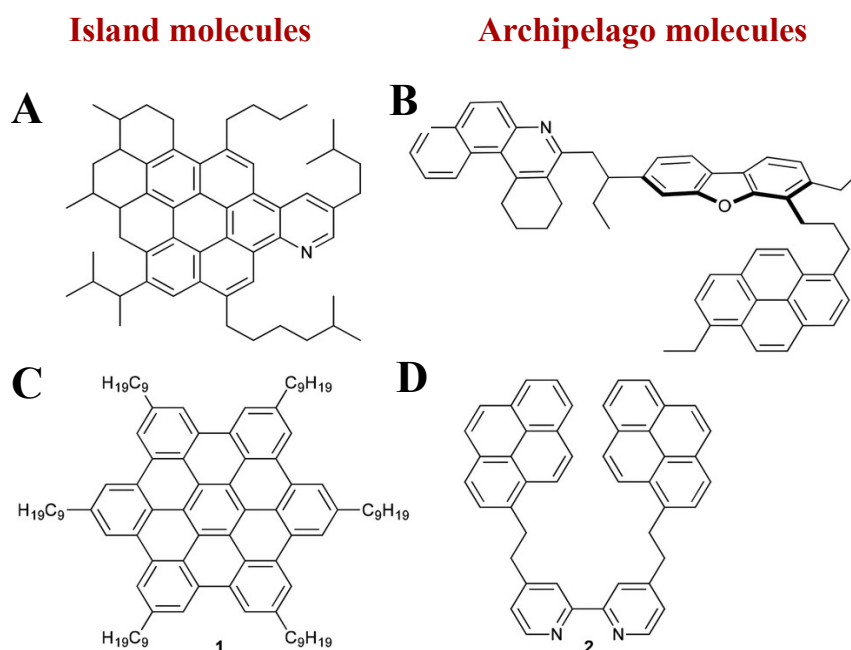
Figure 2.2: A. Schematic molecules of an island asphaltene type (MW = 756 g mol^{-1}) from Ref. [13]. B. Archipelago asphaltene type (MW = 754 g mol^{-1}) from Ref. [14]. C. Examples of model compounds used to study aggregation of asphaltenes, representing island (MW = 1280 g mol^{-1}) from Ref. [15]. D. Archipelago type molecule (MW = 613 g mol^{-1}) from Ref. [16]. Adapted from Ref. [17].

Due to their amphiphilic characteristic, asphaltenes are known to be interfacially active and capable of stabilizing oil-in-water or water-in-oil

emulsions, since they adsorb at those interfaces and form rigid viscoelastic films [18]. As the main component responsible for emulsion stability, asphaltenes are commonly known to irreversibly adsorb at oil-water interfaces and create an enclosure around oil drops that protects them from coalescence. They can also accumulate on the surface of solids, changing their wettability and impacting on the recovery of crudes [5].

There are different approaches in the literature concerning the interfacial and bulk activity of asphaltenes, like their ability to self-assemble, react and adsorb onto different interfaces (oil-water, air-water or solid surfaces). The self-interaction of asphaltenes, which is well defined by the hierarchical Yen-Mullins model of colloidal aggregation proposed by Mullins *et al.* [13], pictures asphaltenes as nanoaggregates and clusters rather than single molecules at certain concentrations in bulk (usually greater than 2 g/L, the cluster configuration is dominant). Many studies indicate that these aggregation states are more prone to adsorb and change physical-chemical properties of interfaces [6, 19, 20].

Langevin and coworkers [6] measure the thickness of interfacial layers from oil-water emulsions through neutron scattering techniques. Asphaltenes were dissolved in xylene (a solvent very similiar to toluene) at a concentration of 3 g/L (larger clusters). They found that the interfacial layer is similar to the diameter of the asphaltene cluster (7 nm twice their gyration radius), suggesting their total adsorption at the oil-water interface, which is no longer considered a single monolayer. Lobato *et al.* [19] also show by air-water interface isotherms the evidence of whole adsorption of asphaltene cluster at concentrations beyond 2 g/L. Even though the recently developed studies give insights on asphaltene self-aggregation, there is still a lot of debate on the different crude oil sources that originate distinct active asphaltene moieties. [21].

2.2
Naphthenic acids

Although asphaltenes are considered the dominant surface-active specie in petroleum and the most problematic one, other heavy oil components deserve special attention. Among them, naphthenic acids (NAs) have been extensively studied due to its complex chemical composition and physical-chemical behaviour, which has been linked to crude oil production issues, like emulsions desestabilization and facilities corrosion [22–28]. Broadly speaking, NAs are classified as monocarboxylic acids represented by the general formula $C_nH_{2n-z}O_2$, where n refers to the carbon number and z indicates

the homologous series. The value of z can vary from z=0 (fully saturated aliphatic acid) to z=2 (one-ring naphthenic acids), z=4 (two-rings naphthenic acids), etc [23, 29, 30]. They can possess distinct cycloaliphatic structures and varied carbon number distribution accordingly to the crude oil source. Lower molecular weight is also observed compared to the asphaltene average values (166 to 450 g/mol versus 1000 g/mol of the asphaltenes) [12, 23, 27]. Typical NA structures are shown in Fig 2.3.
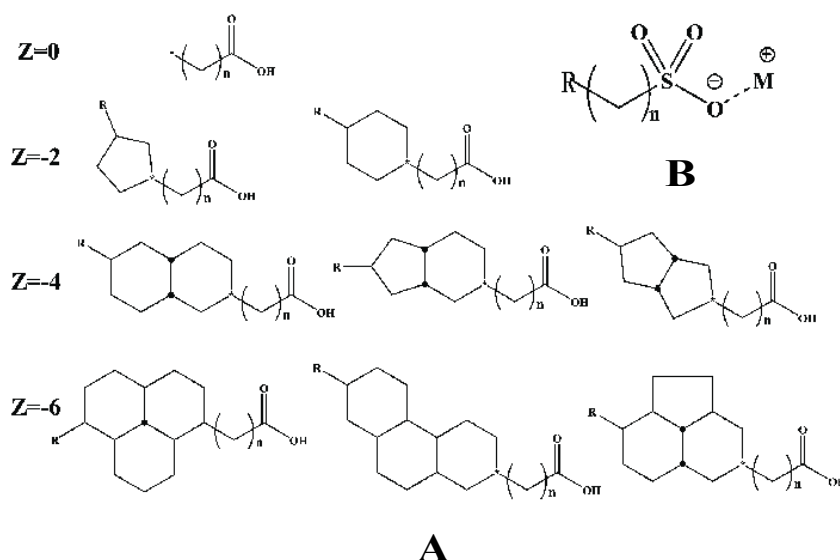
Figure 2.3: Typical naphthenic acid structures. A. Naphthenic acids with distinct carbon numbers and a varying degree of condensation (distinct z values). B. Sulfonic acids or salts with M = H^+, Na^+, K^+, etc., and R representing the generic hydrocarbon tails. Image from initial Ref [29] and also cited by Ref. [30].

Due to their amphiphilic properties, NAs are known to be surface active materials, that is, they can reduce the surface/interfacial tension and induce the consolidation of an interfacial microstructure. Moreover, a marked decrease on interfacial tension is evidenced when the pH of the water phase increases. Alkaline solutions are usually injected in reservoirs to lower capillarity forces and, thereby, promote optimal oil recovery [23]. NAs are easily ionized in alkaline environments, which ultimately favors the accumulation of the species at the oil-water interface as presented in Eq. 2-1.

$$R - COOH^+ \Leftrightarrow R - COOH^- + Na^+ + H_2O \qquad (2\text{-}1)$$
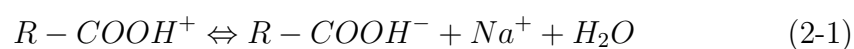
Some researchers have investigated the presence of a special type of naphthenic acid known as ARN (tetracarboxylic naphthenic acids), which is mainly formed of aliphatic molecules with four branches with a carboxylic

terminal group attached to each branch (see Fig. 2.4 [a]). It is potentially problematic to the formation of calcium naphthenates, a hard solid deposit derived from chemical interactions at the oil/water interface, and sodium naphthenates, which have a significant impact on the desalting process [26]. Nonetheless, simpler carboxylic structures are preferably chosen to mimic the interfacial effects of NAs at oil-water stabilization, e.g, the palmitic, oleic and stearic acids (see Fig. 2.4 [b]). Special attention must be taken to stearic acids, since they are broadly used in previous work to elucidate NAs physical-chemical behavior at interfaces [24, 31–33]. The main reasons are the ones that follow: firstly, because stearic acids are widely found in nature with a basic aliphatic chain (no *cis* or *trans* double bonds), secondly due to their preferential adsorption towards the oil-water interface compared to other NAs. For instance, cyclic components are more likely to interact with other co-surfactants at the interface [24].
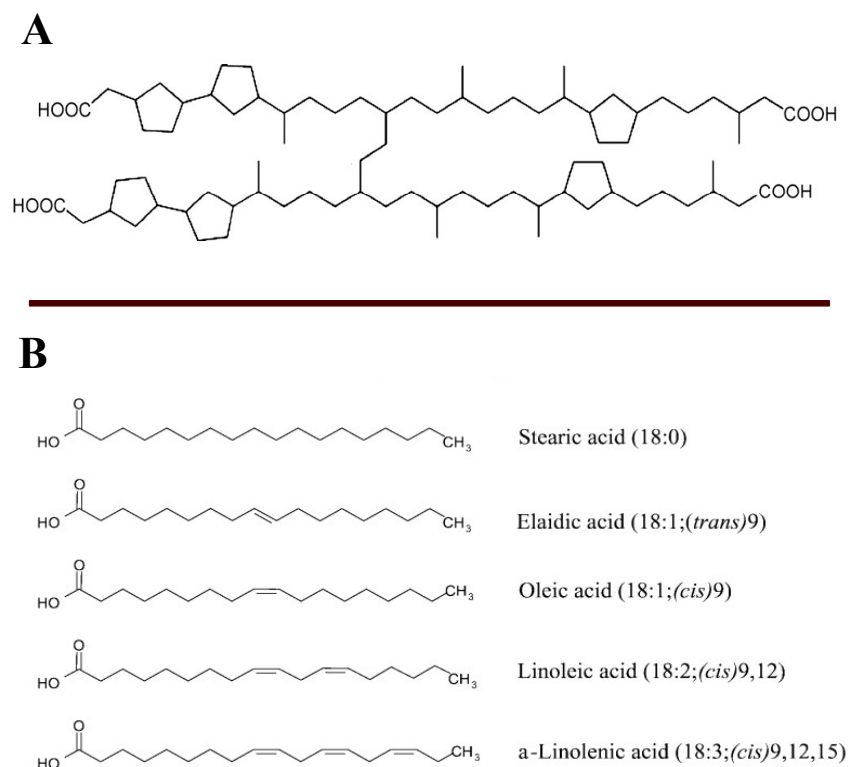
Figure 2.4: A. Structure of the most abundant C_{80} ARN tetraacid. Image from Ref [34]. B. Molecular structures of different carboxylic acids: stearic, elaidic, oleic, linoleic and α-linolenic acids. Image from Ref. [32].

2.3
Rheology of interfacial layers

2.3.1
Overview: the interface upon deformation

Interfaces occur when two immiscible fluids are placed in contact. They can be found in nature, like the membranes of living cells, and in several industrial applications, such as food stability, crude oil emulsification, foaming, liquid-liquid extraction, and so on. The idea of interfaces as a target of investigation begins in the 19th century, when the breakthrough of interfacial phenomenon emerges. Ancherson in 1840 reveals protein patterns at oil-water interface, followed by the work of notable researchers as Benjamin Franklin, Lord Rayleigh and Agnes Pockels [35–37]. Moreover, Plateau proves the presence of molecular forces acting at the interface and the evidence of interfacial viscosity [35].

Surfactant equilibrium and surface properties are extensively studied in a number of works [11, 22, 23, 35–39], being used as preliminary tool to elucidate basic interfacial features. Essentially, interfaces are populated with amphiphilic molecules that induce several dynamic processes as molecular aggregation, deformation, chemical reactions, adsorption/desorption, among others. For instance, the existence of foams and emulsions has been related to the presence of active surface molecules (amphiphilic structures) that adsorb from bulk liquid phases and lows the interfacial tension of the interface. Nonetheless, this property cannot in itself explain the interfacial stability obtained from the emulsification process. In fact, when interfaces are deformed, a resistance to tangential stresses emerges from the presence of distinct material properties. The measurement of these properties is better understood with the aid of the interfacial rheometry, a branch of the well-known 3D rheology, in which the stress-strain response of the 2D adsorbed layer is acquired by means of imposed deformation. In other words, the stresses at the interface are related to their rate of deformation. The rheometer must then be able to measure these fundamental material properties, as well as, the shear rate-dependent viscosity and complex viscoelastic moduli.

Shear and dilation are the main kinds of deformation modes in a rheometric flow, however, there are other types like, bending and torsion stresses, which emerge from specific interfaces (for instance bilayers and biological membranes). The bending modulus of interfacial layers is usually neglected in interfacial rheology [40].

When a rheologically complex interface is deformed or dilated, typical interfacial or surface stresses can emerge. A general expression for the surface stress is presented by Eq. 2-2 [37, 41]:

$$\sigma_s = \sigma_{\alpha\beta}(\Gamma, T)I + \sigma_e \tag{2-2}$$

where $\sigma_{\alpha\beta}$ is the interfacial/surface tension between two phases α and β, a stable variable that depends on surface concentration (Γ) and temperature (T). At a constant T, $\sigma_{\alpha\beta}$ relies only on the surface concentration Γ. The surface unit tensor I is the identity tensor and σ_e is the surface extra stress tensor [11, 41]. σ_e composed of deviatoric and an isotropic contributions, which can be probed by distinct interfacial techniques. As the deviatoric stresses are measured with shear rheology by keeping the interfacial area constant and changing its shape, the isotropic stresses are studied with the aid of dilatational rheology, by inducing changes in area without changing the interfacial shape [11, 37]. There are multiple ways to express the surface stress, however Eq. 2-2 is the simpler and most used approach that considers thermodynamic aspects (it is well represented by $\sigma_{\alpha\beta}(\Gamma, T)$).

In the next sections, we will review the basic equations and experimental measurement techniques of shear and dilatational/compressional rheology, reviewing the basic devices employed to acquire rheological data. The shear and compressional modes receive special attention since they are the focus of this work.

2.3.2
Shear mode of deformation

Interfacial shear rheology aims at measuring the response of the interface to constant area deformations while changing its shape. Basically, two types of experimental methods can be applied: the indirect method, in which, interfacial properties are obtained by the analysis of velocity profiles, and the direct method, in which the interfacial features are obtained through the measurement of force or torque applied to the interface [35, 36]. However, the former methodology tends to be complicated, especially if particles need to be added to track deformation, which can ultimately change the interfacial properties. Therefore, it is easier and more accurate to obtain local shear rates at the probe's surface (direct method) [37].

Nonetheless, one of the main challenges of the direct shear rate method is to deal with the coupling between bulk and interfacial flow fields. For this reason, measurement geometries must provide adequate sensitivity to detect stresses at the interface under the presence of bulk stresses presented in the adjacent films [42]. A good baseline parameter that has been explored extensively is the dimensionless group *Boussinesq number*, which relates the ratio of surface and subphase contributions, as defined in Eq 2-3:

$$B_q = \frac{\eta_s \frac{V}{L_s} P_s}{\eta \frac{V}{L_b} A_b} = \frac{\eta_s L_b P_s}{\eta L_s A_b} = \frac{\eta_s}{\eta a} \tag{2-3}$$

where η_s is the surface or interfacial viscosity (expressed in Pa.s.m) and η is the bulk viscosity of the subphase, V is the characteristic viscosity, L_1 and L_s are the characteristic length scales at which the velocity decays at the interface and in the subphase, respectively, P_1 is the contact perimeter between the rheological probe and the interface and A_b is the contact area between the probe and the bulk phase. The parameter a has the units of length.

Many of the devices used for interfacial shear rheometry are rotational and designed to be conducted in flat interfaces rather than complex curved interfaces, which are commonly found in real life systems. Moreover, the interfacial geometries are mostly comparable to the 3D geometries developed for bulk rheology, like the Couette geometry or the double-wall Couette geometry [35]. The bicone bob rotational rheometer is one of the oldest devices employed to assess the viscoelasticity of interfaces (see Fig 2.5 [a]), and the method has been improved over the years with efficient flow field routines to improve the accuracy of raw data since its sensitivity is smaller (as a in Eq. 2-3 is larger) [37,43]. Fig 2.5 (b) shows the interfacial stress rheometer (ISR), the equivalent of the sliding plate rheometer, which mainly consists of a magnetic rod placed at the interface positioned in the center of a rectangular channel (for this reason, it is also referred to as the magnetic rod ISR). An interfacial shear flow is induced between the rod and the walls of the channel by a magnetic field, and the drag experienced by the rod emerges from interfacial shear stresses (for further information, see the work of Reynart *et al.* and Brooks *et al.* [42,44]).

The Du Noüy ring (see Fig 2.5 [c]), commonly used for interfacial tension measurements, has also been employed in interfacial shear rheometry, however, most bulk rheometers have too low sensitivity and too high inertia to use it in oscillation mode. Therefore, a more accurate replacement is the double-wall ring (DWR), the 2D equivalent of the double-wall Couette geometry (see Fig 2.5 [d]). It has a smaller geometric radio compared to the bicone geometry, thereby presenting greater inherent sensitivity and lower tool inertia (a in Eq. 2-3). The DWR enlarges the perimeter per unit area, which provides better sensitivity and torques, as well as smaller contributions of the bulk phase to the interfacial response. Detailed flow simulations performed by Vandebril *et al.* [45] demonstrate the accuracy and dynamic range of DWR combined with a sensitive rheometer [35,45]. Recently, Renggli *et al.* [23] also proves the remarkable dynamic outreach of the DWR geometry as a direct rheological technique.
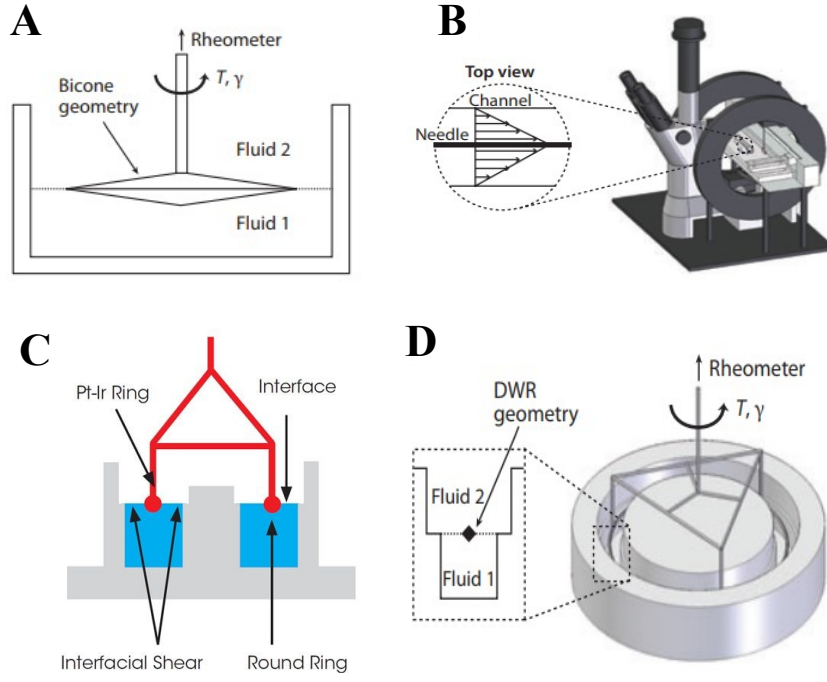
Figure 2.5: Main types of interfacial shear rheometers. A. Bicone geometry (cross section). B. Interfacial rod rheometer with the inset showing magnetic needle and glass channel. C. Du Noüy Ring set up. D. Double-Wall Ring (DWR) geometry set up. Images (a), (b) and (d) adapted from Ref. [35]. Image (c) from TA Instruments available in https://www.tainstruments.com/interfacial-accessories/.

When the interface is subjected to sinusoidal oscillations in the linear regime (small amplitudes), the surface tension oscillates with the same frequency as the area, but with a phase shift δ [46]. The interfacial viscoelastic modulus G can be measured using small amplitude oscillation of the in-plane shear deformation γ:

$$\gamma = \gamma_0 sin(\omega t) \tag{2-4}$$

where γ is performed at angular frequency ω and strain amplitude γ_0, and an out-of-phase response is obtained for the stress tensonr σ with a phase angle δ [47]:

$$\sigma_{\alpha\beta} = \sigma_0 sin(\omega t + \delta) \tag{2-5}$$

The storage (or elastic) modulus G' and loss (or viscous) modulus G'' are obtained as follows:

$$G' = \frac{\tau_0}{\gamma_0} cos(\delta) \tag{2-6}$$

$$G'' = \frac{\tau_0}{\gamma_0} sin(\delta) \tag{2-7}$$

If the deformation is in the linear viscoelastic (LVE) regime, the signal generates only a first harmonic, from which the phase shift and intensity are used to calculate the complex modulus [46]. The deformation of the interface is mainly a superposition of shear and dilatational kinematics, and for this reason, the deformation profile depends on the magnitudes of shear and dilatational complex moduli [35]. In the next section, we explore the mathematical modeling of the dilatational mode applied to complex interfaces.

2.3.3
Dilation mode of deformation

Dilatational measurements are significantly important to obtain a full rheological description of compressible materials, such as polymers or surface species at fluid-fluid interfaces. When the interface is deformed symmetrically retaining its shape, modifications in the interfacial area occurred, followed by changes in excess concentration of the surfactant (Γ) and in the state variables (surface or interfacial tension). The relation between the area and interfacial tension changes leads to the definition of Gibbs elasticity or Gibbs modulus K_Π [11, 37]:

$$K_\Pi = E = \frac{\mathrm{d}\sigma_{\alpha\beta}}{\mathrm{d}lnA} \tag{2-8}$$

where K_Π or E is the resistance to the creation of gradients in surface tension, or more generally known as surface stresses [35]. Similarly to the shear rheology, the total frequency-dependent complex moduli $K_i^*(\omega)$ is obtained and then decomposed in a elastic (K_i') and viscous modulus (K_i''). These contributions are also referred as real and imaginary components E' and E'' respectively [35, 42, 48, 49].

The tangential surface stress $\sigma_{\alpha\beta}$ also causes pressure jump, which can be quantified by a simple force balance that leads to the well-known Young-Laplace (Y-L) equation:

$$p - \rho g z = \sigma_{\alpha\beta}(\kappa_1 + \kappa_2) \tag{2-9}$$

where κ_1 and κ_2 are the principal curvatures, p is the pressure across the interface at z=0, ρ is the density difference, g is the gravitational acceleration and z is the vertical coordinate [37]. The Y-L equation is only valid if the stresses acting in interfacial adsorbed layers are uniform and isotropic, that is, if they do not vary along the interface [35, 37, 49, 50]. In that case, finding the shape of the drop to solve the Eq 2-9 is employed as an effective method since the late 19th century, especially after the invention of electronic cameras, image

digitalisation and software implementation. This approach is often referred as axisymmetric drop shape analysis (ADSA), or simply drop shape analysis (DSA) methodology, in which, Eq 2-9 is transformed into a set of differential equations expressed by means of the geometric parameters obtained by the drop profile. The high-resolution cameras are able to digitalize the drop images via the process of least square fitting of the theoretical shape obtained in the Laplace equation (see Fig 2.7 [b]). Some commercial equipament offer the control of area or volume as a function of time to sinusoidal profiles (see Fig 2.6 [a]). The measurement consists in recording the response of the interfacial tension while the area/volume of the drop is modified with time. Other types of dilatational experiments can be performed in DSA devices that couple shape and pressure measurements (see 2.6 [b]). They are conducted by varying interfacial aging and compressional strain rate [51]. Further mathematical modelling and experimental set-ups can be found in the work of Saad and Neumann, Miller *et al.* and Danov *et al* [36, 49, 52].

The DSA method is the principle employed for most commercially available dilatational apparatus, however, interfacial stresses acting in certain types of interfaces may be anisotropic and non-uniform. Usually, interfaces formed from proteins, asphaltenes, polymers, and phospholipds tend to possess surface viscoelasticity, and for this reason, they are called complex interfaces. Evidence of solid-like properties can be proved by the presence of interfacial wrinkles that arise upon compression, as the ones observed in the image sequence of Fig 2.7 (c). In that case, the drop profile deviates from the Laplacian shape, and consequently, fitting values of stress are composed not only a single value, but instead of two components acting along the "meridians" and "parallels": the σ_s and σ_ϕ respectively (see Fig 2.7 [a]) [37, 49]. Nonetheless, as recently proved by Rodriguez-Hakim *et al.*, if small-step deformations are applied to a pendant drop at short times and quasi-static deformations, the Y-L equation still remains valid [11, 51].

A

B
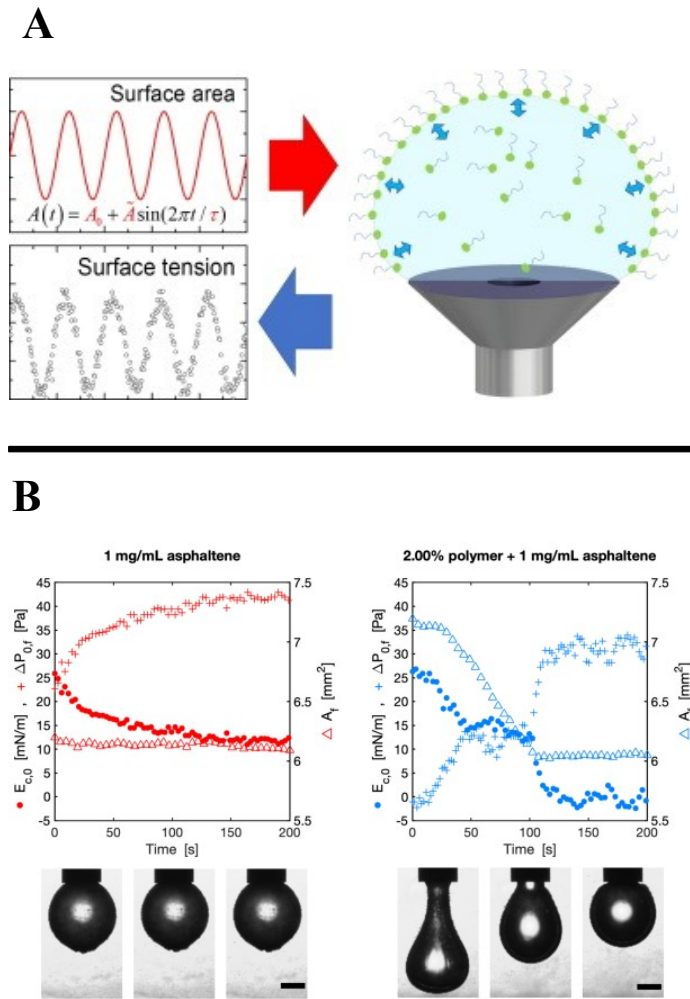
Figure 2.6: A. Schematic of determining the surface dilational rheology by measuring the interfacial tension and controlling the surface area. The cartoon ilustrates the surfactant adsorption process at the interface of an ascending drop. Image from Ref. [53]. B. Compressional step-strain results for 1 mg/mL asphaltene (left) and 1 mg/mL asphaltene + 2:00 % polymer (right) oil solutions at an aging time of 60 minutes and a compressional rate of 0.1 μL/s. Pictures of the deformed drops are shown at times 0, 100, and 200 seconds after stress relaxation begins. Image from Ref. [51].
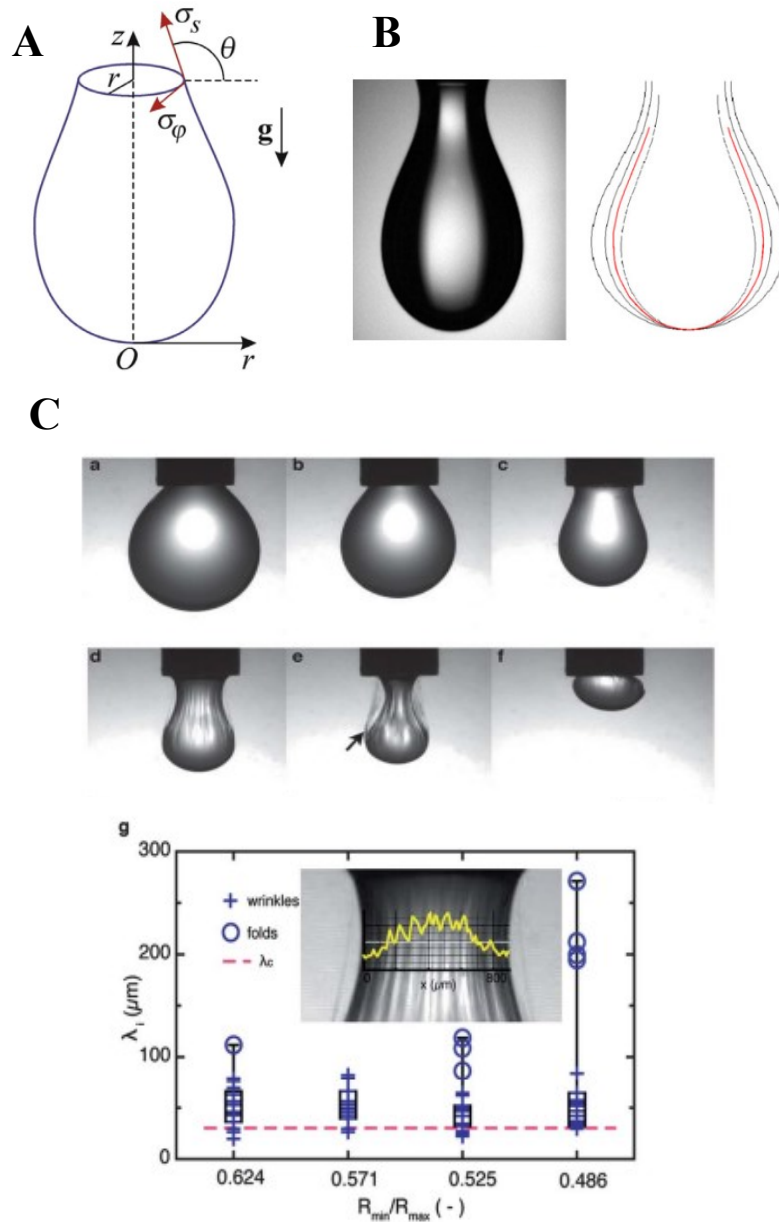
Figure 2.7: A. Scketch of a pendant drop displaying the σ_s and σ_ϕ components of surface/interfacial tension acting along the droplet profile. The vertical coordinate z and droplet radius r are also shown. (image from Ref. [49]). B. Pendant drop (*left*) and calculated profiles in the process of least square method of theoretical Laplace fitting (*right*). Image from Ref [36]. C. Evolution of a drop of β-ionone (oil phase) immersed in a solution of *Acacia* gum (aqueous phase) upon compression driven by negative pressure in the syringe (a-f). A biopolymer film is left behind by the delaminating of oil drop (see arrow). The wrinkles on the drop surface marks the presence of solid-like features. Image (g) shows the analysis of interface wrinkles through a wavelength distribution profile: data in the form of box plots in four different compression states of the same drop can be observed in the graph. (see Ref. [54]). Image adapted from Ref. [54].

2.3.4
Surface pressure isotherms: the Langmuir-Blodgett technique

Besides the DSA methodology, the Langmuir-Blodgett (LB) technique (also called as the Langmuir Trough technique), is widely used to investigate the dilatational properties of fluid-fluid interfaces. One important concept is that fluid interfaces are divided into two main classes: the soluble materials forming the Gibbs monolayers, and insoluble materials that produce the Langmuir films. The latter is what can be observed in the LB process, in which an insoluble layer of amphiphilic molecules is firstly spread on the surface of the aqueous subphase, followed by the compression or dilation of the interface [35, 55]. The experimental set-up of the Langmuir trough is basically composed of a rectangular cell and two movable barriers responsible for the imposed deformation [24, 37, 56].

In the analysis of the surface stresses obtained from compression, typical pressure-area (Π-A) isotherms can be expressed by the equation:

$$\Pi = \sigma_0 - \sigma_{\alpha\beta}(\Gamma, T) \qquad (2\text{-}10)$$

where Π is the surface pressure and σ_0 is the surface (or interfacial) tension of the clean interface. By measuring the surface pressure at a constant temperature, one can obtain the surface pressure as a function of area per molecule, which describes the relation between surface tension and surface concentration of the species adsorbed at the interface [37, 55]. Compression of the monolayer leads to distinct phases which are presented as discontinuities in the pressure isotherm. These phase transitions are mainly determined by the physical-chemical features of the surface-active species, the subphase temperature/composition, and rheological properties. At first, the monolayers exist in the gaseous state (G), however, when compression begins, they undergo a phase transition to liquid state (LE) passing through the G-LE co-existing region. Upon further deformation, the LE phase goes to a liquid-condensate (LC) state (after going through a co-existing region LC-LE), and ultimately to a higher molecular configuration at the solid-state (S) (see Fig 2.8). The monolayer collapse occurs when there is an overcompression of the interfacial film beyond the two-dimensional packing limit of molecules (the 2D molecular state changes to a 3D state) [55, 57].
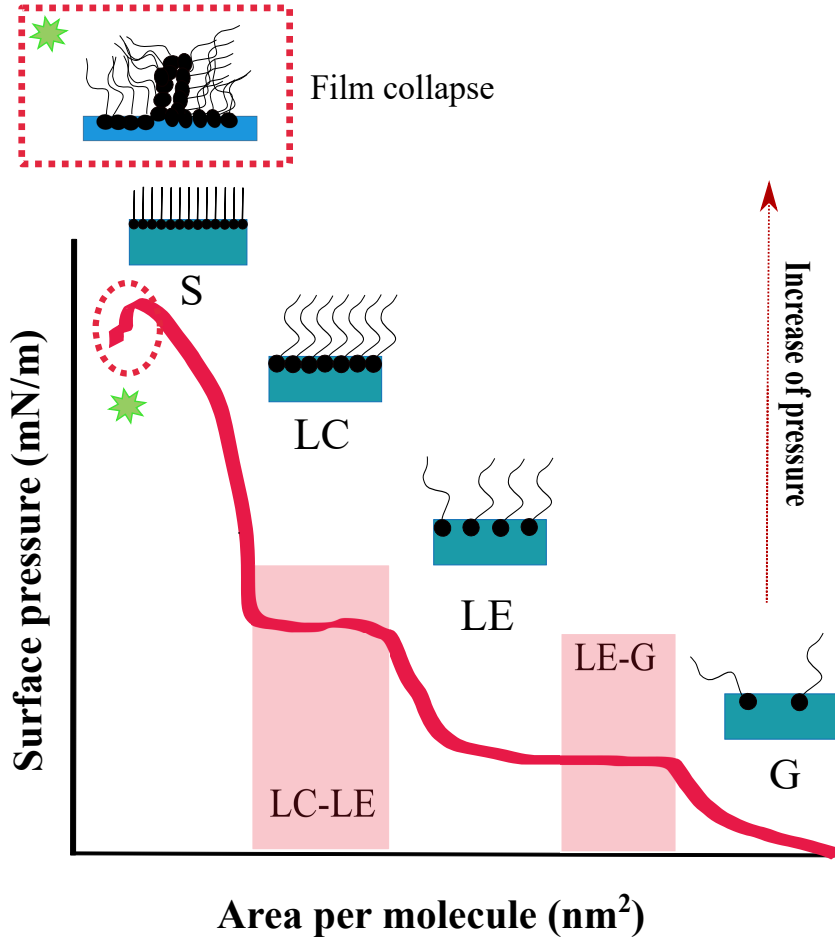
Figure 2.8: Schematic drawing of the Langmuir film phase transitions: gas (G), liquid-expanded (LE) and liquid-condensate (LC), and the in-between states LE-G and LC-LE. Adapted from Refs. [56, 58].

One of the drawbacks of using the rectangular Langmuir trough is that, at significantly high compression rates, the interface may undergo deformations of both area and shape, resulting in mixed shear/dilatational contributions that usually are difficult to decouple [37, 59]. This may impact on the evaluation of solid-like interfacial properties due to the extra stresses as presented in Eq 2-2 [37, 56]. Drop-shape methods applied to complex microstructures can also present similar mixed deformation fields [56].

Nonetheless, it is frequently mentioned in the literature the apparent compressional modulus (K_{app}), which can be calculated from the slope of the compression isotherms as follows [11]:

$$K_{app} = -\frac{\Pi_1 - \Pi_2}{\ln(A_1) - \ln(A_2)} \tag{2-11}$$

where Π is the surface pressure shown in Eq 2-10. In conditions such as slow compression and true equilibrium properties, the $K_{app} \approx K_\Pi (K_\Pi$ is

defined in Eq 2-8 as the Gibbs modulus for dilatational mode of deformation). This simplification implies that pure dilation in plane could be considered as the main mode of deformation.

Several attempts have been made to measure the material functions of interfaces subjected to pure dilation in planar geometries. Methods that include the use of radial troughs (see Fig 2.9 [c]), in which the interface is isotropically strained and the surface pressure is measured by a Wilhelmy rod to keep the radial symmetry, are the most recently investigated, as the initial work of Miyano *et al.*, Matsumo *et al.*, and more recently the work of Pecipelli *et al.*, Fajardo-Rojas *et al.* and Kale *et al.* (for further information on the development and mathematical modelling of radial troughs see Refs [20, 56, 59–61]). In addition to new cell configurations, the Langmuir trough has been modified by assembling it to interfacial geometries in standard rheometers, like the DWR geometry [39, 41] (see Fig 2.9 [b]). Morever, to monitor the interfacial morphology, the use of optical and confocal microscope is a useful way to correlate rheological properties to microstructure visualization under compression/dilation. Brewster Angle microscopy (BAM) is also an alternative to assess interfacial structure formation *in situ* under distinct shear rates and surface coverages [39, 56, 62].
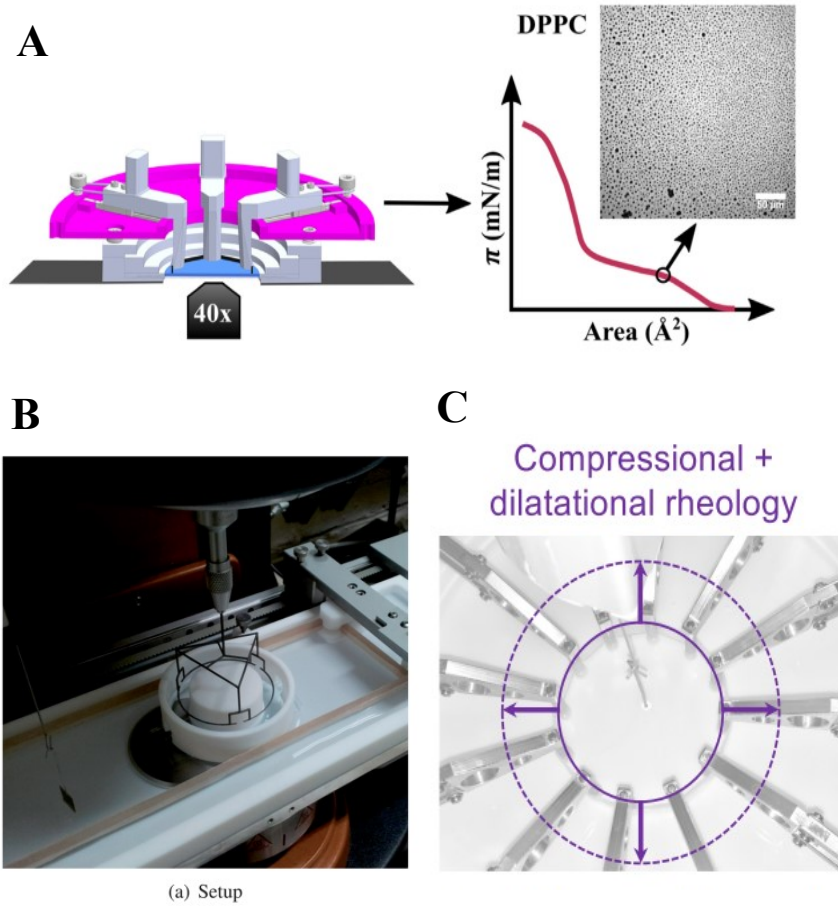
Figure 2.9: Advances on dilation/compression techniques. A. A miniaturized radial Langmuir trough developed to study poly(tert-butyl methacrylate) (PtBMA) and dipalmitoylphosphatidylcholine (DPPC) at an air-water interface under purely dilatational deformations. A conventional inverted microscope is accopled to the experimental apparatus for simultaneous interfacial visualization (image on the *right*). Image from Ref. [56]. B. Langmuir trough with an adapted DWR accessory attached to a stress-controlled rheometer. Image from Ref. [41]. C. Dilatational/compressional rheology in the radial trough. Image from Ref. [11].

2.4
Spontaneous emulsification phenomenon

Complex fluid-fluid interfaces play a significant role in various industrial applications, for instance, in food and emulsion stability, biofilms, and coating phenomena [37]. Understanding these examples throughly involves a major engineering challenge, especially the rheology of emulsions and foams that are

widely found in the petroleum industry [20, 63]. Emulsions are traditionally defined as unstable systems formed by two immiscible liquids where one phase is dispersed into the other [64]. If the interfacial tension of the system is high, a large input of energy (generally by mechanical means) is required to increase the interfacial area. (see Eqs 2-12 and 2-13). The addition of surface-active species (polymers, asphaltenes, or nanoparticles) lower the interfacial tension, and consequently reduces the Gibbs free energy promoting greater dispersion of the droplets, as can be verified from the equations:

$$W = \Delta A * \gamma \tag{2-12}$$

or

$$\Delta G = \Delta A * \gamma \tag{2-13}$$

where ΔG is also expressed as interfacial work W. The stability of an emulsion is enhanced when the surfactants adsorb onto the interface and induce the formation of complex and structured films, which ultimately affects coalescence events by promoting interfacial rigidity. Depending on the surface forces and intermolecular interactions, the phase separation of the system is faster or slow, although as time goes on, the emulsion will separate, returning to its original configuration [51, 65].

Despite the evidence of high-energy input to induce emulsion formation, there is a special type of emulsion that can be formed with no energy cost. This work-free emulsion processing, firstly observed in the XIX century with lauric acid in oil dispersed onto an aqueous alkali phase, is called spontaneous emulsification (SE), and it occurs when the total system free energy is at minimum [66, 67]. Over the years, many researchers have devoted to the understanding of the SE phenomenon [66–71]; however, special attention should be made towards the work of Davies and Rideal, since it addresses the fundamental discoveries on three possible mechanisms of SE based on *interfacial turbulence*, which is basically the result of transient negative values of interfacial tension, and *diffusion and stranding*, when one of the components of a phase has a very strong affinity for the other during the mass transfer. The single constituent can be "stranded" by the other, resulting in a separation out of phase [72]. The main difference between these two mechanisms is that the former is derived from a mechanical instability, whereas the latter is a chemical rather than a mechanical problem [51].

Interfacial turbulence is mainly governed by interfacial tension gradients that are developed due to the non-homogeneous coverage of surfactants at the interface. Marangoni stresses can lead to turbulent flow, which may contribute to greater emulsification rates [68]. On the other hand, when a solvent diffuses

into an immiscible phase, local regions of supersaturation are created , which can ultimately derive in nucleation and drop formation. Lopez-Montilla *et al.* [68] shows a good example of this mechanism when a solution of ethyl alcohol and toluene is placed in contact with water. The alcohol diffuses from the oil to the water and carries part of the oil that is soluble in the alcohol/water mixture. Thus, the oil ends up being "stranded" in the water in the form of droplets. Other mechanisms may explain the SE, like the *interfacial bending*, in which the interfacial free energy resulting from bending stresses (associated with changes in the mean curvature) balances the energy cost from increasing the interfacial area [73].

Recently, Araujo *et al.* showed that indigenous asphaltenes dissolved in toluene can spontaneously emulsify when the solution is placed in contact with water. With the aid of a confocal microscope located at the center of the meniscus, they observed that the number of microdroplets increases over time, which they mainly associate to interfacial turbulence phenomena (see Fig 2.10 [b]). Moreover, a recent study conducted by Duboé and coworkers [72] presents an osmosis-driven phenomenon governed by the differences in the chemical potential of the water in the formed microdroplets and the water in the bulk phase (see Fig 2.10 [c]). They also prove that high-salinity water reduces the number of emulsified droplets at brine-crude oil interfaces. Rodriguez-Hakim *et al.* proves that the diffusion and stranding is the mechanism responsible for SE at asphaltene and asphaltene/polymer laden interfaces. Besides, they find that interfacial viscoelasticity is inversely proportional to the rate of SE, and it is also a time-dependant phenomenon (see Fig 2.10 [a]). In other words, some types of interfaces can supress emulsification, depending on the type of surfactant or/and in the presence of co-species, as the viscoelastic moduli increases with time [51]. This was a breakthrough discovery that correlated interfacial viscoelasticity with the SE process (see Fig 2.11).

Controlling the SE is of great importance to a number of applications where there is a demand for microsized droplets as in emulsion formulation for personal care, cosmetics and health, and the petroleum industry. Alternatively, this process can be undesirable, as in the case of enhanced oil recovery (EOR) by low-salinity water, in which the physical-chemical mechanisms induce the formation of microdispersions at the oil-water interface, thus impairing the quality of oils. Researchers believe that the presence of microdroplets can be helpful to elect oils for the low-salinity process [72, 74–76].
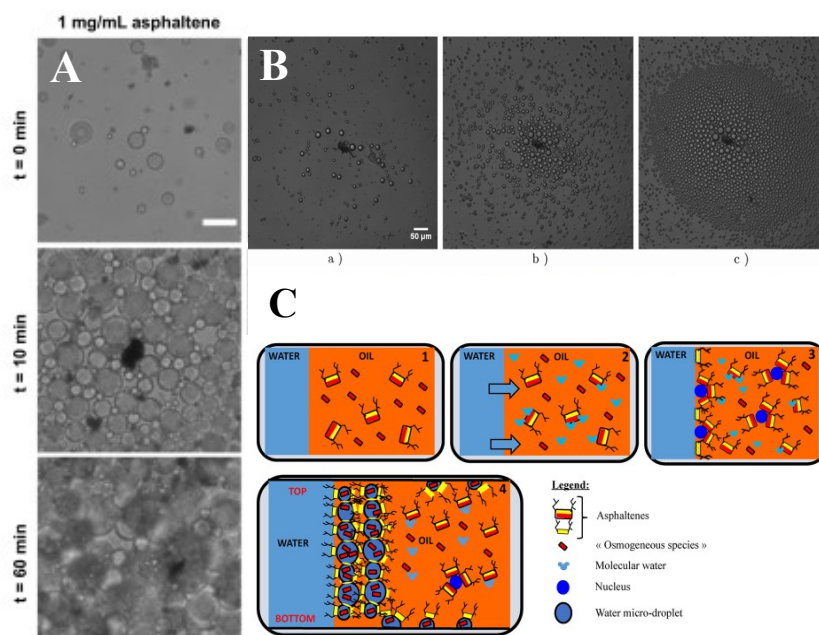
Figure 2.10: A. Spontaneous emulsification (SE) as a function of time for a 1 mg/ml asphaltene solution (100% toluene in volume). The water phases consist of deionized water (DI) and the scale bar is 50 μm. First snapshot: immediately upon contact of water and oil phases. Second snapshot: 10 minutes after contact of water and oil phases. Third snapshot: 60 minutes after contact of water and oil phases. Both pure asphaltene and pure polymer systems spontaneously emulsify. In the presence of asphaltenes, the higher the co-polymer concentration, the lower the degree of emulsion formation. Image from Ref. [51]. B. Another set of images of SE for a distinct asphaltene solution with a concentration of 1.5 mg/ml (100% toluene in volume). The water phases consistis of deionized water (DI) and the scale bar is 50 μm. The images were captured using a confocal microscope. Accumulation towards the meniscus is observed. Image from Ref. [77]. C. Illustration of the mechanism of the water droplets formation in the oil phase. Imagem from Ref. [72].
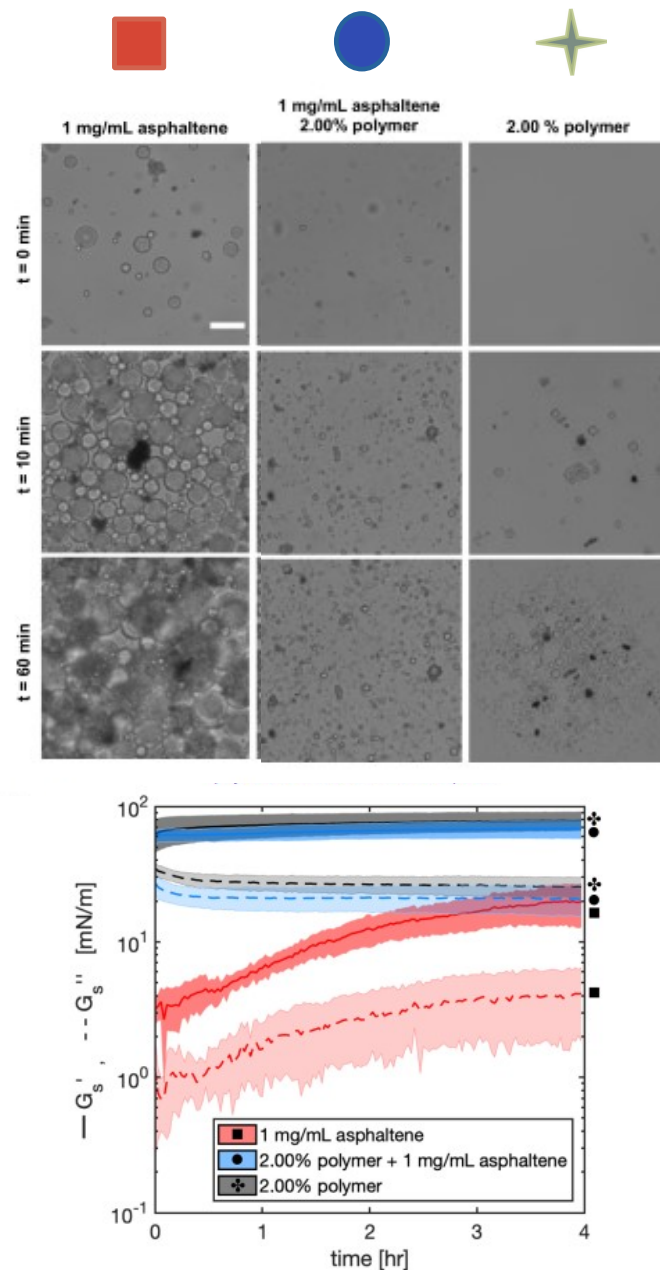
Figure 2.11: The linkage between spontaneous emulsification (SE) and interfacial viscoelasticity. Evolution of droplet formation with different asphaltene polymer concentrations (square symbol corresponds to asphaltene-only surfaces, circle symbol to mixture of asphaltene and polymer, and cross symbol to the polymer-only surface). The top, middle and bottom rows correspond respectively to 0, 10, and 60 minutes after contact of water and oil phases (*top*). Small-amplitude oscillatory interfacial shear rheology of different asphaltene and polymer mixtures as a function of time for a strain rate of 0.3 % and a frequency of 0.1 Hz within the linear viscoelastic regime. The solid lines represent the elastic modulus, whereas the dotted lines represent the viscous modulus (*bottom*). As the interface becomes more viscoelastic (by adding polymers to the asphaltene solution - circle and cross symbols), the rate of emulsification also decreases. Thus, interfacial shear viscoelasticity is inversely correlated to the propensity of a system to emulsify spontaneously. Adapted from Ref. [51]

2.5
Background on interfacial rheology of asphaltenes and advances of measuring techniques

Understanding the behavior of asphaltenes at the interface represents an important challenge to several engineering problems found in crude oil refineries. For instance, the plugging of pipelines, wells and facilities can generate fouling and impair oil production, leading to undesirable shutdowns. The desalting process, an important first unit operation in the refinery, may be affected due to a delay in the coalescence process of droplets, which is essential to a successful separation of oil and water streams. Moreover, the aggregation process of asphaltenes is quite helpful to clarify how the mixture of oil with water occurs when subjected to high shear rates during flow.

All the aforementioned issues have been mainly linked with the presence of asphaltenes, since they are the most interfacially active fraction of crude oil, and consequently, they are more prone to aggregate and adsorb at the oil-water interface [10, 11, 39, 78–80]. Recently, the advances on the interfacial rheometry and tensiometry (e.g, pendant drop dilation and contraction, surface pressure isotherms and shear rheology) has helped researchers to better understand the linkage between the material properties of adsorbed layers with their physical/chemical features.

Different groups have investigated the impact of asphaltene structuring and solvent composition. Spiecker and coworkers [63] selected asphaltenes from distinct crude oils sources and showed by using a bicone bob interfacial rheometer that the aromatic and polar content is inversely proportional to the viscoelastic modulus and yield stress of the layers. They also suggested that the adsorption kinetics of asphaltenes in solvents with greater aromaticity is reduced (poor film forming). Also confirmed by Barré *et al.* [81], the most polar fraction of asphaltenes are able to form the more massive clusters, which can adsorb as a whole at the interface. The solvent effect discovery is later emphasized by Fan *et al.* [47], who showed that, at a given asphaltene concentration, the elastic modulus decreases when increasing the proportion of toluene in the oil phase composition. On the other hand, by reducing the toluene content up to 30 %, the authors reported a much higher storage modulus.

Asphaltenes are also known to irreversibly adsorb at oil-water interfaces and slower the drainage of thin films. Assessing the film lifetime is a good strategy to evaluate water-in-oil emulsion stability. The work of Tchoukov *et al.* [82] pointed out the differences in the film thickness of asphaltenes and maltenes. The evidence of increasing stability and lower drainage dynamics

is supported by the way asphaltenes self-assemble and form a compact 3D network. The buildup of the 3D structure modifies the rheological properties of the liquid film, changing it to a gel-like non-Newtonian interfacial film.

The dynamic competition between asphaltenes and co-surfactants (e.g, polymers, demulsifiers and carboxylic acids) has also been explored in terms of surface activity, since it plays an important role on emulsion stability and the coalescence process. It is known that co-adsorption of lower molecular weight surfactants and asphaltenes can soften the interfacial film and facilitate oil and water separation [83,84]. Liu *et al.* [85] showed a synergetic effect of asphaltenes and resins by means of short and long-terms interfacial adsorption. Adding resins to the oil solution induced the dispersal of asphaltenes, which resulted in smaller values of the dilatational storage modulus. Similar to the work of Zhang *et al.* [86], Wang and coworkers [24] also explored the interactions of asphaltenes and stearic acids (SAs) by conducting washing experiments in a rectangular Langmuir trough. They showed that the SAs preferably stayed attached to the toluene-water interface upon the addition of fresh toluene on top of the film, whereas the loosely asphaltene molecules were displaced from the interface. This result supports the theory that SAs can reduce the rigidity of the toluene-water interface.

Advances on the analysis of surface/interfacial properties of asphaltenes with the aid of visualization techniques have been made recently, as the study conducted by Lin *et al.* [39]. Asphaltene layers and variations (two surface coverages) were prepared by spreading the surface-active content at decane-water or air-water interface. They found that when asphaltenes are spread at the air-water interface, that is, by letting them aggregate in air, the morphology of the film is like a compact layer with a finer grain-like structure and smooth edge, whereas when the asphaltene solution is directly injected at the interface after the oil addition, the asphaltene aggregates hold a less tightly packed configuration, which the authors define as a coarser-grain appearance with rough edges. Swollen asphaltenes entrainment hinders packing of the interface, as also discussed in the studies of Gawrys *et al.* [87] Spiecker *et al.* [63]. Furthermore, Zúniga-Hinojosa and coworkers [88] used Brewster angle microscopy (BAM) and atomic force microscope (AFM) to look into the morphology of asphaltene films and maltenes under compression. Asphaltene films exhibited the most rigid and compact structures, whereas maltenes seem to form thinner films and larger areas of mono- or bi-molecular layers.

Although efforts made over the years, the dynamic aggregation of asphaltenes is still under debate. Despite the numerous analytical and experimental techniques, their self-interaction at the oil-water interface is

among the least understood topics in surface science [9]. Molecular dynamics (MD) simulation is an alternative method to help with the above-mentioned subject. It provides efficient computational calculations to better assess the asphaltene structural properties at a microscopic level. Hence, it is a good strategy to address the fundamental details of their self-arrangement and precipitation. Headen *et al.* [89] performed MD simulations of different generated asphaltene/resin structures in solvent molecules (toluene and heptane), and investigated the energy bindings of asphaltene-asphaltene and resin-resin molecules. Gao *et al.* [27] utilized two distinct asphaltene molecules, namely electroneutral C5 Pe and anionic C5 Pe to study their stacking in crude oil and at the oil-water interfacial. Their findings show that the non-charged molecules preferably remained in the oil phase, while the anionic molecules had a distinct affinity towards the interface. Similarly, in the work of Mikami *et al.* [90], a heptane-asphaltene-water interface is investigated and distinct types of asphaltene configurations are selected (like the "archipelago type" and the "island type"). They observed that with two different island type configurations, the aromatic plane could either form a stable structure parallel to the interface or rearrange as nanoaggregates, changing to a vertical position and inducing molecular oscillations. Moreover, the study shows the relevance of film consolidation to changes in the surface energy of the interface (the interfacial tension values can drop significantly).

In this work, we aim to address the viscoelasticity of asphaltenes and mixed asphaltene and stearic acid laden interfaces by mainly conducting interfacial/rheological experiments (we did not use any type of computational method to study the asphaltene behaviour). In the next section, we will present in details the materials and methods applied within the experimental procedures.

3
Materials and Methods

In this section, we present the materials and experimental methods employed in this work. Almost all equipaments are found in the facilities of the "Grupo de Reologia da PUC-Rio (GReo)". However, the confocal microscopes and the equipament for the asphaltenes chemical characterization are located elsewhere: the confocal experiments were performed at the Laboratory of Microhydrodynamics and Flow in Porous Media (LMMP - PUC-Rio), the NMR analysis at the "Central Analítica Pe. Leopoldo Hainberger" (CAPLH - PUC-Rio) and the Elemental Analysis at the "Centro Analítico de Instrumentação da Universidade de São Paulo (USP)". The confocal microscope used for the spontaneous emulsification study is located at the Fuller Lab (Stanford University - California, USA).

3.1
Chemicals

The main asphaltenes used in this research were extracted from a Brazilian crude oil sample provided by the company Petrobras. They have a density of 989 kg.m^{-3} at 20°C (10.9 °API). The ASTM method implemented was the ASTM DS6560, in which heptane was used as the main solvent for the asphaltene extraction. We will refer to these asphaltenes as "BR asphaltenes"; however, it is worth to recall that, depending on the petroleum source, asphaltenes obtain distinct interfacial/rheological properties. In this work, we evaluate only one type of Brazilian asphaltenes.

Samples of two distinct asphaltenes were donated by the Professor Fuller Research Group from Stanford University. They were used in the studies of Rodríguez-Hankim *et al.* [51] and Araujo *et al.* [77], and the asphaltene properties, as well as the extraction methods employed, are listed in their work (see Refs [51, 77]). We will refer to them as "Asphaltene A" and "Asphaltene B".

Stearic acid (SA) was purchased from Synth ($\leq$ 98 %). It is a completely saturated carboxylic acid (no double bonds) comprising a straight carbon chain with 18 carbon atoms ($C_{17}H_{35}COOH$). SAs are considered one type of linear NAs [24].

For the oil phase, we elected pure toluene from Quemis (purity=95%) to solubilize the asphaltenes. We also chose two different non-aromatic solvents: n-heptane and n-hexadecane from Sigma-Aldrich (purity=99 %) to investigate specific interfacial properties. However, the hexadecane was the only non-polar solvent used as a diluent for the asphaltene fractions. The heptane, purchased from Synth ($\leq$ 95 %), is only employed as a solvent top phase; therefore it was not used as part of the volume mixture (this will be better explained in subsection 3.9.1).

.

3.2
Water subphases

Aqueous subphase of interfacial experiments consisted of ultrapure Mili-Q water (deionized water - DW) with a pH close to 6.5. and condutivity of 0.5 μ.s^{-1}. A brine composed of distinct salts that mimic real ocean water was employed as an aqueous subphase and we referred to it as *synthetic water* (SW). The pH of SW is $\approx$ 8. The preparation of SW was done by following the ASTM Standard D1141-98.2013, "Standard Practice for the Preparation of Substitute Ocean Water" [91]. The composition of SW is presented in Table 3.1.

Table 3.1: Chemical composition of Synthetic Ocean Water.

Compound	Concentration [=] g/l
NaCl	24.53
MgCl$_2$	5.20
Na$_2$SO$_4$	4.09
Ca$_2$Cl$_2$	1.16
KCl	0.695
NaHCO$_3$	0.201
KBr	0.101
H$_3$BO$_3$	0.027
SrCl$_2$	0.025
NaF	0.003
Ba(NO$_3$)$_2$	0.0000994
Mn(NO$_2$)$_2$	0.0000340
Cu(NO$_3$)$_2$	0.0000308
Zn(NO$_3$)$_2$	0.0000096
Pb(NO$_3$)$_2$	0.0000066
AgNO$_3$	0.0000049

Most of investigations examine the individual effects of salts and ions, however, in reality, more than one salt or ions are present in seawater, which is mainly used during the processing of crudes [92]. Therefore, we selected the aforementioned SW to assess the synergetic effects of the asphaltenes and SAs at the interface.

3.3
Oil composition

We prepared an *asphaltene solution* of 1 mg/ml, that is, by solubilizing the asphaltenes in 100 % vol. of the *toluene solvent*. We also prepared a *hextol solution*, which means, the asphaltenes were solubilized in a 80/20 volume mixture of hexadecane and toluene that we named as *hextol solvent*. In order to simplify our study, we investigated the hexadecane only in mixture, keeping the same hexadecane-toluene volume ratio.

To prepare the *hextol solution*, we followed these steps: firstly, we prepared a solution of asphaltenes dissolving them in pure toluene (100 vol. %) at the desired concentration, and then sonicated it for 30 minutes. Secondly, we added the hexadecane to the asphaltene solution and put it in the sonicator for more than 30 minutes. This is a simple strategy to avoid precipitation, since hexadecane is considered a poor solvent for asphaltenes [5, 7]. The so-called *hextol solution* is then different from the *hextol solvent* since the former contains asphaltenes, whereas the latter is an asphaltene-free mixture of distinct solvents. This distinction will be important for discussion in Chapter 4.

Solutions of stearic acid were prepared with pure toluene in the concentrations of 1 mg/ml and 10 mg/ml or by mixing mass fractions of asphaltenes with the acid in the rates of 1:1, 1:10, 3:1 and 3:10, also dissolved in 100 vol. % of the *toluene solvent*. These solutions were used for the dynamic interfacial tension (DIT) experiments. Specifically for the rheological tests, we prepared a *diluted asphaltene-stearic acid solution*. To prepare it, we employed a 1:1 mass mixture of asphaltenes and stearic acid in 7 ml of pure toluene (final concentration of 1 mg/ml), which will be referred as *main solution*. We solubilized 1 ml of the *main solution* with 12 ml of the *toluene solvent*. The final solution was then sonicated for 30 min at room temperature. Detailed steps of the dilution procedure are shown in Fig 3.1.
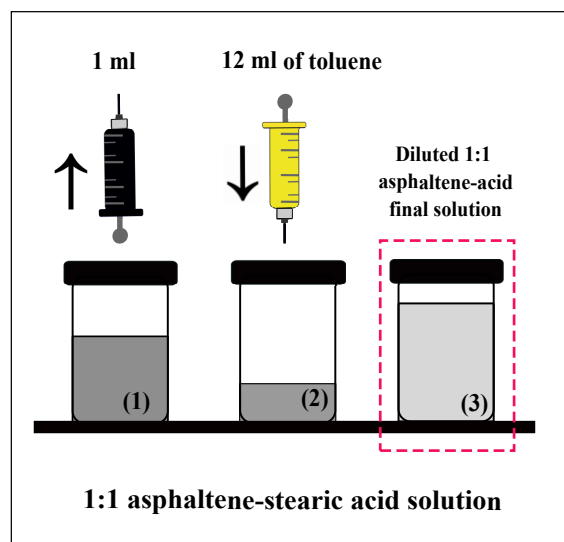
Figure 3.1: Schematic drawing of the asphaltene-stearic acid preparation for the rheological co-adsorption experiments. Black arrow in vial (1) indicates the volume removed from the main solution containing both stearic acid and asphaltenes, whereas black arrow in vial (2) indicates the addition of pure toluene, resulting in the final diluted 1:1 asphaltene-stearic acid solution (vial 3).

3.4
Interfacial energy measurements

In order to assess the surface energy of asphaltenes and stearic acid films in both deionized water (DW) or synthetic water (SW) subphases, we measured the dynamic interfacial tension (DIT) applying the well-known drop shape analysis (DSA) methodology. We used a Teclis Tensiometer (Model T2017 05 15 - Fig 3.2) to conduct the surface energy experiments. The oil phase containing asphaltenes, stearic acids or both was inserted in a "U" shape syringe (Fig 3.2 [b]) that was immersed into the water subphase (aqueous phase is placed in the quartz cuvette shown in Fig 3.2 [b]). Before each trial, we carefully washed, at least three times, the cuvette, the needle, and the syringe with deionized water, ethanol and acetone. We also dried the pieces with compressed air and soft wipes. The solutions were previously sonicated for 30 min before each experiment.

The DIT was performed by acquiring the digitalized image of the oil drops, obtained by means of a CCD camera and the equipament software. The Laplace equation of capillarity was employed to fit the drop shape coordinates to a set of first-order differential equations by the geometric parameters of the drop/bubble profile. We set the equipament software to a "None" deformation

mode, so the droplet remained static until the end of the experiment. DIT was measured for 1h without interfacial aging at room temperature.
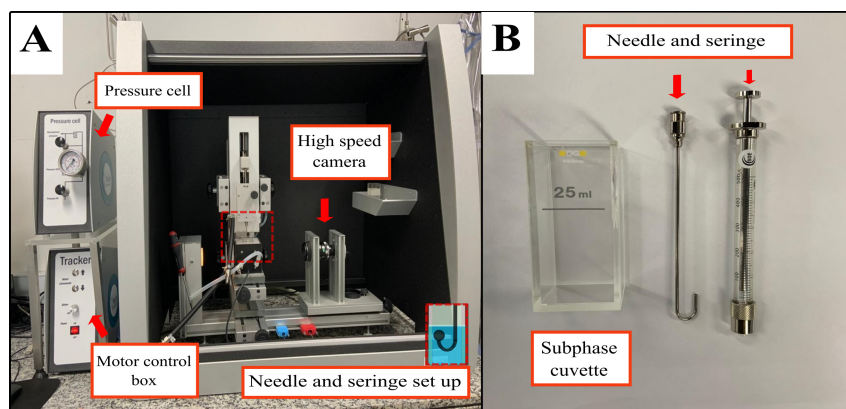
Figure 3.2: Overview of the Teclis Tensiometer. A. Complete apparatus. B. Details of the cuvette and syringe used in the DIT experiments.

3.5
Pressure Isotherms

Surface pressure isotherms were obtained using a rectangular liquid-liquid computer controlled Langmuir trough from KVS NIMA 1004 (Biolin Scientific) depicted in Fig 3.3 (a). It is coupled with two-movable barriers, which allow the compression tests, a bottom compartment that holds the liquid subphase and a top compartment to hold the oil phase. Also, a Wilhelmy plate is gently placed at the water-air interface for each trial (see Fig 3.3 [b]). Deionized water (DW) or the synthetic water (SW) is poured into the bottom compartment until it is completely covered. We prepared asphaltene and SA solutions, as well as mixtures of both surfactants to investigate the molecular packing of asphaltene nanoaggregates and their interfacial competition with SA at the air-water and oil-water interface.

Prior to each experiment, we carefully washed the trough and barriers with water and detergent drops, rinsed them with DW at least three times and carefully dry them with a suction pump. A similar procedure is carried out with the Wilhelmy plate, in which we rinse it with ethanol and deionized water for three times and flame-treated it to remove any residual organic contaminants. The bottom compartment was, then, filled with 300 mL of DW or SW and the Wilhelmy plate was gently placed at the air-water interface. After closing the barriers and cleaning all the remaining impurities, we opened them to the limit of the trough area and injected 25 μL of the desired samples (asphaltene,

SA or the binary system) dropwise onto the air-water interface with the aid of a 50 μL syringe from Hamilton.

Three-hour interfacial aging was set before the compression of the movable barriers to guarantee the total evaporation of the solvents and the network consolidation. For the tests performed at the air-water interface, once the aging time expired, the compression of the trough started. As for the oil-water measures, we poured roughly 200 mL of heptane, hexadecane, or toluene on top of the adsorbed asphaltene-SA layers before the onset of compression. All compression experiments were carried out with a fixed compression rate of 10 mm/min at a temperature of 25°C.
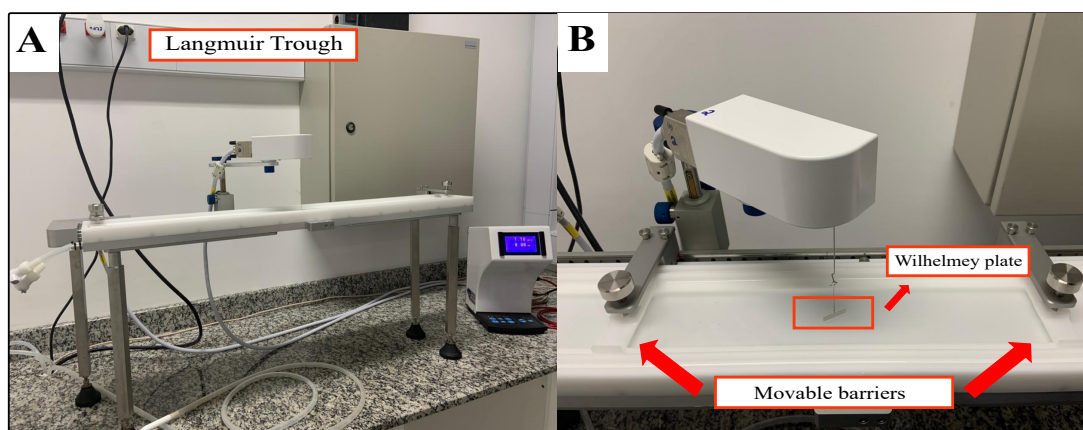
Figure 3.3: Overview of the Langmuir Trough apparatus. A. The Langmuir trough setup. B. Top view of the compression-expansion compartiments. Red arrows indicate the Wilhelmy plate and movable barriers of the trough setup.

3.6
^{1}H and ^{13}C nuclear magnetic resonance (NMR) and Elemental Analysis

Nuclear magnetic resonance (NMR) was employed to evaluate the asphaltene chemical structure. ^{1}H and ^{13}C spectra were acquired in a Bruker Advance 400 Equipment operating at 9.397 T. For the experiment, 20 mg of asphaltene was dissolved in 0.6 mL of deuterated chloroform and tetramethylsilane was used as reference for chemical shifts and for ^{13}C spectrum (Cr(acac)$_3$ 50 mmol L^{-1} is employed as a relaxation agent). For ^{1}H NMR a spectral width of 8012.8Hz with a relaxation delay of 1.0s and 128 scans were accumulated, with a pulse flip angle of 30°. For the ^{13}C NMR, a spectral width of 240038.5 Hz, a relaxation delay of 10 s and 7200 scans, with a pulse flip angle of 90° was used. The decoupler mode was set to invert gated to avoid the nuclear Overhauser enhancement effect (NOE).

To prepare the samples for the Elemental Analysis, it was injected $\approx$ 1 mg of the asphaltene samples (weighed on a highly precise scale) inside the Elemental Analyzer 2400 CHN (Perkin Elmer) calibrated with acetanilide standard, where combustion occurs in the presence of pure oxygen at a temperature of 925°C. All carbon is transformed into CO_2, hydrogen into H_2O and nitrogen oxides are reduced to nitrogen (N_2) in a copper metallic column at 640°. These gases were displaced by ultra pure helium gas, and separated by a chromatographic column packed in silica. Quantification took place in the TCD detector (Thermal Conductivity Detector). The result of the analysis was expressed as a percentage of carbon, hydrogen, and nitrogen (C,H,N).

3.7
Scanning electron microscopy (SEM) and confocal microscopy

We conducted a study on the morphology of precipitate asphaltenes (solid- state), asphaltenes dissolved in a 100 % vol. of *toluene solvent* and in the *hextol solution* by employing Scanning Electron Microscopy (SEM). We used a TESCAN CLARA equipped with a BrightBeam^{TM} electron optics column. Small fragments (approximately 0,7 mg) and one drop of each solution were placed on aluminum stabs that were previously stamped with carbon ribbons. The holders were coated with gold since asphaltenes are non-conductive material. For the liquid samples, we waited until the total evaporation of the solvents to begin vizualization. This coating enabled a more precise and detailed analysis of the surface topography and particle sizes. We employed a back-scattered electron detector in conjunction with a high-energy, high-resolution mode to produce high magnifications and high-quality images on a micrometer scale.

Optical microscopy was conducted using a LEICA STCS SP8 inverted confocal microscope. For this technique, we studied the asphaltenes only in *hextol solution*. We sonicated it for 30 min before each trial, and after, we placed a drop of the solution on top of pre-cleaned glass slides. A HC PL APO CS2 63x/1.40 oil objective was used with a zoom factor of 1.28 to scan the sample. We also applied a PMT-transmitted light with a 340V gain.

3.8
Confocal experiments: Analysis of Spontaneous Emulsification over time

The evolution of spontaneously emulsified droplets of BR asphaltenes at the toluene-water interface was investigated over time by using a Nikon Ti2-E inverted microscope. A 20x objective was selected to vertically scan the interface. To hold the water and oil phases, a glass chamber was built by

glueing a cylindrical capillary to a glass cover slide with a thickness of 0.1 mm (5 mm diameter by 10 mm height). Prior to each test, we carefully rinsed the chamber at least three times with toluene, deionized water, and acetone. After the cleaning, it was plasma treated to offer the glass hydrophilic and ensure the presence of smooth contact lines to help imaging [51].

At the beginning of each experiment, 10 μL of DW was added inside the chamber with the aid of a glass syringe. The chamber was positioned onto the microscope stage and the center of the glass was located (water-air meniscus). Then, 20 μL of asphaltene solution was injected on top of the water subphase using a separate glass syringe. The chamber was immediately covered with a glass slide to avoid evaporation. The water-toluene interface was located through the presence of the emulsified drops. The spontaneous evolution of droplet formation was recorded after 4, 10, 40, and 60 minutes the oil and water phases were placed in contact. The methodology for the spontaneous emulsification (SE) experiments is the same employed by Rodriguez-Hakim *et al.* [51].

3.9
Interfacial Rheological Experiments

The mechanical shear properties of asphaltene and stearic acid films were measured by using a stress-controlled Discovery Hybrid Rheometer (DHR-3) from TA Instruments (USA) (see Fig 3.4 [a]) coupled with a double wall-ring (DWR) and a custom-made steel cup to hold the water and oil subphases (see Fig 3.4 [b]). The physical dimensions of the DWR geometry are described in the TA instruments report APN031 and also by Lin et al. [39] (inner radii are 31 mm for the subphase and 30 mm for the upper phase, and outer radii are 39.5mm for the subphase and 40.5 mm for the upper phase).

Cleaning and sample preparation were similar to the Langmuir trough procedure. Firstly, the DWR was carefully washed at least three times with toluene, ethanol, deionized water and finally rinsed with acetone. The steel cup was also washed with some drops of detergent and water, and then rinsed with ethanol, DW and acetone to eliminate all impurities. After placing the ring and the cup base in the rheometer (see Fig 3.4 [a]), we started the calibration of the geometry before the beginning of the experiments.

Measurements of both viscosity and complex viscoelastic moduli of air-water and oil-water interfaces were acquired via steady-state and low amplitude oscillatory experiments respectively. Rotational and oscillatory mappings at specific amplitudes and frequencies values were carried out before the beginning of the tests. The rheometer transducer mode was set to "soft"

to guarantee better device control for sensitive interfaces. Previous amplitude and frequency sweeps were carried out to establish the rheological parameters (strain and frequency). A frequency value of 1Hz and a strain range of 10^{-4} to 0.1 % were selected for the strain tests, whereas a deformation of 0.1 % and a frequency range between 0.1 and 10 Hz were established for the frequency sweeps. Strain and frequency values were defined within the linear viscoelastic regime as input values to the next rheological experiments. All tests were performed at room temperature ($\approx 25°$C).
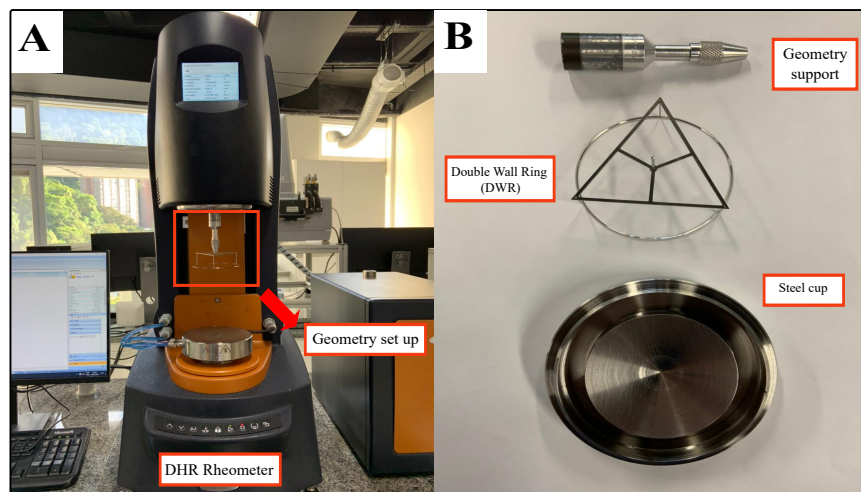
Figure 3.4: Overview of the DHR Rheometer. A. Total view of the rheometer with the geometry setup attached to the instrument head. B. Details of the accessories used in the rheological tests.

3.9.1 Protocols

Interfacial layers were formed in a set of novel protocols named from [A] to [F]. In general terms, the protocols investigated the rheological outcome of adsorbed asphaltene layers upon the addition of distinct top phases, that can either induce or hinder microstructure buildup. However, each protocol aimed at certain features of the adsorbed layers. To do so, we used the *asphaltene solution* with 7 mg of asphaltenes dissolved in 3 ml of toluene and the *hextol solution* with a concentration of 1 mg/ml. Our greatest concern was to maintain initially the same amount of asphaltenes poured onto the interface for all six protocols. Before setting the target concentration, we acquired data with *asphaltene solution* and the *hextol solution* with concentrations below 1 mg/ml; however, we did not observe significant changes in the interfacial rheological tests. On the other hand, for concentrations greater than one, we noted asphaltene deposition close to the walls. Therefore, we elected the
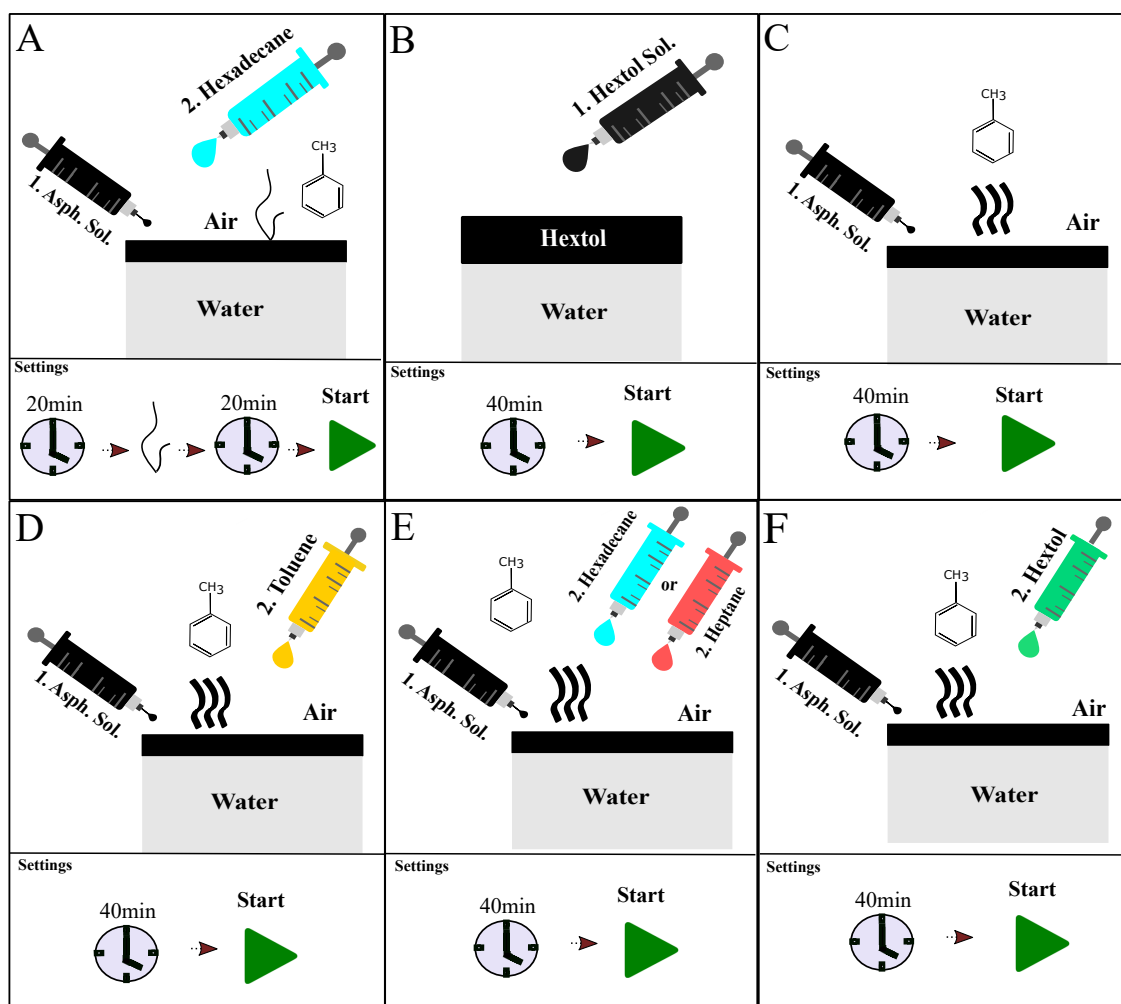
Figure 3.5: Schematic drawing for experimental procedures of Protocols [A] to [F]. Aging time settings are also summarized with the aid of the bottom cartoon depicted for each protocol. Partial and total evaporation of the toluene fraction are represented by the symbols (〜) and (〰).

concentration of 1 mg/ml as ideal for the experimental procedure. As for the *diluted asphaltene-stearic acid solution*, we prepared the *main solution*, prior to dilution, at the same concentration of 1 mg/ml.

As our experiments required detailed ways of forming and measuring the adsorbed interfacial films, we scrutinized the steps for each protocol [Fig 3.5(a) to Fig 3.5(f)], presented in the following items.

- Protocol [A]: we solubilized the asphaltenes in 3 ml of pure toluene and gently added the *asphaltene solution* with the aid of an Arti Glass syringe onto the water subphase. We waited 20 min for a partial evaporation (〜) of the toluene phase, and then inserted 4 ml of hexadecane on top of the remaining asphaltene solution (we estimated that a little over 50% of the *toluene solvent* evaporates). Evaporation occurred by not capping the geometry-cup set with the acrylic covers. We

tried to maintain the volume ratio of hexadecane-toluene (80/20), and especially, the same mass of asphaltenes in solution. After we had waited for more than 20 min, we started measuring (a total aging time of 40 min). In this first protocol, a hextol-water interface (Htol/W interface - A) was formed since part of toluene remained as the oil phase, and ultimately mixed with the top phase (hexadecane). So, we basically aimed to assess the interfacial rheology of an oil-water interface, in which the oil phase was composed of two different solvents.

○ Protocol [B]: the hextol-water interface (Htol/W interface - B) was formed by pouring 7ml of the *hextol solution* on top of the water subphase. We kept the same quantity of 7 mg by preparing 1 mg/ml of the *hextol solution* and adding 7 ml of this solution onto the aqueous phase. After setting an aging time of 40 min, we start to measure and cap the geometry-cup set with the acrylic covers to prevent evaporation. Similar to protocol [A], in protocol [B] we interrogate the effect of the oil-water interface, however with a pre-mixed solution of asphaltenes in hexadecane and toluene.

○ Protocol [C]: we simply added the *asphaltene solution* at the aqueous subphase, and by not covering the geometry-cup set, we induced a total evaporation of toluene (〰). We applied 40 min of interfacial aging before measuring (the sample was kept on hold, that is, no deformation was applied). The rheological response of the toluene-water interface (T/W interface) was measured, followed by the air-water interface (A/W interface) when all toluene fraction was gone.

○ Protocol [D]: in this protocol we obtained the same interfaces of Protocol [C] (T/W and A/W) in order to assess the asphaltene film reversibility. To this end, we quantified twice the interfacial moduli of T/W and A/W interfaces. This double measure was referred as "first cycle" and "second cycle". In the first cycle, we added 3ml of the *asphaltene solution* on the aqueous bulk phase and, after 40 min of aging, the rheometer acquired the stress-strain response of the T/W interface. When the toluene fraction was gone (acrylic covers were removed from the top of geometry-cup set to help the evaporation process), the rheometer started measuring the complex moduli of the A/W interface (similarly to Protocol C). We re-injected fresh pure toluene onto the asphaltene layer formed at the A/W interface, which marks the onset of the second cycle. The rheometer measures again the film at the T/W interface, and after the second evaporation of toluene, the interfacial layer at the A/W interface. This is an *in situ* process where reversibility can be assessed.

○ Protocol [E]: similarly to Protocol [D], in Protocol [E] we explored the reversibility of asphaltenes films, however re-injecting 7ml of pure heptane or hexadecane on top of the previously formed asphaltene layer, as dictated by Protocol [C] (T/W followed by A/W interface after total evaporation of toluene). Nonetheless, we placed the geometry-cap set to avoid evaporation, since we aimed to evaluate the effect of these solvents as an oil-water interface.

○ Protocol [F]: this was the third and last protocol where Protocol [C] was employed as the initial step (T/W and A/W interfaces were created) followed by the methodology presented in Protocol [E] (non-polar solvent addition). We poured 7ml of the *hextol solvent* (asphaltene-free mixture of hexadecane and toluene) on the A/W interface laden with asphaltenes. Here, we focus on understanding the influence of this mixture on film reversibility, just as explored in Protocols [D] and [E].

4
Results and discussion: single asphaltenes at the air-water and oil-water interface

In this section, the interfacial properties of the BR asphaltenes are measured. We begin this chapter with the novel results of asphaltene stress-strain response using shear rheology and the layer compression by employing the Langmuir trough technique. We investigate the aggregation dynamics by assessing the morphology of asphaltenes with the aid of the SEM technique. At the end of the chapter, we show the results of spontaneous emulsification (SE) of BR asphaltenes, and we link it with their viscoelasticity. Moreover, we compare the differences in droplet formation and rheological properties of our samples with two distinguished asphaltenes.

4.1
^{1}H and ^{13}C nuclear magnetic resonance results: effect of asphaltene molecular type

In order to obtain more information concerning how the carbons and hydrogens are arranged in the asphaltene structure, ^{1}H NMR and ^{13}C NMR experiments are performed in deuterated chloroform solutions. The results are summarized in Table A.1 (Appendix). The chemical shift used for assignment is based on literature [93]. The asphaltene molecule displays 92 % of aliphatic hydrogens and only 8.0 % of aromatic hydrogens. This result suggests either a highly polycondensed aromatic structure or a predominance of aliphatic chains and rings on the asphaltene main core. The ^{13}C NMR data excludes the latter, since 60.8% of aromatic carbons are detected along with 39.2% of aliphatic ones. In this way, the lower percentage of aromatic hydrogen in conjunction with the highly aromatic carbon content indicates the prevalence of an island-type asphaltene structure [94]. A closer inspection in the aliphatic hydrogen region also implies a low prevalence of methyl-substituted aromatics, since 17.2 % of α aromatic hydrogen is detected in comparison with 74.8 % of β, γ or terminal hydrogens. Moreover, 8.2 % of aromatic carbons bonded to alkyl chains are identified. These findings indicate that BR asphaltenes may be pictured as a highly polycondensed aromatic island-type structure substituted with small paraffinic and naphthenic units.

4.2
Interfacial rheology of BR asphaltenes: effect of solvent addition

4.2.1
Protocols [C] and [E]: Preliminary strain and frequency sweeps

Strain and frequency sweeps are initially conducted to establish input rheological parameters required for the time sweep tests. The asphaltene content at the interface was set at 7 mg, as already shown in the experimental section, and the protocols chosen were [C] and [E]. They were selected due to their simpler procedure, and also because we could perform the oscillatory measurements at both air-water and oil-water interface configurations. We report considerable repeatability between the trials, and all moduli are independent of strain with a solid-like feature (as shown in Fig. 4.1). Additionally, for the frequency sweep tests, we also observe a non-dependent relation between the viscoelastic modulus and the selected frequency range (see Fig. 4.2). Based on these results, the strain value chosen within the viscoelastic regime was 0.1 %, and the frequency value was 0.5 Hz.
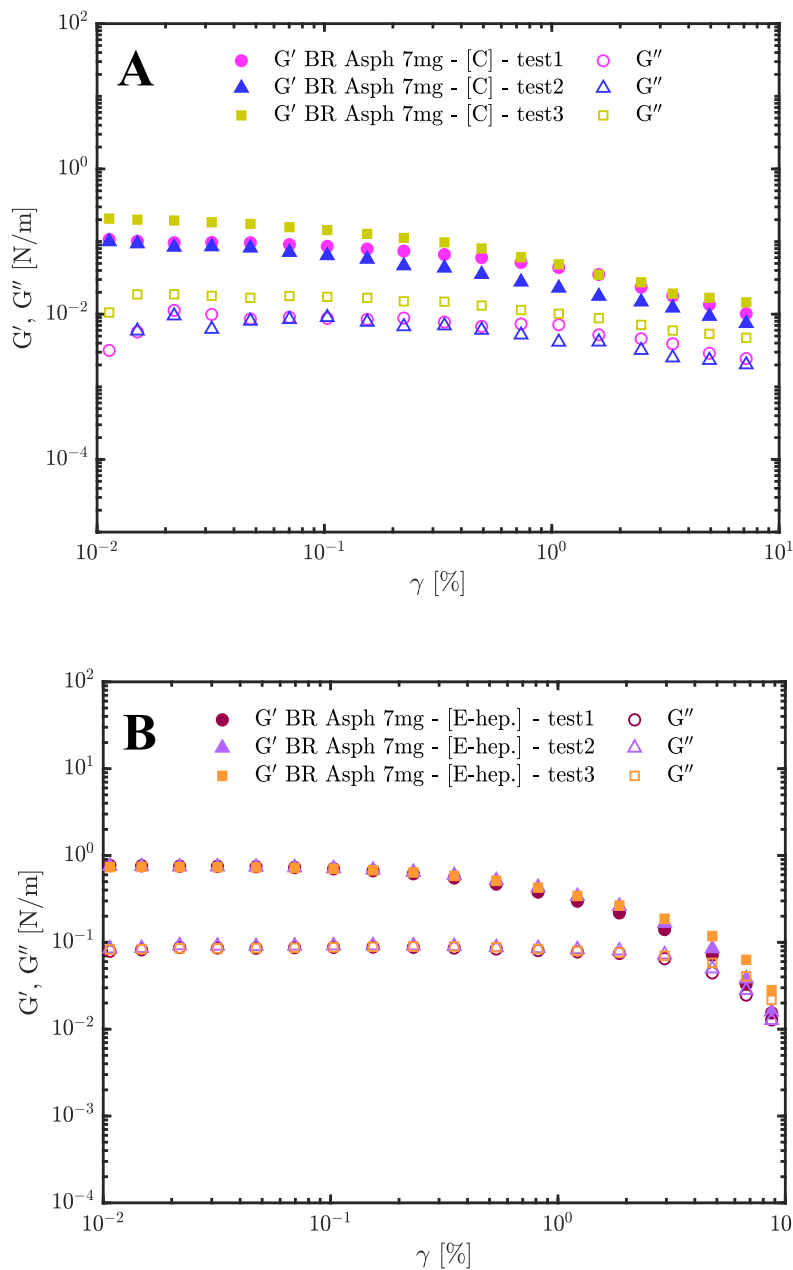
Figure 4.1: Strain sweep results of BR asphaltenes in Protocols [C] and [E]. The solvent selected as the oil top phase for Protocol [E] is heptane. The experiment was performed in triplicates.
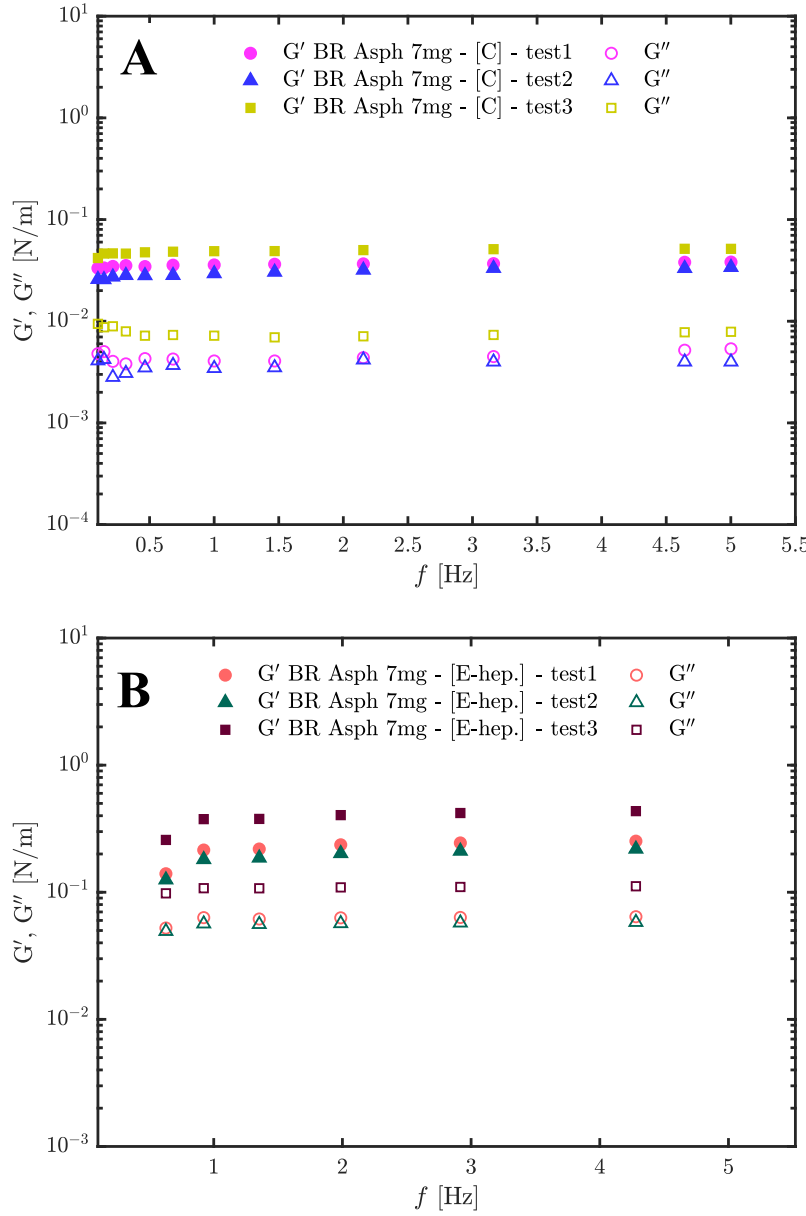
Figure 4.2: Frequency sweep results of BR asphaltenes in Protocols [C] and [E]. The solvent selected as the oil top phase for Protocol [E] is heptane. The experiment was also performed in triplicates.

4.2.2
Protocols [A] and [B]

Rheological properties of BR asphaltenes are examined by small-amplitude-oscillatory-shear (SAOS) experiments within the linear viscoelastic regime. Figure 4.3 plots the results of time sweep experiments of Htol/water interfaces formed in Protocols [A] and [B] with 7 mg of asphaltenes added to the interface within an experimental time of 5h. The time t=0 marks the beginning of the experiment after the aging time, as explained in the

experimental section (this is established for all time sweep graphs).
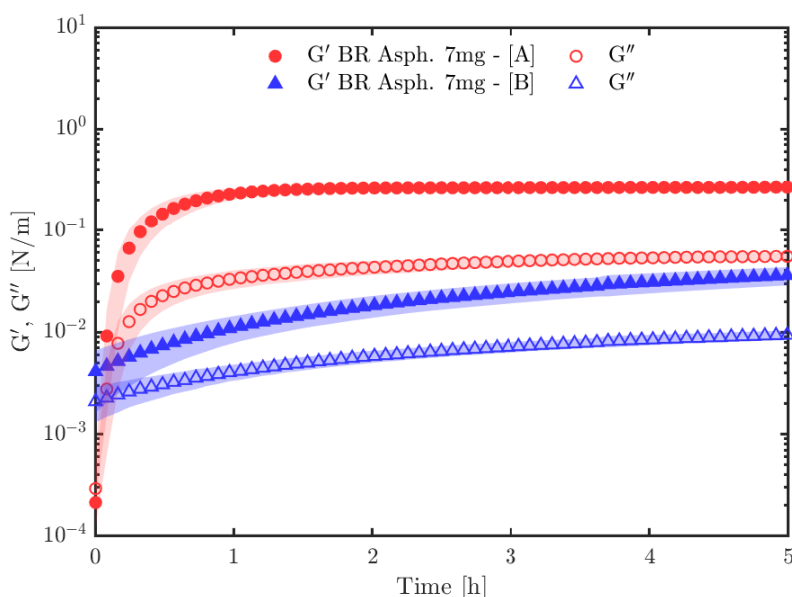
Figure 4.3: Time sweep results of BR asphaltenes at the Htol/water interfaces formed in Protocols [A] and [B]. The filled symbols represent the elastic modulus, and the open symbols represent the viscous modulus. Shaded error bar indicates the repeatability of the experiments.

From an overall perspective, the asphaltene layer in both protocols reveals viscoelastic features, which characterize it as a solid interface (G' is greater than G'' for the total duration of the experiment). However, in Protocol [A], where toluene evaporates partially, and pure hexadecane is poured on the interface, asphaltene film yields a higher elastic moduli (G'), whereas in Protocol [B], G' reaches lower values.

In Protocol [A], there is a gradual buildup of storage and loss moduli as the asphaltene network develops, which we believe is due to higher surface coverage at the air-water interface. This can be better discussed with the aid of the cartoon of Fig 4.4 (a), which illustrates a greater number of nanoaggregates populating the Htol/water interface. Asphaltenes follow a hierarchic molecular configuration that has been well-described by the Yen-Mullis model [21], in which molecules assemble firstly as nanoaggregates, and finally, as clusters. Figure 4.4 (c) displays the possible asphaltene configuration that occurs in the *hextol solution* described by the Yen-Mullis model. This assembly can be affected by the solvent composition, temperature, concentration, molecular architecture and energy binding [6, 9, 39, 47]. Lanvegin *et al.* [5] show that nanoaggregates can be formed due to the attractive interactions between the π electrons of the rings (π-π *stacking*), which ultimately affect their colloidal behavior in solution. At a higher concentration of asphaltenes, larger aggregates start forming, that is, they form clusters, which contain about 20
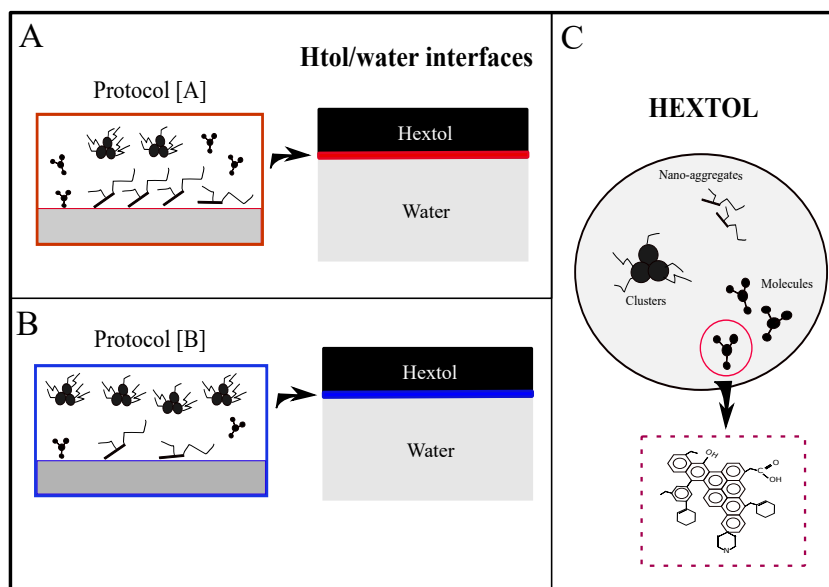
Figure 4.4: A. Asphaltenes molecular arrangement at Htol/W interfaces in Protocols [A] B. Asphaltenes molecular arrangement at Htol/W interfaces in Protocols [B]. C. Possible hierarchic molecular configuration in the *hextol* solution.

solvated nanoaggregates [5]. Regarding the interfacial activity, most studies propose that the asphaltenes adsorb at the interface as nanoaggregates and clusters rather than single molecules [20, 81].

In contrast, Protocol [B] reveals a different trend: elastic moduli values are significantly lower than the ones obtained in Protocol [A] and the interfacial microstructure develops much slower. This is in line with previous studies that claim that aggregation kinetics is much slower in oil-water interfaces [20, 95]. The rigidity of the asphaltene film is reduced when a limited number of nanoaggregates and molecules populate the interface, which can be justified by the viscoelastic moduli observed in Fig. 4.3, and by the schematic drawing of Fig 4.4 (b) (it illustrates the Htol/w interface formed in Protocol [B]). Hexadecane in the *asphaltene solution* may cause the formation of stronger aggregate units in which remaining asphaltene molecules are unable to penetrate [6,9]. Thereby, they end up diffusing to the interface in a slower pace, but maybe as single molecules, and not as nanoaggregates, which suggests the formation of a weaker film at the Htol/W interface.

As shown in the protocols explanation section, the *asphaltene solution* in Protocol [A] is placed on the water subphase and only part of toluene evaporates. Differently from Protocol [B], in Protocol [A] pure hexadecane is poured at the asphaltene/toluene-water interface, and, for this reason, we guess the hexadecane works as a barrier from where asphaltene nanoaggregates/clusters do not solubilize. Due to the fact that these structures

cannot migrate to the upper phase, they promptly bond with each other and rapidly build a strong interfacial network that is revealed by rheological data. Although we state that the faster buildup of a network is due to more or less interfacial coverage, it is also valid to underscore the asphaltene-asphaltene interaction that can be altered when the hexadecane is poured onto the interfacial film. Disturbance of the π-π interactions may alter the stacking distance and the corresponding binding energy in the π system, which ultimately affects the extent of clustering [98, 99]. The work of Kuznicki *et al.* [10] shows that the stacking behaviour of polyaromatic rings is more pronounced in non-polar than in polar solvents. Furthermore, Mousavi *et al.* [98] investigates how interactions of amide-type bio binder with asphaltenes disturbs the uniformity of π density in stacks. MD simulations and high-resolution transmission electron microscopy (HRTEM) are some of the techniques employed to support the charge polarization in the aromatic core.

The results of Protocols [A] and [B] also support our theory that the inclusion of a non-polar solvent to the *hextol solution* may lock up nanoaggregates inside the *hextol mixture* and, therefore, impair their interfacial activity. Previous authors as Gawrys *et al.* [87] and Lin *et al.* [39] also explain that swollen asphaltenes entrained with solvents are unable to form well-organized and packed interfacial layers. In the end, eventual nanoaggregates and clusters may finally adsorb at the Htol/W interface and induce mechanical changes.

4.2.3
Protocol [C]

A five-hour time sweep experiment is conducted in Protocol [C] where toluene-water (T/W) and air-water (A/W) interfaces are formed. Interfacial films exhibit different moduli magnitudes when the interface shifts from T/W to A/W as shown in Fig 4.5. In the T/W zone - 0h to 1.5h - torques are below the equipament limit (minimum torque of 0.5 µN.m^{-1} for the DHR-3 series), thereby no reliable data can be acquired.

The rise of mechanical strength matches the jump of torque (as shown in the upper graph of Fig 4.5) at the point where we observe the onset of the microstructure buildup, which is revealed when all the toluene fraction evaporates. Then, the rheometer begins to measure the stress-strain response of the A/W interface, and the plateau value of G' is reached immediately for all tests. A steep increase of G' is observed for all tests, however we report a lack of repeatability, sustained by the difficulty in controlling asphaltene

aggregation at the A/W interface. This can be supported with the aid of Fig 4.6, in which one can note non-homogeneous interfacial skins in different spots of the double-wall setup [Fig 4.6 (a), (b) and (c) corresponds to tests 1, 2 and 3 respectively]. Yet, the same tendency is noted for all trials.
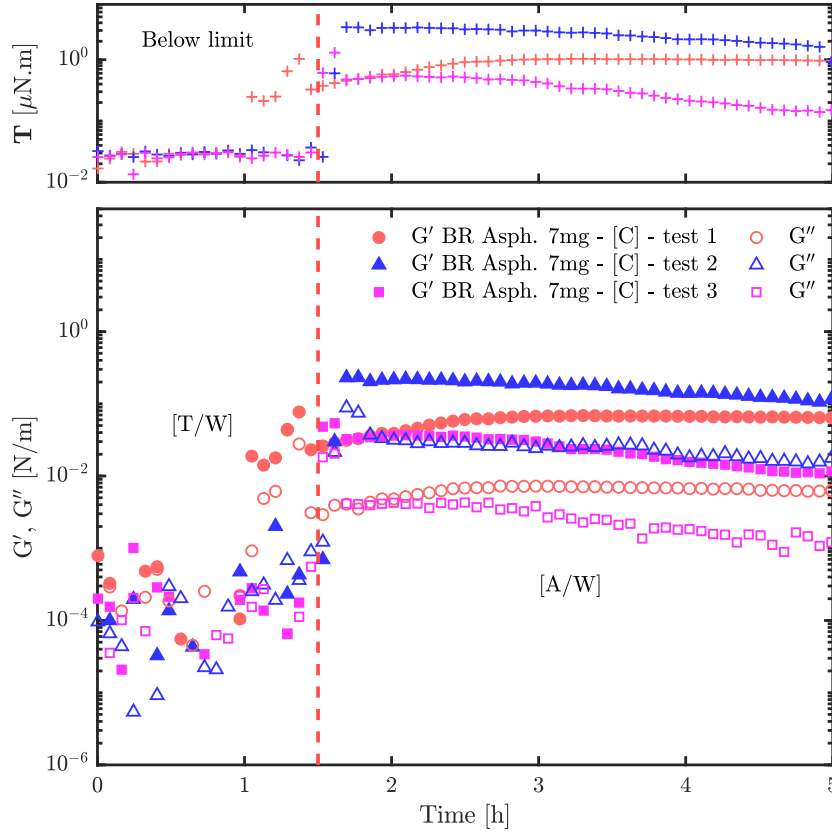
Figure 4.5: Effect of toluene evaporation in the time sweep results of Protocol [C]. The peak of viscous and elastic moduli is noted 1.5h after the beginning of the experiment followed by the increase of torque values.

The discrepancy in the rheological measures of T/W and A/W interfaces are mainly due to the lack of adsorbed asphaltene nanoaggregates at the former, since they prefer to stay in the toluene phase rather than migrate to the interface. Nonetheless, once the toluene is gone, a reconfiguration of the interface takes place, which is accompanied by the formation of a dense and solid network capable of responding to imposed strain.

Rheologically complex interfaces hold significant microstructure that is mainly formed because of high surface coverage and lateral interactions between the surface activity moieties [37, 49]. Therefore, interfacial viscoelasticity is measured when these moieties populate the interface. Differently from what we report, previous authors as Fan *et al.*, Rodríguez-Hakim *et al.* and Araujo *et al.* succeeded at measuring complex moduli of asphaltene laden toluene-water interfaces, where they observe the effect of film buildup also from time sweep experiments [47, 51, 77].
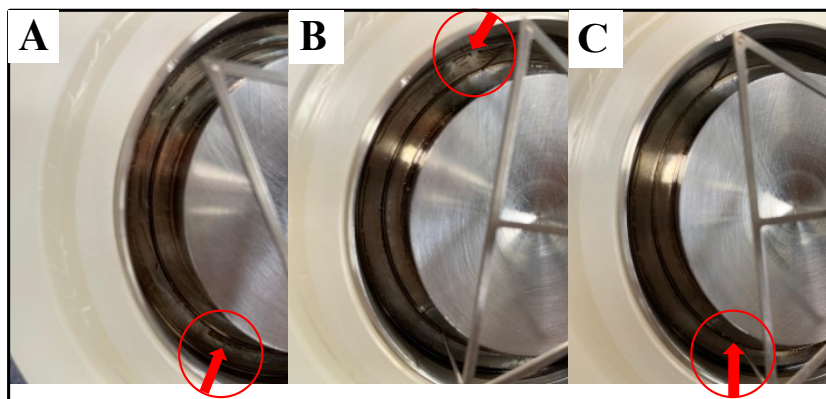
Figure 4.6: Interfacial skins of asphaltenes located in different spots of the DWR setup. Figures (a), (b), and (c) corresponds to tests 1, 2 and 3 respectively.

.

The inability to form rigid films at T/W interface may be related to the presence of uncharged three-dimensional structures and the fewer presence of polar entities that are known to induce greater interfacial activity. Consequently, the asphaltene nanoaggregate remains in the bulk phase. This pattern is well reported by the work of Kuznicki and co-authors [10] that explores MD simulations to show that uncharged asphaltene molecules do not adsorb at toluene-water interface, whereas molecules with charged terminal groups congregate at the interface. Furthermore, they observe that the continental type (or island type) asphaltene molecules have lower tendency towards stacking if compared to the archipelago type, which might be attributed to the steric interference of the aliphatic side chains. The stacking process of polyaromatic units is of great importance to the formation of 3D aggregate architectures, which render considerable rigidity to the oil-water interface. Therefore, their results support our rheological findings, in which we show that BR asphaltenes have no affinity towards the T/W interface, possibly due to the presumed absence of charged portions. Moreover, our asphaltene polycondensate island-type, revealed by the NMR experiments, appears to obtain a less stacking behaviour compared to other asphaltene configurations, yet sufficient to impart viscoelasticity to the A/W interface.

4.2.4
Protocols [D] to [F]: film reversibility

As previously mentioned, Protocols [D] to [F] comprise the investigation of asphaltene film reversibility when solvents with distinct aromaticities are added onto the A/W interface, earlier formed as described in Protocol [C] (the

A/W interface is formed when all the toluene fraction is gone). Fig 4.7 exhibits the results of eight-hour time sweep tests of Protocol [D], where toluene is re-injected after the measured strain-stress response of the asphaltene laden A/W interface.
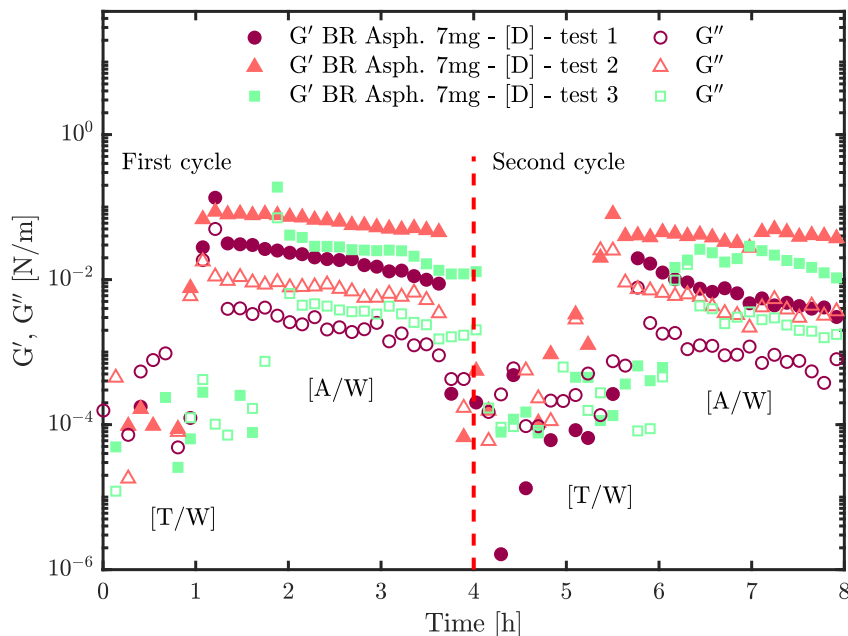
Figure 4.7: Effect of toluene on asphaltene film reversibility. First cycle comprises the T/W and A/W interfaces followed by the second cycle, in which the toluene is re-injected onto the asphaltene network formed in air.

Similarly to what is discussed in subsection 4.2.3, an increase in viscoelastic modululi is detected after toluene evaporates (roughly 1.5h after the beginning of the experiment) and an instantaneous buildup of the interfacial network occurs ("First cycle"). However, when we place toluene back onto the asphaltene layer, a remarkable and sudden decay of G' and G'' values is noted, which may indicate the desorption of the asphaltene molecules back to the toluene top phase. After the second evaporation of toluene ("Second cycle"), we observe an almost perfect re-adsorption, as presented in the second cycle measures of G' and G'' depicted in Fig 4.7.

To the best of our knowledge, the reversibility of asphaltene films has not been shown by means of interfacial rheology experiments. Most authors report that asphaltenes do not migrate from the toluene-water interface to the water subphase or to the toluene top phase, instead, they will rather stay as a unit, suggesting irreversible adsorption [51, 63, 86, 100]. Zhang *et al.* demonstrate through Langmuir trough experiments, UV spectroscopic measurements, and atomic force microscopy (AFM), the formation of an asphaltene monolayer at the toluene-water interface when fresh toluene is placed on top of a previously formed multilayer [86]. In our case, not even the monolayer remains at the

oil-water interface after the re-injection of the toluene, which explains the drastic drop in viscoelasticity [Figs 4.5 and 4.7]. This outcome confirms the trend observed in Protocol [C]: the lack of asphaltene molecules at the T/W interface is justified when fresh toluene is re-used as top phase solvent of the *in situ* addition. On the other hand, the peak in the viscoelasticity is possibly associated to the 3D stacking of polyaromatic rings at the A/W interface, as mentioned by Kuznicki *et al.* [10]. The stacking behaviour is a relevant structural feature that, although its predominance is in favor of archipelago-type molecules, renders considerable stiffness to the interface [9, 10].

Figure 4.8 exhibits asphaltene reversibility considering the addition of heptane, hexadecane, and the *hextol mixture* onto the asphaltene layer formed at the A/W interface. Time sweeps are also carried out within an eight-hour measuring time of the interfacial network. Unlike the trend noticed in Fig 4.7, one can perceive a subtle increase on viscoelastic moduli when apolar solvents are directly poured at the interface, which suggests greater mechanical strength. However, differently from what we expected, the stress-strain response contemplating non-polar solvents with distinct chain lengths (C_7 and C_{16}) or the mixing of polar and non-polar diluents (*hextol solvent*), does not vary meaningfully. Instead, we can state that, from a rheological perspective, the viscoelastic moduli values are practically the same regardless of the hydrocarbon type (we can notice only a slight increase on G' values with hexadecane as the top phase).

This behavior implies that the effect of the aliphatic tail length of non-polar solvents has little impact on the mechanical properties of our asphaltene film, suggesting that the response to imposed strain on the film within an oscillatory test may be essentially dependent on chemical structure rather than solvent quality. Silva *et al.* [9] present an extensive and meticulous work on how asphaltenes self-assembly and interact with water, heptane and toluene. Using molecular dynamics (MD) simulations, they highlight the relevance of asphaltene-solvent interactions based on a function of lateral chain lengths that can either promote or hamper the interplay between aggregates. Heptane interacts selectively with the asphaltene molecules depending on their molecular architecture: longer lateral chains interact more with n-heptane molecules and may form less packed clusters compared with shorter chains. Moreover, the authors summarize that the side of the conjugated core may impact the self-assembly of asphaltenes as well as the eventual presence of polar groups capable of forming H-bonds. Possibly, BR asphaltenes interact with non-polar solvents at the same rheological level regardless their chain

size, and their interfacial viscoelasticity is mainly governed by the stacking of the island-type molecules.
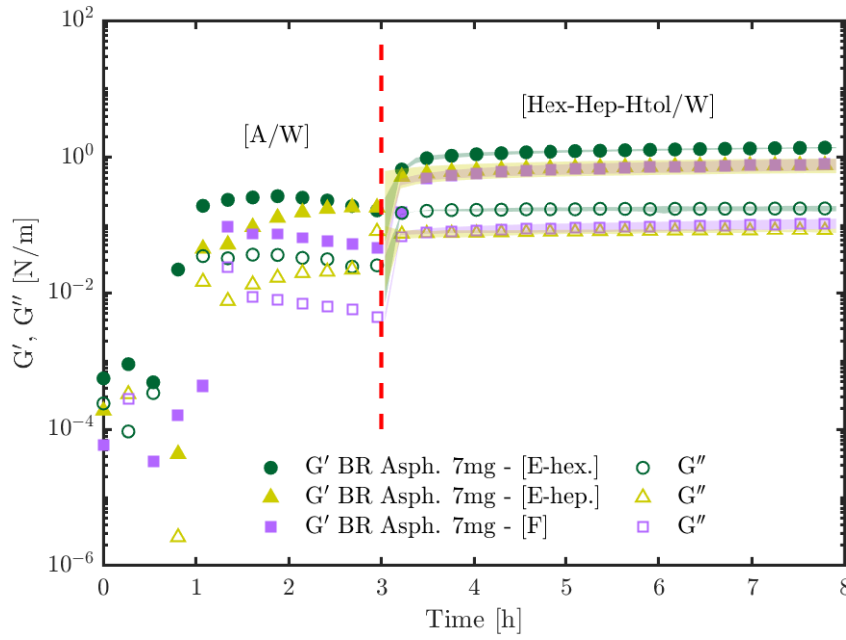
Figure 4.8: Effect of non-polar solvents in the asphaltene film reversibility. Dashed line marks the increase of interfacial viscoelastic moduli under the addition of heptane, hexadecane and the *hextol* mixture.

4.2.5
Protocols [A], [B], [E-hep.] and [E-hex.]: steady state experiments

We chose Protocols [A], [B], [E-hep.] and [E-hex.] to interrogate the non-linear behaviour of loaded asphaltene interfaces. They were formed similar to the steps exposed in the experimental section for the protocols employed. We fit the shear viscosity to the power-law model, as follows:

$$\eta(\dot{\gamma}) = K\dot{\gamma}^{(n-1)} \tag{4-1}$$

where η, $\dot{\gamma}$, K and n are surface viscosity, shear rate, consistency index and flow behaviour index, respectively. When n<1, the interface, similarly to the bulk environment, presents a shear-thinning behavior, typically for pseudoplastic fluids, where the viscosity decreases with increasing shear rate.

Shear data fit is depicted in Fig 4.9, in which the solid lines represent the fitting results along with the shaded error bars that indicate the experimental uncertainties. Table 4.1 also shows the fitting results of the constancy index k, the power-law index n, and the coefficient of determination (R^2) of the three protocols studied. Based on R^2 values, we conclude that the power-law is a good fit for the acquired data (Protocol [E-hep.] presented the lowest value of R^2; however the power-law fitting is satisfactory). The value of the

exponent n in Protocol [A] is lower (0.1407) compared to the values acquired in [B] and [E-hex.] (0.5248 and 0.3470 respectively), which indicates a more shear-thinning interface. Samaniuk *et al.* [101] also report non-linear viscosity of asphaltenes at water-hexadecane interface with similar power-law index.

The onset of the non-linear response is marked throughout the entire flow curve experiment and the viscosity progressively decay until its end. We report higher interfacial viscosity for Protocols [A] and [E-hex.], which is in good agreement with the time sweep results of the same scenarios: in the former, the greater number of asphaltene nanoaggregates at the interface results in higher interfacial viscoelasticity and hinders asphaltenes disassociation, whereas in the latter, asphaltene film promptly gains mechanical resistance upon the *in situ* addition of the poor solvent hexadecane. On the other hand, the steady-state result for Protocol [B] exhibit greater index value (n=0.5248) and lower interfacial viscosity, which upholds the idea of interfaces loaded to a lesser extent when asphaltenes are solubilized in the *hextol* mixture.

Differently from what we note in the oscillatory measurements, the interfaces formed in Protocols [E-hex] and [E-hep] demonstrates distinct responses with the increase of shear rate. For the time-dependent data, the interfacial films render significant mechanical rigidity when heptane and hexadecane are poured, and the viscoelastic moduli do not vary considerably between them. In contrast, in the flow sweep tests, although the slope of the power-law fit reaches similar values (0.3270 for the [E-hep] and 0.3470 for the [E-hex]) the interfacial viscosity changes considerably. Heptane addition is known to accelerate the asphaltene flocculation process, changing their colloidal state [102]. Consequently, the interface formed in Protocol [E-hep] may be more brittle and susceptible to disrupt under stress. We suppose that steady-shear viscosity is directly correlated to the adsorption of the aggregates/clusters and unravels the pseudoplastic behaviour of asphaltene films. In addition, the steady-shear outcome also highlights the distinguished results obtained for *in situ* inclusions of non-polar solvents.

	k	n	R^2
Protocol [A]	0.0005	0.1407	0.9917
Protocol [B]	0.0001	0.5248	0.9912
Protocol [E-hep.]	0.0001	0.3270	0.9489
Protocol [E-hex.]	0.0004	0.3470	0.9963

Table 4.1: Power law parameters obtained by curve fitting of experimental curves from Protocols [A], [B], [E-hep.] and [E-hex.].
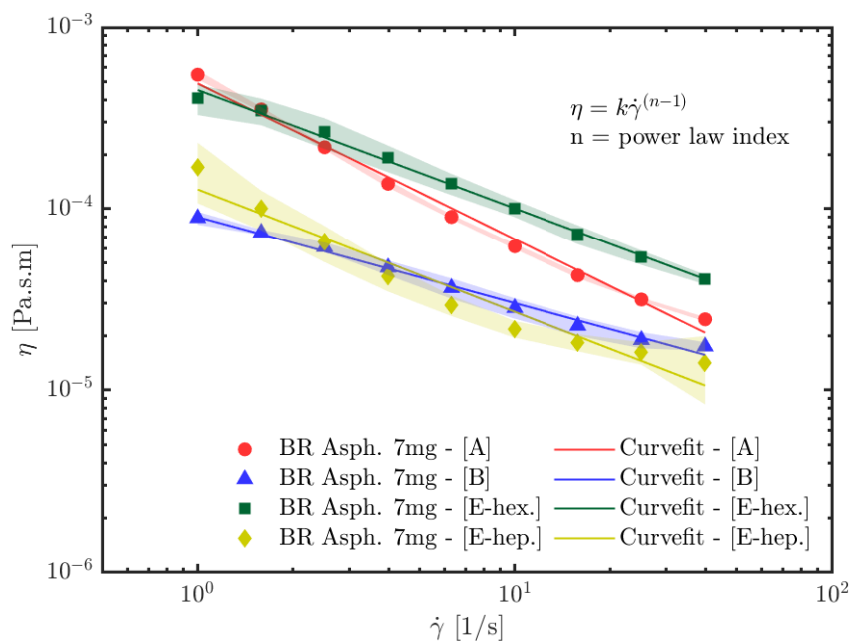
Figure 4.9: Steady-shear results of asphaltene films formed in Protocols [A], [B], [E-hep.] and [E-hex.].

4.2.6
Compression curves of asphaltenes of air-water and solvent-water interfaces

Fig 4.10 shows the pressure isotherms (Π - A) of asphaltenes at air-water and solvent-water interfaces. We reproduce part of the interfaces formed in Protocols [A] to [E]: air-water (A/W), toluene-water (Tol/water), heptane-water (Hep/W) and hexadecane-water (Hex/W) with the exception of the hextol-water interface (Htol/W). All experiments are repeated three times and shaded error bars are plotted. For all trials, we initially spread 25 μl of the asphaltene solution (1mg/ml) and wait three hours to consolidate the air-aggregation. Compression begins just after the aging time expires (A/W measurement) or after the addition of the solvents (Tol/water, Hep/W andHex/W measurements). The A/W isotherm exhibit the rise of pressure at a trough area of roughly 150 cm^2. As compression develops, increasing surface pressure is noticed and a significant pressure value of 58 mN.m^{-1} is obtained, before reaching the limit of the trough compression. We do not observe a clear phase transition in the π - A results, instead, a steep rise is noticed, which may be caused by a jamming of asphaltenes at the A/W interface. This behaviour, detected in our A/W isotherms, is consistent with the study of Lin *et al* [39]. They monitor asphaltene microstructure by using a Langmuir trough combined with a Brewster angle microscopy (BAM) and show that further compression resulted in a 2D "skin" of asphaltenes that leads to instabilities such as surface

wrinkling and multilayer aggregates [39]. A max surface pressure of 48 mN m^{-1} is reported before reaching the limit of the trough.

Regarding the oil-water interfaces, we observe differences in the final pressure if compared to the aggregation in air. Firstly, the almost zero pressure for the T/W interface can validate its rheological outcome: not even a monolayer of asphaltenes remains when fresh toluene is poured over the interface. Instead, the toluene injection suppresses their interfacial activity, thereby confirming the reversibility observed in the time sweep experiments. Secondly, lower values of surface pressure at Hep/W and Hex/W interfaces suggests an interaction of asphaltene nanoaggregates with the upper phase rather than lateral interactions between them. We note a slight difference in the area per molecule of heptane and hexadecane compared to air. The values are 98.39 and 91.57 nm^2/molecule for the Hep/W and Hex/W versus 77.75 for the A/W interface, which means that, although the same amount of asphaltenes is spread at the interface, they associate differently.

One possible explanation is that the aliphatic tails of asphaltenes interact better with hexadecane and heptane rather than with the air phase as also pointed out by Alicke *et al.* [11]. In their recent work, the authors claim the differences in molecular packing of indigenous asphaltene nanoaggregates at air-water versus hexadecane-water interfaces that may occur due to the interactions with the aqueous subphase and top phase. At the air-water interface, the carboxylic groups that comprise the asphaltene molecule have affinity towards water, whereas the alkyl chains do not interact with air. Instead, these chains interact better with hexadecane, therefore, leading to weaker lateral interactions between asphaltene nanoaggregates. It is also worth mentioning that, in our work, small differences are observed among hexadecane and heptane pressure results, however, mildly higher values are obtained for the Hex/W interface (≈ 28 mN m^{-1} versus 20 mN m^{-1}), indicating a well-favorable interaction with heptane.

The compression isotherms obtained for the distinct interfacial films are an extra attempt to better elucidate the molecular packing and re-arrangement of the asphaltene nanoaggregates/clusters under the addition of distinct aromatic solvents. Nonetheless, most importantly, we demonstrate that the BR asphaltenes desorption can occur with toluene as oil top phase, as initially shown in the rheological studied conducted in Protocols [C] and [D]. The absence of a monolayer of asphaltenes justifies our inability to measure the mechanical response of interfacial films at the toluene-water interface.
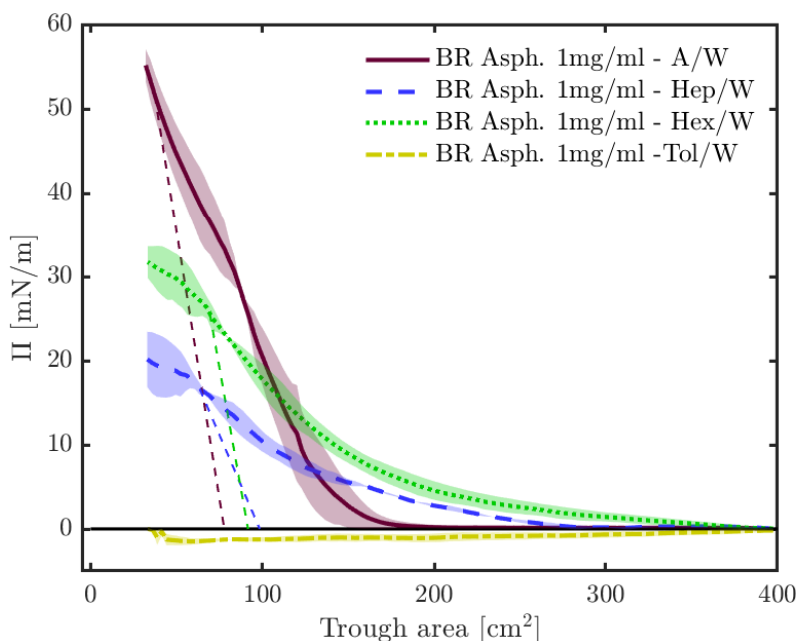
Figure 4.10: Compression isotherms of A/W, Hep/, Hex/W and Tol/W interfaces. Dashed lines crossing the abscissa axis indicate the area/per molecule for each interface.

4.2.7
Scanning electron images of asphaltenes

BR asphaltenes dissolved in toluene and in the *hextol solution* are studied by using the confocal microscopy and SEM analysis. Figure 4.11 shows the confocal micrograph of asphaltenes precipitated from the *hextol solution*. Precipitation in pure toluene is not observed, even with the magnification of 63x, which is why we limit this first microscope analysis to the *hextol solution*. Similar images proving asphaltene precipitation by confocal microscopy are found in the literature with non-aromatic solvents as heptane or heptol mixtures [103, 104]. For the *hextol solution*, it appears that the asphaltene precipitates are akin to the ones noted in heptane systems, suggesting that the solvent quality has a significant effect on clusters formation. Roux *et al*. [105] and Fenistein *et al*. [106] also reports the effect of temperature and solvent quality on the mean radius of asphaltene clusters, pointing to an increase of 50 % in radius considering a solution of 45% heptane in toluene.

The morphology of asphaltene fragments prior to solubilization is studied by using the SEM microscope magnified 178 times. An uneven surface can be observed in Fig 4.12 (a) with distinguishing irregularities. Fig 4.12(b) explores a region of this surface more deeply where one can note what seems to be very small fragments. Figs 4.13 (a) and (b) exhibit the SEM results of asphaltenes after evaporation of the toluene solution whereas Figs 4.13 (c) and (d) show

the micrographs after the evaporation of the *hextol solution*. We applied magnification of 50,0000 times [Figs 4.13 (a) and (c)] and 10,0000 times [Figs 4.13 (b) and (d)]. Broadly speaking, we observe a remarkable change in the asphaltene morphology when they are solubilized in solvents. After evaporation of toluene and the *hextol mixture*, asphaltenes congregate in a globular shape which we define as *agglomerate particles*. Nonetheless, differences in the size of the spheres are attributed to the type of solvent: we believe that the addition of hexadecane to a previous-made asphaltene solution in 100 % *toluene solvent* can induce the agglomerates to interact selectively with their counterparts and hold a more close-packed aspect. Once the *hextol mixture* evaporates, the conjugated unit of asphaltenes appears.

However, these agglomerates cannot be considered as asphaltene clusters for two main reasons: firstly, because there is an extensive literature background that reports, by using scattering techniques such as small-angle neutron scattering (SANS) and small-angle X-ray scattering, the size of asphaltene clusters in the range of 5-6 nm in high concentrations, accordingly to the Yen - Mullins model [21, 77]. It is significantly smaller compared to the size of our particles that are close to 100 nm in the *hextol solution*, the scenario with more compact spheres. Secondly, the nanoaggregates and clusters definition are applied to asphaltenes solubilized in bulk, which is different from the samples we study in SEM that requires evaporation before being submitted to the analysis. Our findings suggest the meaningful effect on interfacial assembly of asphaltenes regarding the presence of distinct aromatic solvents.
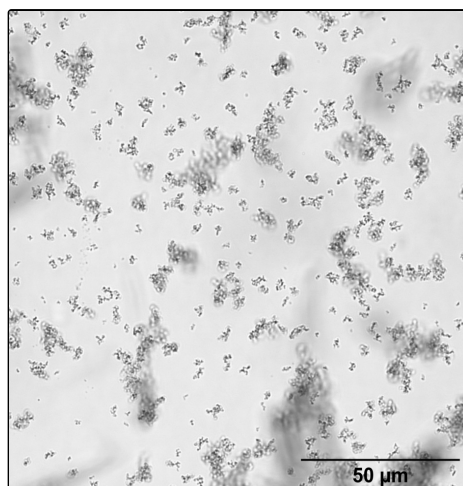
Figure 4.11: BR asphaltene precipitation in *hextol solution* by using confocal microscopy. The scale bar is 50μm.
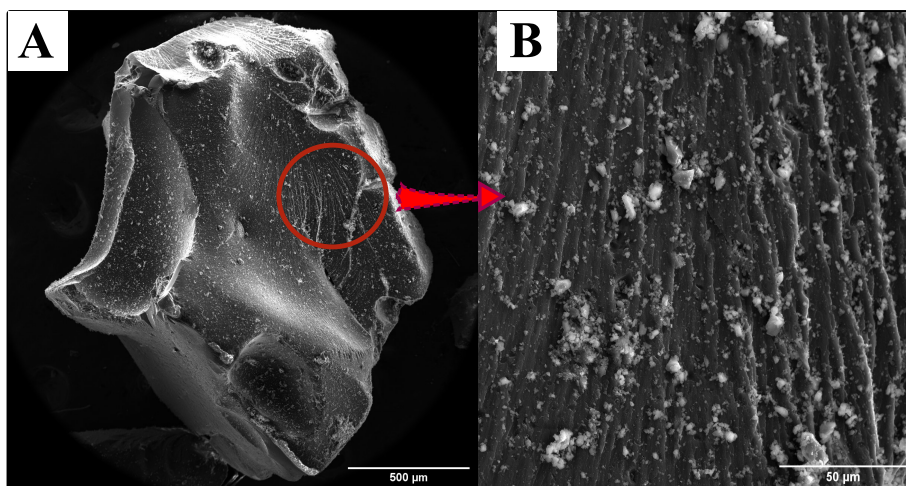
Figure 4.12: A. BR asphaltene precipitate (solid state) seen in SEM microscope. B. Magnification of its surface.
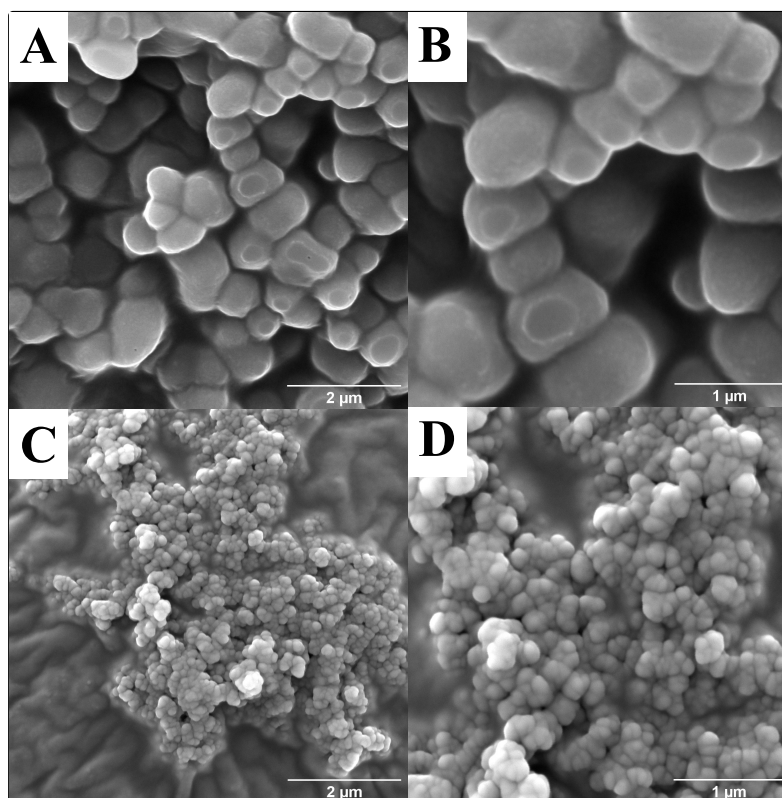
Figure 4.13: SEM images of BR asphaltene agglomerate particles. A. Asphaltene agglomerates are revealed after evaporation of toluene B. Magnification of image A. C. Asphaltene agglomerates are revealed after evaporation of the *hextol mixture*. D. Magnification of image C. The scale bar is 2μm for (a) and (c), whereas for (b) and (d) it is 1μm.

4.2.8
Spontaneous emulsification of BR asphaltenes at the toluene-water interface

The evidence of spontaneous emulsification (SE) is assessed by means of a confocal microscopy as described in chapter 3. Fig. 4.14 displays a time sequence of droplets spontaneously created at the toluene-water interface. Top rows correspond to the snapshots of the interface at the concentration of 1 mg/ml (images [a]-[d]), and bottom rows to the interface at a concentration of 3 mg/ml (images [e]-[h]). A few number of droplets is observed at the first minutes of phase contact and, due to gravitational setling (see Fig 4.15 [d] and [h]), they gather at the interface and migrate towards the water-oil meniscus. The images reveal the occurrence of some larger droplets, possibly due to coalescence events, but they mainly show smaller droplets (especially for the lower concentration). This is supported by the results presented in Figs 4.15 (a) and (b) that exhibit the number of droplets as a function of size and time. Graphs are obtained by measuring the radii size of each droplet in the center of the meniscus. One can note the dominance of emulsified droplets, for both concentrations, at t = 60 min with a droplet size ranging from [5 7] to [7 11]. For the highest concentration, more droplets were formed in the range of [5 7] at t = 40 min and t = 60 min.
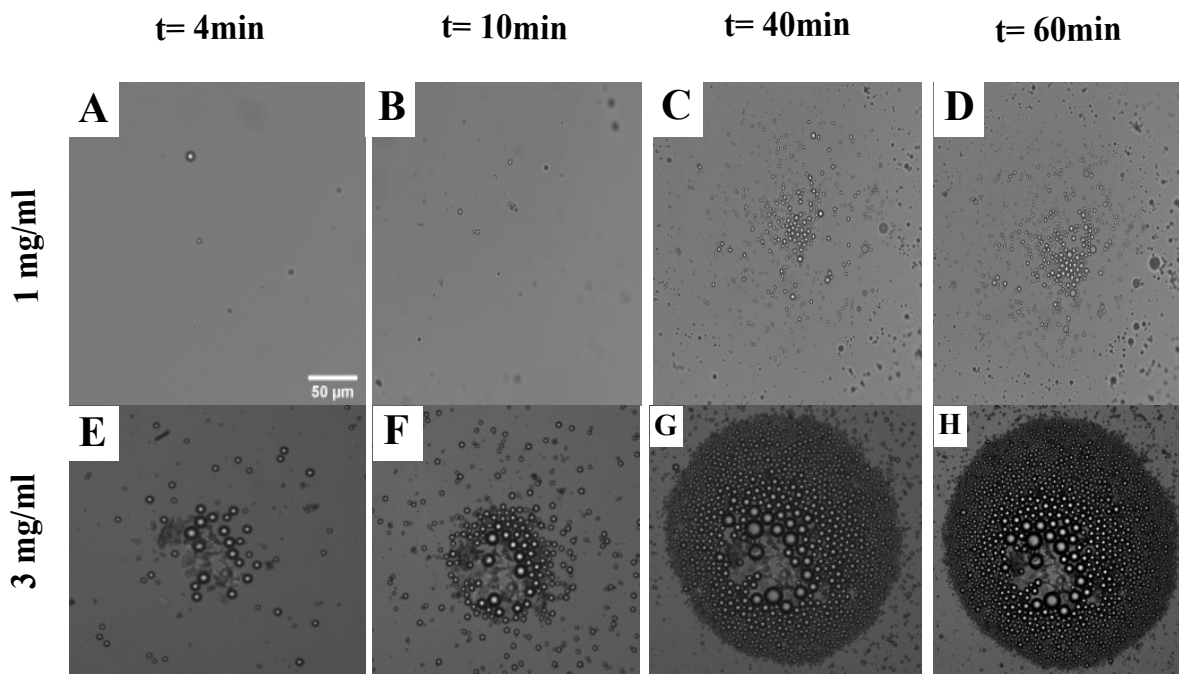
Figure 4.14: Images of SE process for the BR asphaltenes at the toluene/water interface for a 1 mg/ml and 3 mg/ml solution.

We observe that more droplets appear as the asphaltene concentration

increases (see Fig 4.15 [c]). After 10 min, the droplet content for the concentration of 3 mg/ml increases significantly, and a dense layer of accumulated droplets is formed. There is a jump from almost 150 droplets for the concentration of 1 mg/ml to a value close to 450 for the asphaltene concentration of 3 mg/ml. This is in accordance with the work of Araujo *et al.* [77] that reported the same trend for the SE phenomenon considering asphaltene solutions in the concentration of 1, 1.5 and 3 mg/ml. The authors claim that at the highest concentration, the consolidation of an asphaltene multilayer impaired the quantification of the droplets. Moreover, the same observation is presented by Rodriguez-Hakim and coworkers [51]; however the multiple layers of spontaneously emulsified droplets occurs with asphaltene-only systems at a concentration of 1 mg/ml.

The above-mentioned results endorse the theory that the asphaltene structure influences the SE process. Based on the references cited above, one can note that, although the concentration of asphaltenes is the same, the experimental outcome is different. In our tests, we show very few droplets after 1h of interfacial aging at the concentration of 1mg/ml, which is quite low if compared to previous work that reports a number close to 800 emulsified droplets for the same asphaltene concentration [77]. We believe that the mechanism responsible for the formation of droplets is similar to the one recently described by Rodriguez-Hakim *et al.*: when asphaltenes adsorb at the oil-water interface, they minimize the free energy of the system. This process occurs due to differences in the chemical potential gradients across the bulk phases that induce the diffusion of water molecules, and ultimately their nucleation to active polar sites of asphaltene molecules. As we can see for the concentration of 1 mg/ml, in the presence of fewer asphaltene moities, the water droplets have fewer anchoring points to bind and nucleate. On the other hand, with a higher concentration, the number of droplets increases substantially.
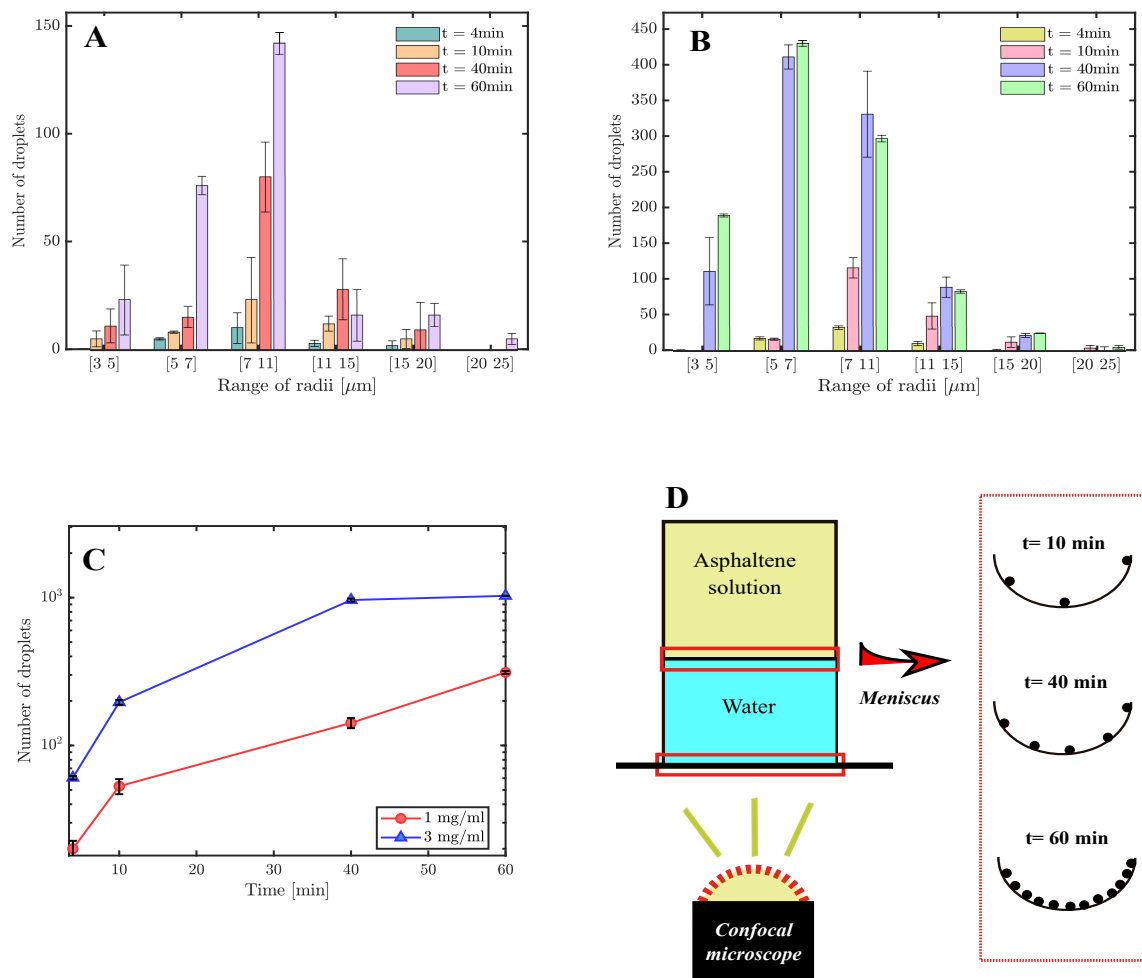
Figure 4.15: A. Number of droplets as a function of time and range of radii for the asphaltene concentration of 1 mg/ml. B. Number of droplets as a function of of time and range of radii for the asphaltene concentration of 3 mg/ml. C. Total number of emulsified droplets as a function of time for the concentration of 1 mg/ml and 3 mg/ml. D. Schematic diagram of the emulsification process in the confocal microscope: the accumulation of droplets occurs at the water-oil meniscus.

The island-type configuration of our asphaltenes may also justify the differences observed in the diffusion-aggregation process. As discussed in section 4.2.3, the island-type (or continental-type) configuration is less prone to induce molecular stacking, since the molecules do not fold efficiently. This can be related to the differences in the SE process with other asphaltene fractions that may possess distinct structural configurations [51, 77]. We believe that the polar content of the asphaltene structure alongside the ability to stack at the interface is possibly the central grounds that lead to SE phenomenon. In the next section, we will show by means of shear rheology experiments that

the interfacial viscoelasticity of asphaltenes can help to clarify the SE results. We will compare the asphaltenes employed in the work of Rodriguez-Hakim *et al.* [51] and Araujo *et al.* [77] with the BR asphaltenes. They will be respectively referred to as "Asphaltene A" and "Asphaltene B".

4.2.9
Effect of distinct asphaltenes on the interfacial viscoelasticity

To better elucidate the structure and dynamics of three distinct asphaltene structures (BR asphaltenes, Asphaltenes A and B) on the SE process, we conducted time sweep experiments considering the same frequency and strain values established for the studies with single BR asphaltenes. Protocol [C] was selected to assess the rheology of the three asphaltenes due to its simplicity (no solvent was added onto the adsorbed layer and we simply measured the asphaltene layer at the air-water interface). The experiment was performed at triplicates, but we display one trial of each asphaltene used (we did not include the error bars due to the difficulty of reproducibility as presented in section 4.2.3). Fig 4.16 (a) shows how the interfacial moduli develop at the T/W and A/W interfaces formed in Protocol [C]. Prior to evaporation (t = 1.5h), data for BR asphaltene and asphaltene B look very scattered, which we assume it is due to the absence of a mechanical resistant at the interface, which generates torque values below the equipment torque range. On the other hand, the viscoelastic moduli for asphaltene A starts forming at the first seconds of the test, and practically remains constant until the total evaporation of toluene, which evidences the consolidation of a structured interface (torque values are also within the equipment range). This is a significant result, since the magnitude of the elastic moduli measured at the interface is $\mathcal{O}(10^{-3})$, which corresponds to a bulk value of $\mathcal{O}(10^5)$. It suggests how strong is the viscoelastic film at this stage. The calculus is done by estimating the film thickness (it is ≈ 10 mn, see in Refs. [11, 107, 108]).
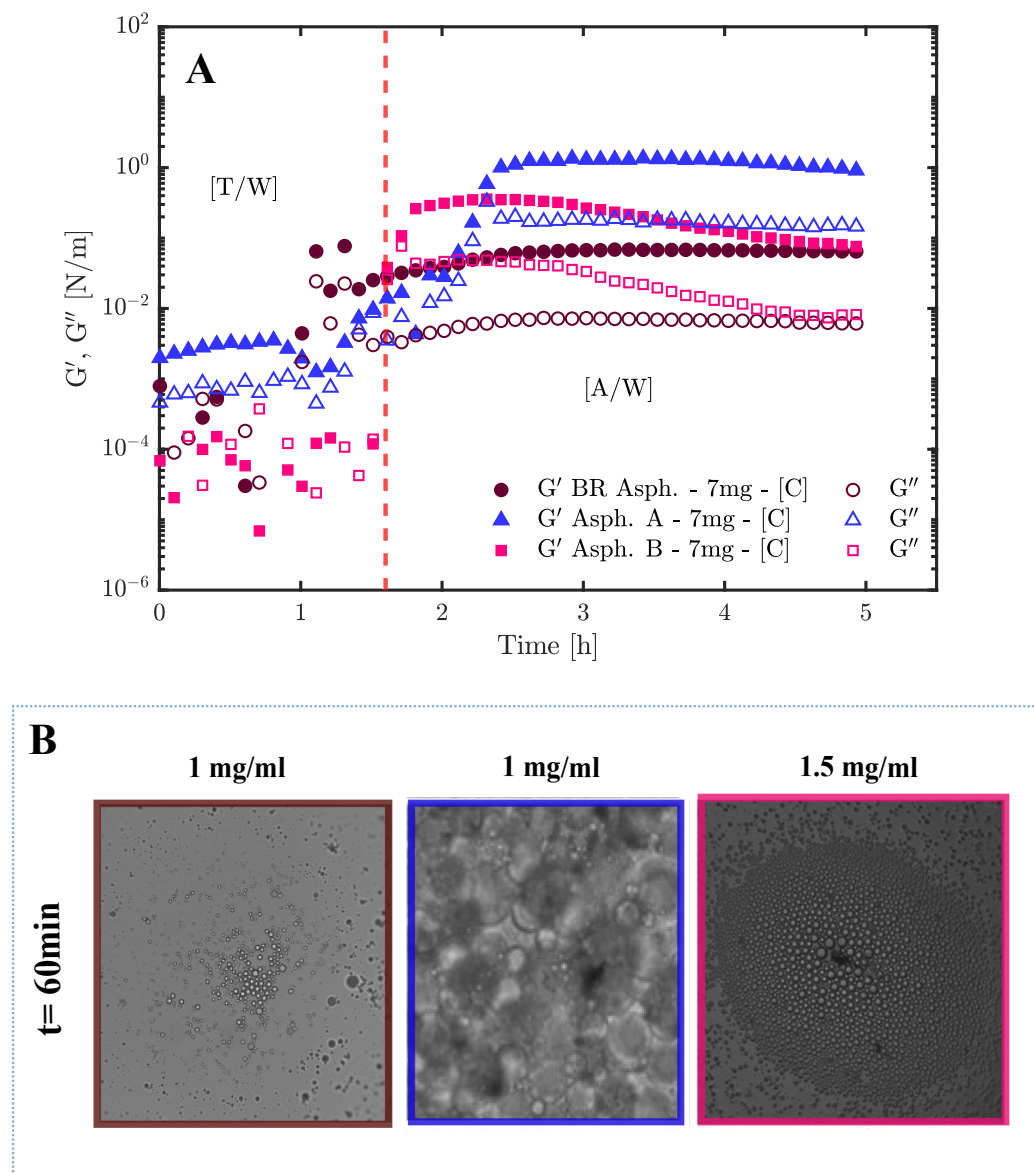
Figure 4.16: A. Small-amplitude oscillatory interfacial shear rheology of the three asphaltenes (BR Asph., Asph. A and Asph. B) as a function of time. B. Evidence of SE for the three asphaltenes: snapshots at t = 60 min are presented with the concentrations employed. Images of Asph. A and B can also be found in Refs. [51, 77].

As time goes by and the toluene fraction evaporates (1.5h after the beginning of the test), the buildup of the interfacial network is even more pronounced for asphaltene A, reaching a final G' value close to $\mathcal{O}(10^0)$. The G' and G'' values of asphaltene B abruptly increase; however they are lower than the values for asphaltene A and also decline over time, reaching the same final plateau of BR asphaltenes.

It has been observed that asphaltenes fastly adsorb at the interface governed by a diffusion mechanism (first step), followed by a slower adsorption

stage (second step) that may leads to the formation of multilayers [11]. We showed in section 4.3.2 that BR asphaltenes have little affinity towards the T/W interface, which impairs their adsorption at a initial stage and the consolidation of a measurable film. This may be linked to their low propensity to emulsify spontaneously. Considering the diffusion and nucleation theory, less molecules of water will be prone to attach to the active sites of asphaltenes, since fewer moieties are available at the interface (see Fig. 4.16 [b] first snapshot). One the other hand, if we compare the shear rheology of asphaltene A with its SE image after t = 60 min, it can be noted the highest interfacial moduli associated with a greater number of emulsified droplets at the same asphaltene concentration (1 mg/ml). The second snapshot in Fig. 4.16 is the evidence of an asphaltene multilayer [51]. Conversely, BR asphaltenes and asphaltene B are less viscoelastic and possess very similar interfacial modulus at the end of the experiment, yet the SE outcome is different. Araujo *et al.* [77] only display the microscope images for the concentration of 1.5 mg/ml (see Fig. 4.16 [b] third snapshot), but the authors report the number of emulsified droplets for the concentration of 1 mg/ml, and it is twice the number of the droplets obtained for the BR asphaltenes (450 for the BR asphaltenes versus 800 for Asph.B). These results help us to hypothesize that, for asphaltene-only oil-water interfaces, the propensity of a system to spontaneously emulsify is directly related to the rigidity of the interfacial network, which also depends on the asphaltene molecular architecture that will influence the nucleation process. We emphasize that this assumption may be restricted for interfaces free of co-surfactants, that is, interfaces loaded only with asphaltene molecules. Rodriguez-Hakim and coworkers showed a distinct trend for systems with both asphaltenes and co-polymers. They argue that as the interface develops and becomes more elastic, the rate of emulsification decreases, which is mainly justified due to a highly surface network that decreases molecular diffusion rate across the interface [51].

To confirm the parallels we set for the differences in the chemical structures of the asphaltenes used in this work, a simple elemental analysis for the three asphaltenes was performed. The results are presented in Table 4.2.

Table 4.2: Elemental analysis for the three asphaltenes.

	Asph. A	BR Asph.	Asph. B
% C	76.35	87.64	77.9
% H	7.55	7.69	7.63
% N	1.74	1.26	1.01
C/H molar ratio	0.84	0.95	0.85

^{1}H NMR and ^{13}C NMR experiments were also performed for the Asph. A and B, and are shown in the Appendix section. We highlight in Tabel 4.2 the percentage of nitrogen (% N), following the sequence Aspha. A > BR Asph. > Asph. B. Greater content of nitrogen may be linked to the greater polarity of the material. Furthermore, due to the basic characteristics of nitrogenous heterocycles, these portions end up being sensitive to pH changes: they can protonate in contact with water, resulting in charged moieties. Therefore, asphaltene A possesses more polar active sites, which may explain the greater number of emulsified droplets and interfacial activity. This assumption is also supported by the ^{1}H NMR result (see Table A.3) that reveals the higher proportion of naphthenic or paraffinic CH and CH_2, indicating larger and/or more numerous alkyl chains. In addition, the ^{13}C NMR analysis (see Table A.5) corroborates the above-mentioned premise: the high % of aromatic carbon linked to alkyl chains (17.8 %) accompanied by the highest % of peripheral carbon (23.7 %) and the lowest % of bridgehead carbon (40 %) indicates that this asphaltene has polycondensate units smaller than the other two.

On the other hand, the ^{1}H NMR of BR asphaltenes shows a greater number of aromatic hydrogens than Asph. A and B, which may indicate a smaller size of the polycondensates units and/or alkyl groups attached to the main aromatic core. In addition, BR asphaltene has a higher proportion of isolated methyls (CH_3), which validates the evidence of smaller alkyl chains (more CH_3 units than CH and CH_2). These findings can help to better understand the low interfacial activity of BR asphaltenes in toluene. Silva *et al.* [9] proposes through MD simulations that, in toluene, molecules having longer lateral chains with polar groups attached at the end of the branch have a propensity to interact more strongly than molecules having shorter chains with the same groups or polar content.

At last, $\%$ C$_{aromatic-bridgehead}$ in the following order Asph. B > BR asphaltene > Asph. A together with $\%$ C peripherals in the order Asph. A > BR asphaltene > Asph. B (see Fig. 4.17) indicates that the size of polycondensate units follows the order Asph. A > BR asphaltene > Asph. B. This trend also corroborates the supposition of the island-type configuration.
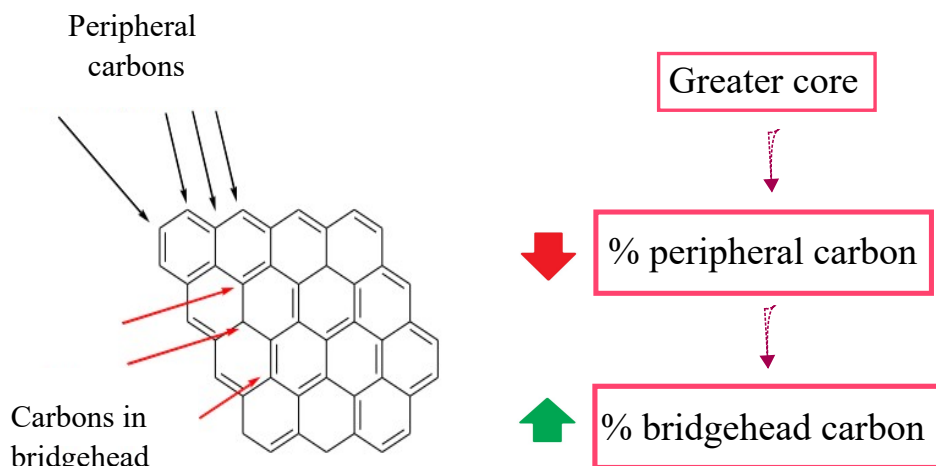
Figure 4.17: The linkage between the number of bridged head carbons with the asphaltene policondensate units: the greater the percentage of bridged head carbons the lower is the percentage of peripheral carbon.

.

4.3
Brief conclusions of Chapter 4

The effect of aromatic and non-aromatic solvents were investigated by studying the rheological response of asphaltene-only laden interfaces. We assessed the mechanical characteristics of adsorbed layers at the air-water and solvent-water interfaces with the main purpose of interrogating their stress-strain response upon the addition of distinct oil phase aromaticities. Π-A isotherms were also explored to interrogate the asphaltene behavior upon compression. Moreover, confocal and SEM microscope were used to elucidate the morphology of asphaltenes in distinct solvent aromaticities. The SE of BR asphaltenes was studied and compared with other asphaltenes reported the literature. Some brief conclusions can be made in order to consolidate the exposed:

○ BR asphaltenes are a polycondensed aromatic island-type structure that form reversible films when pure toluene is poured onto the asphaltene layer formed at the air-water interface;

○ The practical absence of charged groups on the asphaltene structure, as well as the lower tendency towards stacking at the interface, are the main reasons for the lack of activity at the toluene-water interface;

○ Network growth increases with decreasing solvent aromaticity, leading to higher elastic modulus;

○ Asphaltene laden interfaces attain a pseudoplastic behavior under the application of shear stress;

○ Additional Langmuir trough experiments confirms the desorption of asphaltenes in toluene, which supports the reversibility discussed in the time sweep experiments;

○ SEM micrographs revealed that lower aromatic content leads to more tightly packed agglomerates configuration;

○ Greater polarity due to the presence of nitrogen in the asphaltene structure may induce greater viscoelasticity and more propensity of a single asphaltene system to spontaneously emulsify.

.

5
Results and discussion: co-adsorption of asphaltenes and stearic acids at the air-water and oil-water interface

This chapter presents the study on the surface energy and co-effects of binary systems composed of BR asphaltenes and stearic acids. Initially, we show the results of DIT with different asphaltene-SA ratios, followed by the analysis of Π-A isotherms. We employed both DW and SW to deepen our investigation on the influence of electrolytes. The final discussion is related to the interfacial shear rheology experiments performed with the *diluted asphaltene-stearic acid solution.*

5.1
Interfacial tension results

To better understand the interplay between the BR asphaltenes with stearic acids (SAs), we initially performed dynamic interfacial tension (DIT) measurements of individual asphaltene and stearic acid laden interfaces, followed by the measurement of their mixtures. Although the DIT is a simple interfacial parameter, we highlight the importance of its measurement for the asphaltene systems, since their features vary significantly according to the source and extraction method. Toluene was employed as the oil phase and DW and synthetic water (SW) were used as the water subphase. The chemical composition of the SW was previously described in Chapter 3. It is basically formed by distinct salts, yet with the prevalence of the monovalent cation Na^+ (concentration = 24.53 g/l) and the divalent cation Mg^{2+} (concentration = 5.20 g/l). During the refining of petroleum, it is known that the pH of the co-produced water is enhanced due to the release of CO_2 during flow transportation, which induces the dissociation of acid monomers, like carboxylic acids and charged asphaltene moieties. These entities can react with the cations dispersed in the brine, forming a complex microstructure that stabilizes the interface [22].

We explored the interfacial tension as a function of the concentration of surfactants, as displayed in Fig. 5.1. For the asphaltene-only interfaces, we measured the surface energy of six distinct concentrations (0.1; 0.5; 1; 2 and 3 - Fig. 5.1 [a]) for the toluene-DW system and two concentrations for the

toluene-SW interface (1 and 3 - Fig. 5.1 [b]). For the interfaces loaded with stearic acids, we selected three distinct concentrations for the DW aqueous phase (1; 5 and 10 - Fig. 5.1 [c]) and for the SW systems, we also chose two concentrations as for the asphaltene only interface (1 and 10 - Fig. 5.1 [d]). All data points are obtained after an equilibrium time of 60 min and the standard deviation is expressed by the plotted error bars.
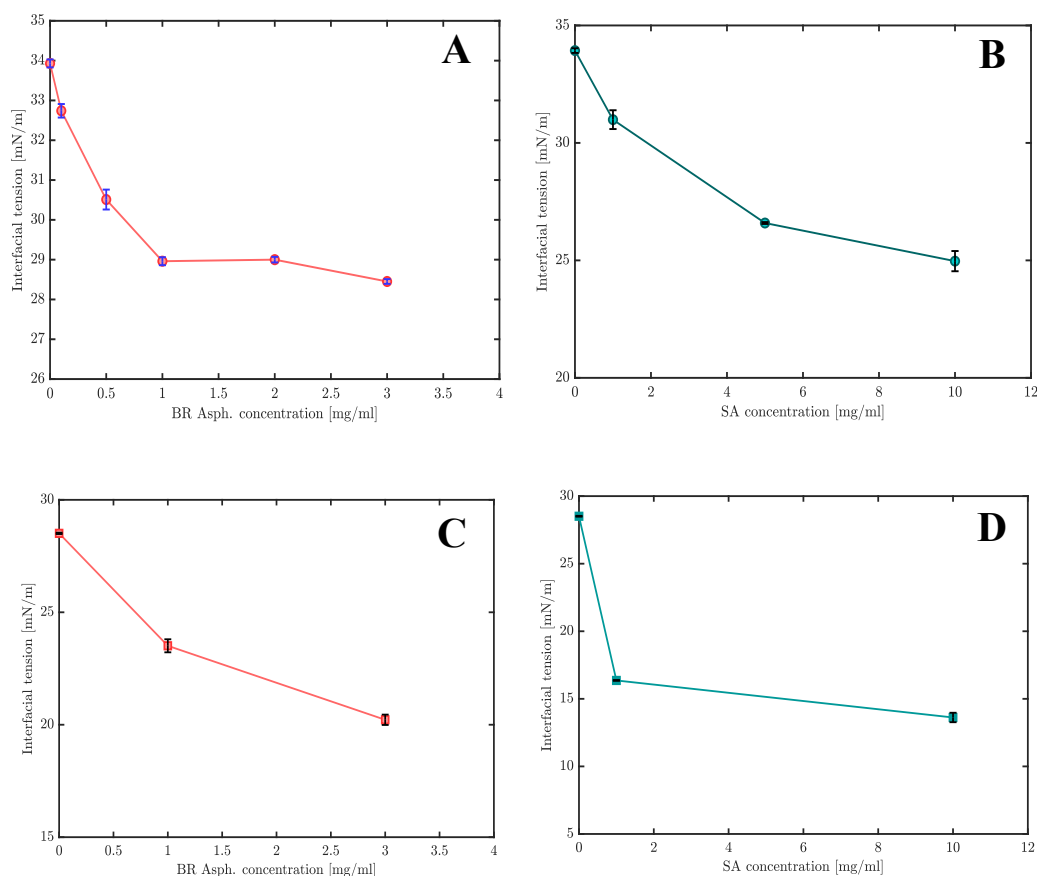
Figure 5.1: A. DIT of individual BR asphaltenes at the toluene-DW interface. B. DIT of individual SA at the toluene-DW interface. C. DIT of individual BR asphaltenes at the toluene-SW interface. D. DIT of individual SA at the toluene-SW interface.

In Fig. 5.1 (a) we observe the effect of asphaltene adsorption at the toluene-water interface by assessing the gradual decrease in the surface energy as the concentration of the asphaltenes increases. There is a drop from 34 mN/m, the value of DIT for the toluene-water interface free of asphaltenes, to almost 28 mN/m for the highest asphaltene content (3 mg/ml). Similar trend is verified for the asphaltene-SW systems (Fig. 5.1 [b]); however, lower values of

interfacial tension are obtained (for the 3 mg/ml concentration, the final value is close to 20 mN/m compared to a 28 mN/m for a bare toluene-SW interface). Figs 5.1 (c) and (d) exhibit the dynamics of SAs at also toluene-DW and toluene-SW interfaces respectively, and we also state that the surface energy is inversely related to the concentration of SAs; however, the final values reached are slightly lower than the DIT values obtained for the asphaltene systems.

Our results are in line with a large number of studies [18, 22, 48, 109, 110] that report changes on DIT due to asphaltene and carboxylic acid adsorption, especially with the work of Sauerer *et al.*, which shows the same DIT trend with both asphaltenes and SAs. Once the acidic or acid groups ionize at the toluene-water interface, they increase their hydrophilic character, leading to greater affinity towards the interface [110] and changings in the surface energy. This feature is even more pronounced in the presence of cations, as well discussed by Alves and coworkers [48], who concluded that the presence of salt in aqueous phase increase the rigidity of the interfacial film, hence improving the interfacial activity of the surfactants and the film compressibility.

Fig 5.2 compares the influence of the co-effect of asphaltenes and SAs on the surface energy of toluene-water interfaces. The equilibrium time here is also obtained after 60 minutes of experimental measurement. The DIT for the lower asphaltene concentration does not change significantly as the SA content increase. The same behaviour could be noted for the SA solutions with increased asphaltene content and vice-versa: the concentration of surfactant lowers the surface energy. However, it is valid to highlight some differences observed with the asphaltene-SA ratios: for instance, for the 1:10 asphaltene-SA ratio, the DIT is greater than the individual SA-DIT for the 10 mg/ml concentration. Similarly, the 3:1 asphaltene-SA ratio shows a higher DIT if also compared to its individuals. We assume that for the binary systems, a competition between the species takes place, and it may be initially favored to the SAs, since they are much smaller and have more mobile molecules if compared to the asphaltenes [18]. However, as the asphaltene content increases, it is reasonable to suggest that the interface will be crowded by these structures, which may ultimately affect the SAs adsorption. This is observed in Fig 5.2 (b). On the other hand, if the SAs concentration is potentially higher than the asphaltenes (see Fig 5.2 [c]), they seem to dominate the adsorption process by lowering the surface energy.

We were unable to perform the same systems with the SW as the aqueous phase because, over time, significant changes in the pendant drop profile occurs as the adsorption mechanism develops. The droplet could not sustain sufficient stresses to maintain its shape (the DIT values were ver low for the mixtures),

which invalidates the Young-Laplace equation from an isotropic interfacial tension. So, we only show the results of co-adsorption regarding simple DW as the aqueous subphase. To circumvent this issue, we suggest other methods to measure the DIT, for instance, force tensiometers that can be highly accurate automatic measures at flat oil-water interfaces.
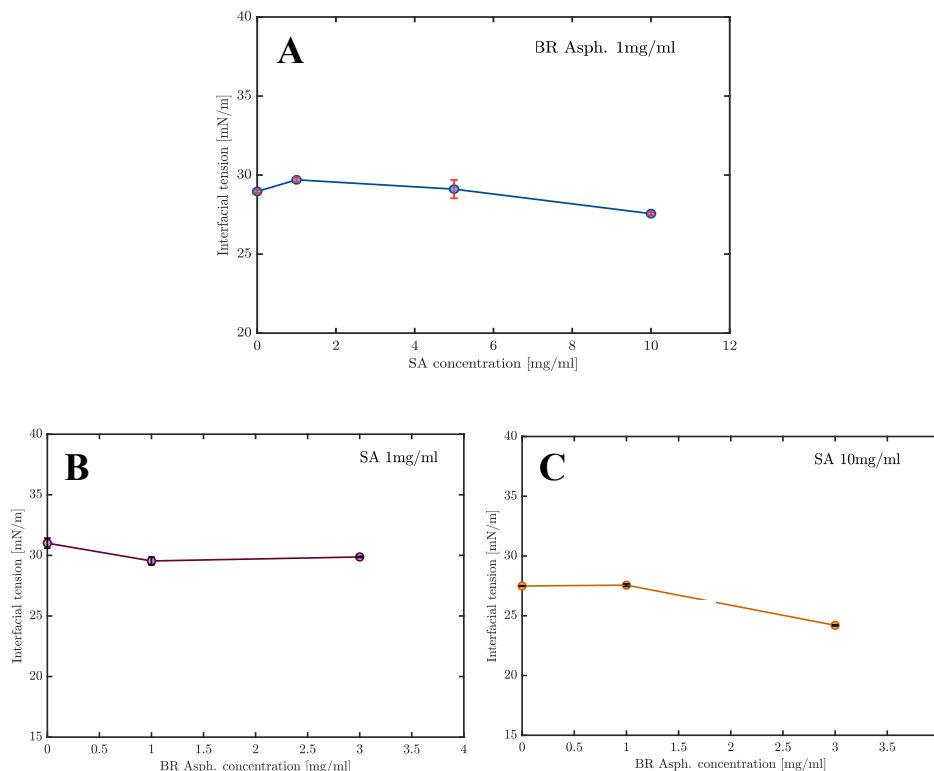
Figure 5.2: A. DIT of the binary asphaltene-1 mg/ml-SA mixture. The SA concentration varies while the asphaltene remains constant. B. DIT of the binary asphaltene-SA-1 mg/ml. The asphaltene concentration varies while the SA remains constant. C. DIT of the binary asphaltene-SA-10 mg/ml mixture varying the SA concentration. The asphaltene concentration varies while the SA remains constant.

5.2
Surface pressure isotherms at air-water and air-SW interfaces

Results for experimentally surface pressure Π versus trough area of single component asphaltenes and stearic acids solutions are presented in Fig 5.3 (a). Shaded error bars display the repeatability of the tests. We maintained the initially spreading of 25 μl of the asphaltene solution (1mg/ml - 100% toluene), as explained in chapter 4. The solutions considered for the SAs were 1 mg/ml and 10 mg/ml, and they were also spread onto the water subphase (25 μl). A three-hour aging time was equally employed to induce solvent evaporation

and interfacial strengthening at the water interface. This step was made prior to the beginning of compression. For the lower SA concentration (1 mg/ml), the surface pressure starts rising at a higher surface area around 250 cm^2 (Π values for BR asphaltenes evidences a similar increase at a trough area of ≈ 150 cm^2), exhibiting a steep growth with an apparent kink at the surface pressure of 52 mN m^{-1}. However, at the end of compression, it yields a final Π value close to the one obtained for the BR asphaltene (≈ 57 mN m^{-1}). When the monolayer is compressed, phase or *collapse* transitions may appear as the Π-A isotherm progresses. The latter has received much attention since it is related to change the dimension from 2D to 3D, and usually is described in the form of kinks followed by either a plateau or a subsequent pressure rise (even a decrease can be observed) [57]. 2D-3D transition has been characterized as a nucleation and growth process, in which the overcompression of the film reaches a maximum pressure value [57, 111, 112]. The interfacial collapsing that occurs for the lower concentration of SA (1 mg/ml) may be justified by the packing of the C$_{18}$ fatty acid molecules that have a propensity to be expelled of the water in order to minimize the free energy of the system [32]. Thus, they tend to arrange themselves at tightly packed configuration at the adsorbed monolayer, leading to the formation of rigid films at the LC and S phases (most compact stages).

Slope changes at the SA-10 mg/ml system are striking: the surface pressure begins to rise at the first seconds of the compression, reaching a maximum pressure value of ≈ 33 mN m^{-1}. By comparing these disparities between the SA profiles, one can note the relevance of the concentration as the Π-A isotherm measurements change completely when the concentration is 10 times greater. The evident kink is followed by a plateau and a slight rise until the end of the experiment. This trend has already been shown for unionized fatty acids – stearic (octadecanoic) acid by Rises and coworkers [113, 114] in their research on collapse. The authors propose an organized trilayers type of collapse, where the monolayers can fold out of the aqueous phase resulting in a sudden drop on the surface pressure values. These folds can bend and fall over the monolayer domain and ultimately form the trilayers, which cover the interface (the plateau region seen in Fig 5.3 (a) after the kink) and are stabilized by head group hydrogen-bonding.

Fig 5.3 (b) presents the re-plot of the individual asphaltenes and SA isotherms with their binary mixtures. The asphaltene concentration was kept the same (1 mg/ml) whereas the SA concentration employed was of 1 and 10 mg/ml. For the 1:1 BR-SA mixture, we clearly observe the dominant effect of SA at the initial compression stages, since the binary curve starts rising at

the surface area value of the individual SA-1 mg/ml isotherm. As the surface pressure increases, we observe a change of the profile in favor of the single asphaltene isotherm, which suggests that asphaltenes competitively adsorb onto the air-water interface. The final surface pressure value reaches $\approx$ 70 mN m^{-1}. Also, the monolayer kink is no longer observed. The 1:10 BR-SA mixture shows a tendency that strongly evidences the early SA adsorption, as the curve progresses similarly to its individual equivalent. Our findings are in line with the work of Sauerer *et al.* [18], which reports that initial values of binary asphaltene-SA curves are close to those of single SA systems. We propose that the initial contribution of SA to the surface adsorption occurs due to the fact that in mixtures, large asphaltene molecules need much more time to rearrange and adsorb onto the interface, hence the initial dynamics is primarily controlled by smaller and lighter molecules like the SA.
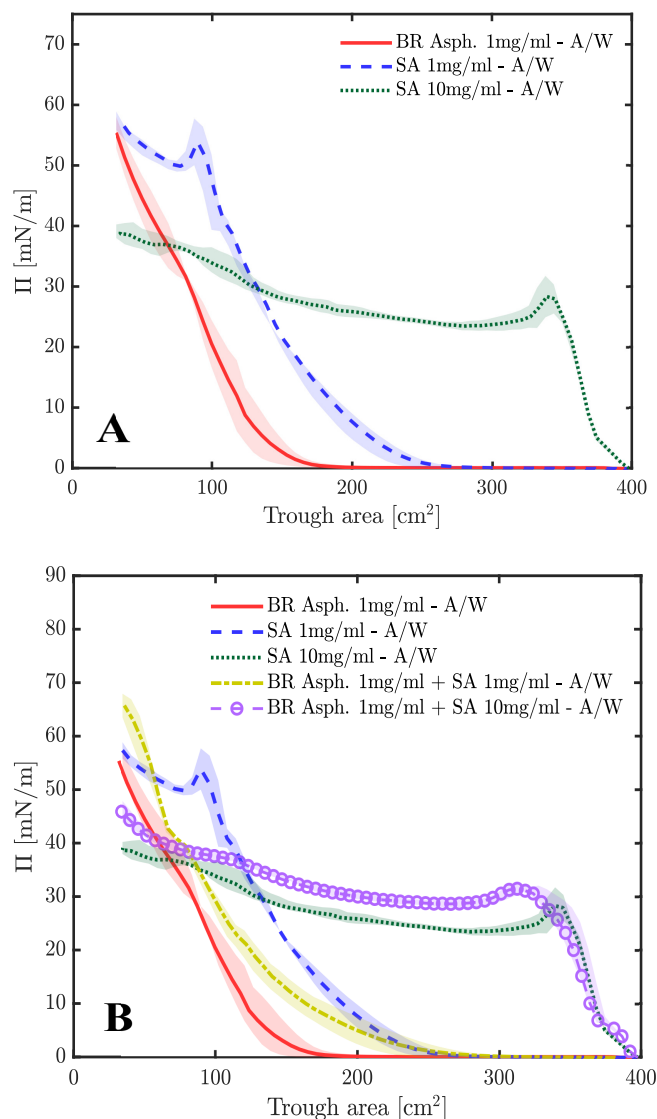
Figure 5.3: (Π-A) Compression isotherms of single BR asphaltenes and SA systems with their binary mixtures at the A/W interface. A. Individual species. B. Binary mixtures at 1:1 and 1:10 ratios.

In order to better understand the influence of the synthetic water (SW) on the compression of adsorbed layers, we studied single asphaltenes and SA with their mixtures at only the 1:1 asphaltene-SA ratio. Salt is a relevant factor that can influence the behavior of asphaltenes and acids, since it can influences acid-base equilibrium, stabilizes ionic species and can also react with oil species. Results for the individual isotherms are also presented with the SW curves for better comparison. Fig 5.4 reveals that the surface pressure is strongly related to the presence of salts in water for both asphaltenes and SA, as it begins to rise as the trough starts to compress. The worth mentioning

point is that, initially, Π values are practically the same for the binary systems, however as the surface area decreases, the asphaltene curve shows a linear trend reaching a final pressure value of ≈ 41 mN m^{-1} (green curve), whereas the SA isotherm exhibits a steep increase close to the surface area of 100 cm^2, reaching a plateau and a final Π value of ≈ 55 mN m^{-1}. Differently from the asphaltenes, the SA monolayers in SW seem to present smooth gas, liquid and solid phases transitions, however the collapsing process is different from the one noticed for SA films formed onto the DW subphase. For the SW systems, instead of a kink, the Π remains constant (pink curve) until the end of compression. These findings are in line with the studies of Gmira *et al.* [116] that points the ion dependency of SA monolayers applied for studies in smartwater flooding. Moreover, an interesting trend is observed for the binary mixture of the surfactants: the initial profile and phase transitions are very similar to the one verified for the SA slope, yet, as time progresses the isotherm reaches the highest Π values (close to 65 m^{-1}). We dot not re-plot the 1:1 mixture in DW for a better visualization (see image 5.3). This confirms the previously mentioned theory that, at first compression stages, SA populates the interface due to its simpler mobility and smaller units, however, as time progresses, the interface may be occupied by the asphaltene nanoaggregates that competitively adsorb with the SA molecules.

In general, our findings suggest that the adsorption kinetics of asphaltenes and SAs is enhanced by the presence of salts in the aqueous subphase. It is well referenced in the literature the increasing of pH, salinity and ions as key factors to the deprotonation of COOH groups that makes them more active at the interface [116]. This process is mainly governed by the pH of the bulk and the pKa of the acid, which represents the ionic environment of the solution where 50 % of the acid groups are protonated (hydrogen atoms are removed from the carboxyl group and remain as OH$^-$ ions in the solution). Since the pH of the SW is greater than the DW (pH ≈ 8 versus the pH ≈ 6.5 for the DW) and the pKa of the SA is 10.15 [32], we propose that some SA molecules are in the protonated state, and consequently, they may interact with the dissociated salts and also with the unionized acid groups through ion-dipole interactions. Hydrogen bonding cannot be discarded as a possible attraction that induces greater interfacial activity [117].

As for the asphaltenes, we can propose that the possible acidic moieties within the nanoaggregates may behave like the SA molecules. Although we cannot confirm its acidic content, the elemental analysis indicates that the island-type BR asphaltenes have a relevant polar portion, which may induce strong hydrogen bonding. As presented by Xu *et al.* [118] and latter confirmed

by Kuznicki *et al*. [10], interactions with molecules that comprise polar functional groups are likely the most relevant when water molecules bind to the asphaltene hydrophilic portions. Besides, the percentage of carbon and the C/H ratio of BR asphaltenes are meaningful. As naphthenic portions and mainly portions aromatics are richer in carbon and less rich in H, this may indicate greater aromatic/naphthenic proportions and low paraffin content, which justifies the presence of carboxylic groups. Last, but not least, the positive protonated group of nitrogen, can also interact with acidic groups of the SA, leading to strong attractive complexation, which leads to higher interfacial activity.

Finally, it is worth mentioning that the SW is mainly constituted by the monovalent salt NaCl (24.53 g/L) and the divalent salt $MgCl_2$ (5.20 g/L). Our assumptions are in consonance with studies reporting the effect of monovalent salts in the interfacial activity of adsorbed SA and asphaltene layers. Nonetheless, as exposed by Schwartz *et al*. [119], divalent cation as Ca^{+2} and Mg^{+2} are inclined to have a strong affinity towards the negative acid groups, and Ca tends to bind more strongly to the SA head groups than Mg^{+2} [116]. Moreover, the ion type may also influence on the surface energy and compression/shear features of the adsorbed film [92]. A study on the single contributions of mono and divalent cations is a noteworthy direction to future work.
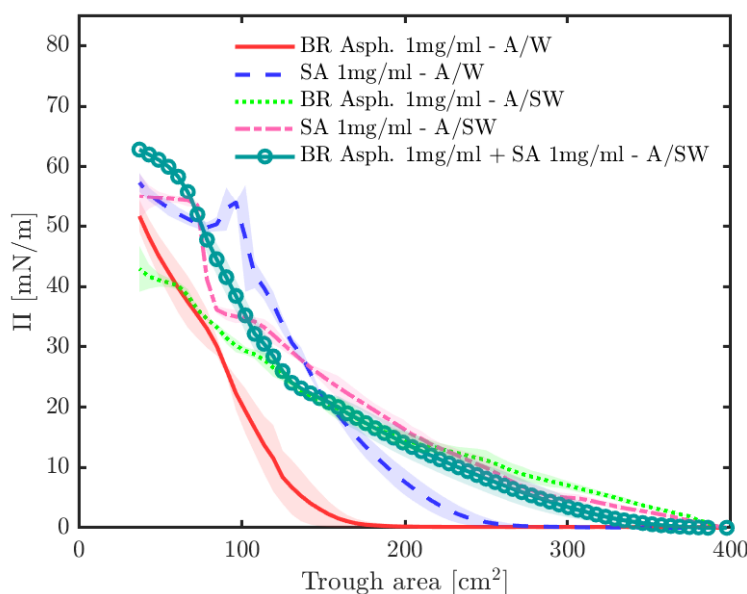
Figure 5.4: (Π-A) Compression isotherms of single BR asphaltenes and SA systems with their binary mixtures in DW (W) and SW.

5.3

Interfacial rheology of SA and SA-asphaltene laden interfaces

Time sweep experiments were performed to evaluate the mechanical response of SA adsorbed layers and their binary systems with BR asphaltenes. To simplify our analysis, we elected Protocols [C], [D] and [E] to form the interfaces in the co-adsorption study. The protocols description presented in chapter 3 were maintained. The stress-strain response of SA was initially assessed in order to provide a better discussion upon mixing with the BR asphaltenes.

Figure 5.5 (a) displays the shear rheology of single SAs at T/W and A/W interface (Protocol [C]) with three distinct experimental trials. SA was solubilized in pure toluene at the same asphaltene content (7mg) employed in the individual study. We re-plotted Fig. 4.5 from chapter 4 in Fig. 5.5 (b) for a better comparison. It is valid to note the scattered data at the T/W interface during the first 1.5h, which may be indicative of low interfacial activity. Weakly SA adsorption has been proposed by Wang and coworkers [24], who shows that, when single SA molecules are dissolved in aromatic solvents as toluene, they are more likely to stay in bulk rather than at the interface. The low torque values were noted prior to the toluene evaporation and were also verified for the asphaltene film (see Fig. 5.5 [b]). However, at the A/W interface, the interfacial loss modulus G'' does not seem to arise abruptly (this trend was observed for the G' asphaltenes initial value), but instead, it suggests that the interfacial network develops over time. G'' continues greater than G' until the end of the experiment, indicating a liquid-like interfacial film with only viscous features. After 8h of the experiment, one can note that the loss modulus is still greater than the storage modulus.

We hypothesize that, although the interfacial activity may be the initial factor that triggers microstructure buildup, it is not enough to impart rigidity to the interface. Other factors, like the surfactant structuring, are essential to define the rheological features. This can be concluded with the aid of the Π-A isotherms of SA monolayers presented in section 5.4. For instance, if we suppose the amount of SA spread at the A/W interface - 25 μl of a 1 mg/ml of a solution equals a SA mass of 25 μg - it represents 0.025 mg, a value that is significantly low if compared to the mass of 7 mg used in the time sweep tests. Even so, the final surface pressure is fairly high yet the shear rheology indicates a liquid-like behaviour, proving the consolidation of a weaker viscoelastic film.
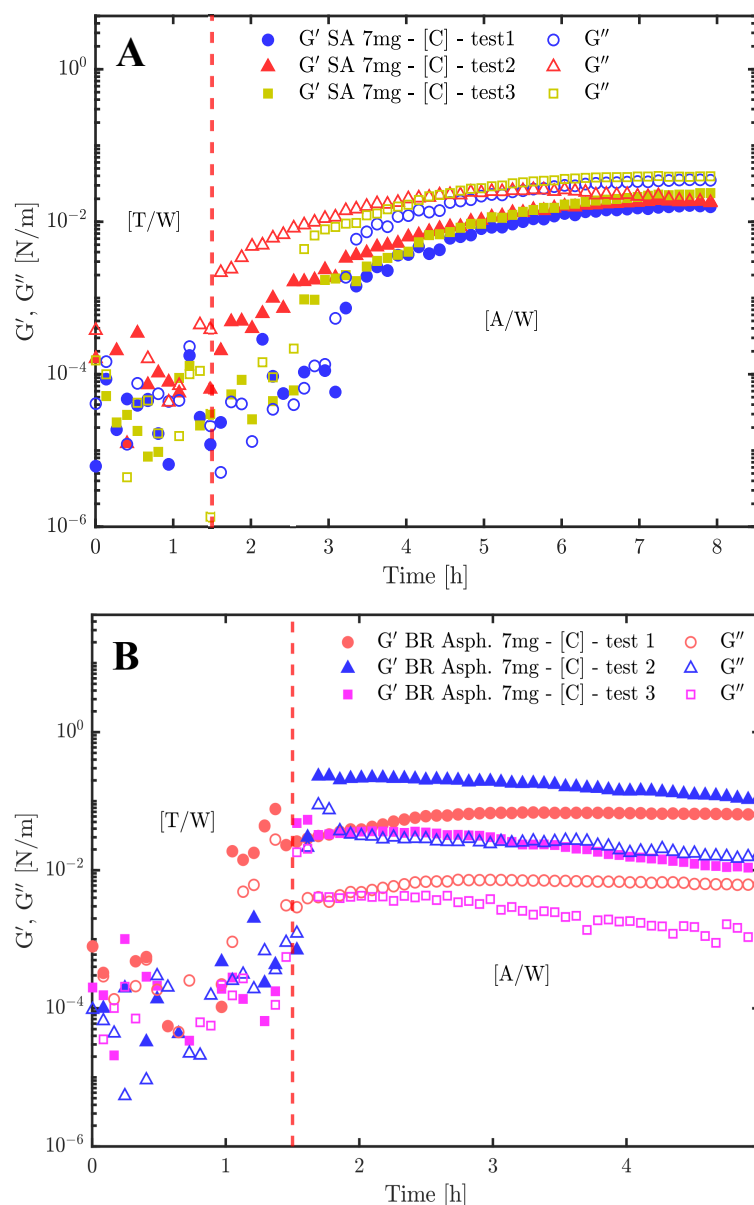
Figure 5.5: A. Interfacial shear rheology of single SA laden interfaces. B. SAOS shear rheology of asphaltene-only interfaces. This result has been shown in Chapter 4. We repeat it to better discuss the distinct effects of the surface active species.

Similarly to the asphaltenes, the reversibility of the SA layers is assessed. Fig 5.6 (a) reveals the interfacial moduli acquired during the "First" and "Second" cycles of the double measures of T/W and A/W interfaces formed in Protocol [D] (dashed red marks off the limits of the cycle zones). One can note the complete destabilisation of the SA film when fresh toluene is re-injected onto the interface, followed by the almost complete re-adsorption onto the A/W interface when all toluene fraction evaporates for the second time. It is

also valid to point out the differences in kinetis of film formation (16h versus 8h if compared to the asphaltene system). Polar solvents like toluene exert a strong influence on the interactions with the carboxyl groups, which indicates the drop of the viscoelastic moduli. In addition, the absence of ionized SA molecules due to the pH of DW (pH = 6 < pK$_a$ of the acid = 10.15), may be related to less surface coverage, and therefore, the consolidation of a weaker rheologically interface.

Fig 5.6 (b) screens a similar drop in G' and G'' when heptane is poured onto the adsorbed SA layer. This procedure is the one performed in Protocol [E], also used in chapter 4 for the rheological study of single asphaltene laden interfaces. However, differently from the asphaltene outcome, the addition of heptane unfolds an opposite effect: no increase in viscoelasticity was observed, instead, we verify a dramatic fall in viscoelasticity, which is evidenced by the scattered data at 8h. It is valid to mention that, weakly polar solvents as heptane interact well with n-alkanes [120]. Besides, as we mentioned previously, the SAs have a tendency to be expelled from water to minimize the free energy, so we believe that it may benefit the solubilization in heptane. From the obtained results, we can infer that SA film strength is independent of solvent aromaticity.
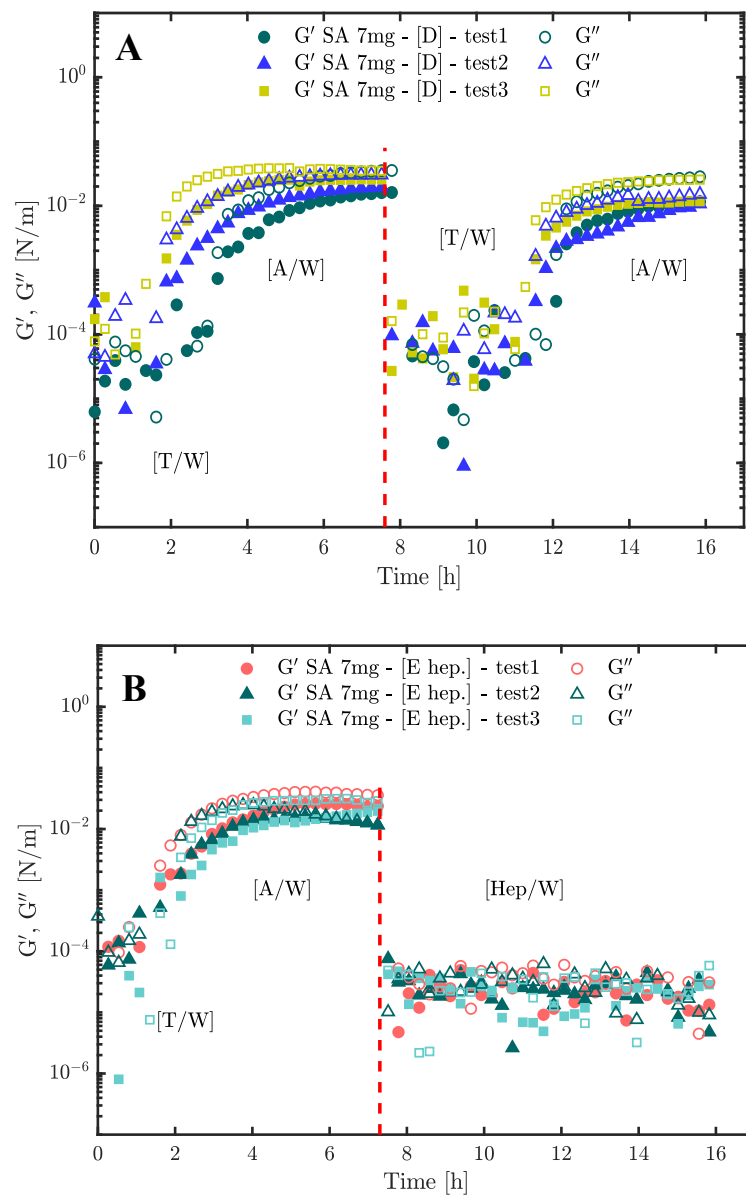
Figure 5.6: A. Interfacial shear rheology of single SA laden interfaces in Protocol [D]. B. SAOS shear rheology of single SA laden interfaces in Protocol [E].
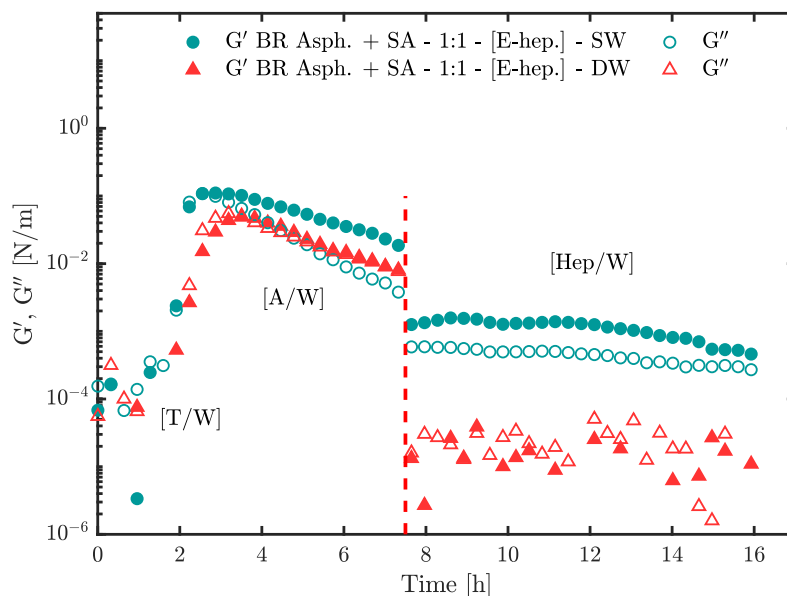
Figure 5.7: Interfacial shear rheology of the 1:1 asphaltene-SA binary mixture. Dashed red line marks the change on viscoelasticity due to the heptane addition.

A preliminary study on the rheology of the binary mixtures of BR asphaltenes and SAs were conducted and it is presented in Fig 5.7. We chose only the 1:1 asphaltene-SA ratio to simplify our analysis. DW and SW were employed as an aqueous phase to also broaden the investigation. Protocol [D] was selected since it encloses both air- and oil-water interfaces, yet, only one solvent was used to form the latter (heptane). Shaded error bars are not ploted due to the scattered data, but the time sweeps were performed at triplicates.

For the two aqueous subphases, Fig 5.7 points to the accurrence of interfacial competition between the asphaltene nanoaggregates and SA molecules at the first hours of the test, expressed by the upward trend at the time range of 0h to 3h. At $\approx$ 3h, the elastic modulus G' equals the viscous modulus G'' in the DW system, and they slightly decrease until the heptane addition (this is limited by the dashed red line). Nevertheless, for the SW phase, the storage moduli develops and remains greater than the loss moduli, which denotes an increase in viscoelasticity.

The differences observed for the DW and SW systems at the same asphaltene-SA ratio confirms the completely dominance of fatty acid molecules at the interface and the influence of ions on the enhancement of interfacial activity. Although asphaltenes are the most responsible for film rigidity, we can note that when they are in a mixture, their interfacial dynamics are altered in favor of SA. This was also shown by the small effect of asphaltenes on

the DIT as individual and binary entities (see 5.1). Moreover, we can infer that the G' magnitude of the mixture is very close to the G'' value obtained for single SA interfaces, which corroborates the preferential SA adsorption. The elastic and viscous modulus of $\mathcal{O}(10^{-2})$ Pa m correspond to a bulk value of $\mathcal{O}(10^{6})$ Pa, and, despite they are considered weaker films if compared to asphaltenes (G' magnitudes of $\mathcal{O}(10^{0}$ Pa.m$)$ corresponding to $\mathcal{O}(10^{10})$ Pa in bulk rheology), they attain relevant film strength for interfacial references [11,47]. Despite the amount of asphaltenes dispersed in solution is lower than the individual concentration, good measurements were only possible with the *diluted asphaltene-stearic acid solution* (see chapter 3, section 3.3).

The above-mentioned discussion is sustained if we observe the stress-strain response of the binary layers when heptane is added as top phase. Differences in the viscoelastic modulus are striking when electrolytes are present in the aqueous phase. When examining the composite system in DW, it is clear that the strongly bonded interfacial network of asphaltenes suggested in chapter 4 (see discussion in section 4.2.4) is replaced by a SA microstructure, since there is no indication of solid-like features at the interface, and in the presence of heptane, the viscoelastic modules fall drastically. On the other hand, for the SW aqueous phase, it is observed a decrease in the moduli values; however, the interface remains quite elastic until the end of the experimental time. This is confirmed by good torque values reported beyond the dashed line zone, indicating the presence of a rheologically measurable interface.

Straight alkyl chains acids like the ones verified in SA tend to pack much tighter in an adsorbed layer and it is more pronounced as their length increases due to the greater van der Waals interactions between them [32,121]. The closer-molecule evidence, associated with faster diffusion-adsorption, reasonably explains the shear rheology results of Fig. 5.7. Besides, the deprotonated carboxyl moities, favored by the presence of ions and mono/divalent cations, play an important role in the film consolidation, as well explored in section 5.2. It is valid to highlight that, although the heptane interacts well with SA molecules, its surface energy and mechanical strength are more affected by film ionization, and ultimately overtake the effect of solvent aromaticity.

5.4
Brief conclusions of Chapter 5

Interactions of BR asphaltenes with SA at the air-water and oil-water interfaces were explored. We used the DSA methodology to measure the DIT

of the interfaces, the Langmuir trough technique to address film consolidation upon compression and small-amplitude oscillatory interfacial shear rheology to investigate the viscoelastic features of the mixtures. We highlight the main conclusions of Chapter 5 as follows:

- BR asphaltenes have little influence on the DIT values, however, at the toluene-SW interface, they seem to be more sensitive to energy changes;

- SA systems present lower values for the DIT compared to the asphaltenes, which indicates that they are more prone to firstly adsorb at interfaces. At toluene-SW interfaces, the DIT is significantly reduced;

- The surface pressure of SA monolayers are clearly dependent of the surfactant concentration and electrolyte content in the water bulk. The binary systems revels a dominant effect in surface pressure values as time progresses;

- SA films hold a liquid-like behaviour and are reversible in the presence of toluene. SAs desorb promptly in heptane;

- Competitive adsorption is evidenced in the first hours of the time sweep experiments, and the interfacial film exhibits an elastic feature. Upon addition of heptane it destabilizes in DW, however in SW, it keeps meaningful values of storage and loss modulus.

6
Conclusions and final remarks

6.1
Conclusions

The surface and rheological properties of indigenous Brazilian asphaltenes at the air-water and oil-interface are studied. Initially, we evaluate the effect of aromatic and non-aromatic solvents on the viscoelasticity of adsorbed layers. We assess their mechanical features with the main purpose of interrogating their stress-strain response upon the addition of distinct solvent aromaticities. To do so, we design a set of novel experimental protocols that comprise adsorption/desorption steps. The Langmuir trough technique is used to explore the interfacial behaviour of our asphaltenes in a compression deformation mode. Additionally, SEM and confocal microscopy provides relevant information concerning the morphology and aggregation in the bulk of the asphaltenes considering distinct solvents. Our findings reveal that BR asphaltenes are a polycondensed aromatic island-type structure that forms reversible films when pure toluene is poured onto the asphaltene film formed at the air-water interface. We believe the lack of charged groups may be the main reason for the lower interfacial activity, yet other factors like the interfacial stacking may be the reason for the observed outcome. Furthermore, we assume that asphaltene-asphaltene interactions are affected by the presence of hexadecane, which also justifies the rheological trend observed. The *in situ* rheological protocols show that asphaltene molecules tend to form more packed nanoaggregates in the presence of hexadecane and heptane, resulting in greater interfacial viscoelasticity. By means of distinct solvent additions, we find that network growth increases with decreasing solvent aromaticity, leading to the higher elastic modulus. Also, we observe that asphaltene laden interfaces obtain a pseudoplastic behavior under the application of shear rate stress, and the interfacial viscosity is directly related to the amount of adsorbed nanoaggregates.

Additional Langmuir trough experiments confirms the desorption of asphaltenes back to toluene, which supports the reversibility shown in the time sweep experiments. The asphaltene-solvent interaction is also evidenced by the

decrease in the surface pressure values. The investigation of the *hextol solution* by means of the confocal microscopy confirms the asphaltene precipitation in less aromatic oil phases. SEM micrographs show that asphaltenes in less polar solutions (i.e, the *hextol solution*) tend to form agglomerates with a more tightly packed configuration.

We also explore the evidence of SE in asphaltenes systems and related it to the viscoelasticty of the adsorbed layers. We used a confocal microscope to map the evolution of droplet formation and interfacial shear rheology to obtain the elastic and viscous modulus. Two asphaltenes originated from distinguished extraction methods are also investigated. We give indications that the asphaltene molecular architecture and composition (the percentage of polar sites) are relevant to the propensity of a system to spontaneously emulsify. Furthermore, we propose that interfacial viscoelasticity is directly related to the growth of droplets at asphaltene-only interfaces.

DIT is analyzed for oil droplets of asphaltene, SA and binary solutions in DW and SW. We conclude from the experiments that the DIT reaches an equilibrium within 1h of experimental time, and the SA lowers the surface energy more significantly than asphaltenes, especially in the presence of the brine. Small-amplitude-oscillatory-shear (SAOS) experiments are performed to assess the viscoelasticity of single SA layers considering the experimental protocols used for individual asphaltene systems. We detected the buildup of a viscous interface for the SA systems and a greater equilibrium time. Moreover, SA can form reversible films when fresh toluene is re-injected on top of the adsorbed layer. Oppositely to the asphaltenes, the SA viscoelastic moduli drastically decreases with heptane addition, which may indicate the disruption of the film. Finally, the co-adsorption of the asphaltene-SA binary system in the rheology of the interfacial layers is explored. We conclude that SA initially dominates the interface, however the asphaltene nanoaggregates and clusters also compete to adsorb at the interface. The SA films obtain a reduced elastic feature (loss modulus greater than elastic modulus), yet, in the presence of asphaltenes, all moduli reach equal values. It suggests the influence of asphaltene attachment to the interface. We also observed the remarkable consequence of adding salts to the water subphase in the binary mixtures. Both storage modulus G' and loss modulus G'' are detectable and remain constant until the end of the experiment, confirming the solid-like behavior of the adsorbed layer.

Interfacial rheology of asphaltenes is a subject that is not fully understood. There are several parameters that impact film consolidation and asphaltenes kinetics, which have been optimized with the improvement

of standard measuring techniques and computational methods like MD simulations. This work is an attempt to contribute to the asphaltene science by addressing their individual surface/rheological contributions, and in the presence of co-surfactants. We also tried to explore real operational variables that induce/hinder interfacial microstructure (like the composition of oil and water phases) in order to apply these discussions to help solving, or at least better understand, real processing issues. Effects of solvent aromaticity on self-assembly and rheology of asphaltenes has not been well explored in experimental study. Besides the operational issues generated by the colloidal or supramolecular aggregation of asphaltenes (i.e, blocking pipelines and processing lines), they can also be responsible for coke deposits, catalysis deactivation and low yield in fuels [9]. In this way, a clear and better awareness of the link between asphaltene structuring and solvent nature is highly significant to avoid these undesirable operational issues. For instance, findings like the reversability effect upon toluene addition may help to address problems related to deposition and emulsion stability, as well as, the spontaneous emulsification results that indicates the relevance of molecular architecture on film consolidation.

6.2
Future work

Despite the study developed in this thesis, we believe there is still significant work that can be explored. Asphaltene aggregation is a meaningful topic still under development, and due to the advances in alternative experimental and computational approaches, the tendency is that new investigations will be conducted. Besides, understanding the way that asphaltenes self-assemble at the interface may also help to elucidate the interfacial behavior of compounds with similar chemical structure. Below we list the main directions that can be followed to continue this work.

○ Address the effect of solvent aromaticity on the rheology of distinct asphaltene fractions. This may help to consolidate the effects of chemical structuring on viscoelasticity;

○ Perform compression-expansion experiments with distinct asphaltene concentrations in order to study the interfacial effect of expanded films;

○ Include other types of carboxylic acids with different degrees of unsaturation as components of the binary mixture (i.e, elaidic and oleic acid). It is reported in the literature that elaidic acid, for instance, even though organizes nicely at the interface, does not become fully packed

as SAs [32]. Pressure isotherms and rheological studies would be valid to check their self-assembly;

○ Investigate the SE of the mixed films and also in the presence of brines;

○ Advance on the co-adsorption study by changing the SA concentration;

○ Prepare emulsions with the binary systems to assess their stability;

○ Investigate the morphology of the SA films and binary systems by using the SEM technique;

○ Study the effect of monovalent and divalent cations on the surface and rheological properties of single asphaltene laden interfaces and their mixtures with SA;

○ Study the possibility of developing predictive models of the behavior of asphaltene-SA interfaces.

7
Bibliography

1 MAHMOUD, M.; ELKATATNY, S.; ABDELGAWAD, K. Z. Using high- and low-salinity seawater injection to maintain the oil reservoir pressure without damage. **Journal of Petroleum Exploration and Production Technology**, Springer Science and Business Media LLC, v. 7, n. 2, p. 589–596, aug 2016.

2 SHENG, J. J. **Modern Chemical Enhanced Oil Recovery**. [S.l.]: Elsevier, 2011.

3 MOHYALDINN, M. E.; HASSAN, A. M.; AYOUB, M. A. Application of emulsions and microemulsions in enhanced oil recovery and well stimulation. In: **Microemulsion - a Chemical Nanoreactor [Working Title]**. [S.l.]: IntechOpen, 2019.

4 PANNEKENS, M. et al. Oil reservoirs, an exceptional habitat for microorganisms. **New Biotechnology**, Elsevier BV, v. 49, p. 1–9, mar 2019.

5 LANGEVIN, D. Surface shear rheology of monolayers at the surface of water. **Advances in Colloid and Interface Science**, v. 207, p. 121–130, 2014.

6 LANGEVIN, D.; ARGILLIER, J.-F. Interfacial behavior of asphaltenes. **Advances in Colloid and Interface Science**, Elsevier BV, v. 233, p. 83–93, jul 2016.

7 LIU, Y.; KASZUBA, J.; OAKEY, J. Microfluidic investigations of crude oil-brine interface elasticity modifications via brine chemistry to enhance oil recovery. **Fuel**, v. 239, p. 338–346, 2019.

8 SCHULER, B. et al. Unraveling the molecular structures of asphaltenes by atomic force microscopy. **Journal of the American Chemical Society**, American Chemical Society (ACS), v. 137, n. 31, p. 9870–9876, jul 2015.

9 SILVA, H. S. et al. Asphaltene aggregation studied by molecular dynamics simulations: role of the molecular architecture and solvents on the supramolecular or colloidal behavior. **Petroleum Science**, Elsevier BV, v. 16, n. 3, p. 669–684, may 2019.

10 KUZNICKI, T.; MASLIYAH, J. H.; BHATTACHARJEE, S. Molecular dynamics study of model molecules resembling asphaltene-like structures in aqueous organic solvent systems. **Energy & Fuels**, American Chemical Society (ACS), v. 22, n. 4, p. 2379–2389, jul 2008.

11 ALICKE, A. et al. Assessing the interfacial activity of insoluble asphaltene layers: Interfacial rheology versus interfacial tension. **Langmuir**, American Chemical Society (ACS), v. 36, n. 49, p. 14942–14959, dec 2020.

12   BARRERA, D. M.; ORTIZ, D. P.; YARRANTON, H. W. Molecular weight and density distributions of asphaltenes from crude oils. **Energy & Fuels**, American Chemical Society (ACS), v. 27, n. 5, p. 2474–2487, apr 2013.

13   MULLINS, O. C. et al. Advances in asphaltene science and the yen–mullins model. American Chemical Society (ACS), v. 26, n. 7, p. 3986–4003, may 2012.

14   GRAY, M. R. et al. Supramolecular assembly model for aggregation of petroleum asphaltenes. American Chemical Society (ACS), v. 25, n. 7, p. 3125–3134, jul 2011.

15   TAN, X.; FENNIRI, H.; GRAY, M. R. Pyrene derivatives of 2,2′-bipyridine as models for asphaltenes: Synthesis, characterization, and supramolecular organization. American Chemical Society (ACS), v. 22, n. 2, p. 715–720, nov 2007.

16   RAKOTONDRADANY, F. et al. Hexabenzocoronene model compounds for asphaltene fractions: synthesis & characterization. American Chemical Society (ACS), v. 20, n. 6, p. 2439–2447, sep 2006.

17   SCHULZE, M. et al. Aggregation of asphaltene model compounds using a porphyrin tethered to a carboxylic acid. Royal Society of Chemistry (RSC), v. 13, n. 25, p. 6984–6991, 2015.

18   SAUERER, B. et al. Dynamic asphaltene-stearic acid competition at the oil–water interface. **Langmuir**, v. 34, n. 19, p. 5558–5573, 2018.

19   LOBATO, M. D. et al. Optical characterization of asphaltenes at the air-water interface. **Langmuir**, American Chemical Society (ACS), v. 25, n. 3, p. 1377–1384, jan 2009.

20   FAJARDO-ROJAS, F. et al. Probing interfacial structure and dynamics of model and natural asphaltenes at fluid–fluid interfaces. **Langmuir**, American Chemical Society (ACS), v. 36, n. 27, p. 7965–7979, jun 2020.

21   MULLINS, O. C. The modified yen model†. **Energy & Fuels**, v. 24, n. 4, 2010.

22   BRANDAL, Ø.; HANNESETH, A.-M. D.; SJöBLOM, J. Interactions between synthetic and indigenous naphthenic acids and divalent cations across oil–water interfaces: effects of addition of oil-soluble non-ionic surfactants. **Colloid and Polymer Science**, v. 284, n. 2, p. 124–133, 2005.

23   HAVRE, T. E.; SJöBLOM, J.; VINDSTAD, J. E. Oil/water-partitioning and interfacial behavior of naphthenic acids. **Journal of Dispersion Science and Technology**, Informa UK Limited, v. 24, n. 6, p. 789–801, jan 2003.

24   WANG, X. et al. Fatty acid-asphaltene interactions at oil/water interface. **Colloids and Surfaces A: Physicochemical and Engineering Aspects**, v. 513, p. 168–177, 2017.

25   BRANDAL, Ø. et al. Isolation and characterization of naphthenic acids from a metal naphthenate deposit: Molecular properties at oil-water and air-water interfaces. **Journal of Dispersion Science and Technology**, Informa UK Limited, v. 27, n. 3, p. 295–305, may 2006.

26 BERTELLI, J. N. et al. Shear rheology using de noüy ring to evaluate formation and inhibition of calcium naphthenate at the water/oil interface. **Energy & Fuels**, American Chemical Society (ACS), v. 28, n. 3, p. 1726–1735, feb 2014.

27 GAO, S. et al. Role of naphthenic acids in stabilizing water-in-diluted model oil emulsions. **The Journal of Physical Chemistry B**, American Chemical Society (ACS), v. 114, n. 23, p. 7710–7718, may 2010.

28 SLAVCHEVA, E.; SHONE, B.; TURNBULL, A. Review of naphthenic acid corrosion in oilrefining. Informa UK Limited, v. 34, n. 2, p. 125–131, feb 1999.

29 FAN, T. P. Characterization of naphthenic acids in petroleum by fast atom bombardment mass spectrometry. American Chemical Society (ACS), v. 5, n. 3, p. 371–375, may 1991.

30 HE, L. et al. Interfacial sciences in unconventional petroleum production: from fundamentals to applications. Royal Society of Chemistry (RSC), v. 44, n. 15, p. 5446–5494, 2015.

31 ANDERSEN, S. I. et al. Detection and impact of carboxylic acids at the crude oil–water interface. American Chemical Society (ACS), v. 30, n. 6, p. 4475–4485, may 2016.

32 KANICKY, J. R.; SHAH, D. O. Effect of degree, type, and position of unsaturation on the pKa of long-chain fatty acids. Elsevier BV, v. 256, n. 1, p. 201–207, dec 2002.

33 HANNESETH, A.-M. D.; SELSBAK, C.; SJöBLOM, J. Behavior and stability of naphthenic acid/naphthenate stabilized emulsions. mixed c80-tetraacid and stearic acid stabilization. Informa UK Limited, v. 31, n. 6, p. 770–779, may 2010.

34 LUTNAES, B. F. et al. Structure elucidation of c80, c81 and c82 isoprenoid tetraacids responsible for naphthenate deposition in crude oil production. Royal Society of Chemistry (RSC), v. 5, n. 12, p. 1873, 2007.

35 FULLER, G. G.; VERMANT, J. Complex fluid-fluid interfaces: Rheology and structure. **Annual Review of Chemical and Biomolecular Engineering**, v. 3, n. 1, p. 519–543, 2012.

36 MILLER, R. et al. Rheology of interfacial layers. **Colloid and Polymer Science**, Springer Science and Business Media LLC, v. 288, n. 9, p. 937–950, may 2010.

37 JAENSSON, N.; VERMANT, J. Tensiometry and rheology of complex interfaces. **Current Opinion in Colloid & Interface Science**, Elsevier BV, v. 37, p. 136–150, sep 2018.

38 KARBASCHI, M. et al. Rheology of interfacial layers. **Current Opinion in Colloid & Interface Science**, Elsevier BV, v. 19, n. 6, p. 514–519, dec 2014.

39 LIN, Y.-J. et al. Combined interfacial shear rheology and microstructure visualization of asphaltenes at air-water and oil-water interfaces. **Journal of Rheology**, Society of Rheology, v. 62, n. 1, p. 1–10, jan 2018.

40 ERNI, P. Deformation modes of complex fluid interfaces. Royal Society of Chemistry (RSC), v. 7, n. 17, p. 7586, 2011.

41 HERMANS, E. et al. Lung surfactants and different contributions to thin film stability. **Soft Matter**, Royal Society of Chemistry (RSC), v. 11, n. 41, p. 8048–8057, 2015.

42 REYNAERT, S. et al. Analysis of the magnetic rod interfacial stress rheometer. Society of Rheology, v. 52, n. 1, p. 261–285, jan 2008.

43 SÁNCHEZ-PUGA, P. et al. Dynamic measurements with the bicone interfacial shear rheometer: The effects of the numerical implementation of the interfacial boundary condition. MDPI AG, v. 5, n. 1, p. 17, mar 2021.

44 BROOKS, C. F. et al. An interfacial stress rheometer to study rheological transitions in monolayers at the air-water interface. American Chemical Society (ACS), v. 15, n. 7, p. 2450–2459, mar 1999.

45 VANDEBRIL, S. et al. A double wall-ring geometry for interfacial shear rheometry. **Rheologica Acta**, Springer Science and Business Media LLC, v. 49, n. 2, p. 131–144, dec 2009.

46 GIMÉNEZ-RIBES, G.; HABIBI, M.; SAGIS, L. M. Interfacial rheology and relaxation behavior of adsorption layers of the triterpenoid saponin escin. Elsevier BV, v. 563, p. 281–290, mar 2020.

47 FAN, Y.; SIMON, S.; SJöBLOM, J. Interfacial shear rheology of asphaltenes at oil–water interface and its relation to emulsion stability: Influence of concentration, solvent aromaticity and nonionic surfactant. **Colloids and Surfaces A: Physicochemical and Engineering Aspects**, Elsevier BV, v. 366, n. 1-3, p. 120–128, aug 2010.

48 ALVES, D. R. et al. Influence of the salinity on the interfacial properties of a brazilian crude oil–brine systems. **Fuel**, Elsevier BV, v. 118, p. 21–26, feb 2014.

49 DANOV, K. D. et al. Capillary meniscus dynamometry – method for determining the surface tension of drops and bubbles with isotropic and anisotropic surface stress distributions. **Journal of Colloid and Interface Science**, Elsevier BV, v. 440, p. 168–178, feb 2015.

50 LONG, R.; SHULL, K. R.; HUI, C.-Y. Large deformation adhesive contact mechanics of circular membranes with a flat rigid substrate. Elsevier BV, v. 58, n. 9, p. 1225–1242, sep 2010.

51 RODRÍGUEZ-HAKIM, M. et al. Asphaltene-induced spontaneous emulsification: Effects of interfacial co-adsorption and viscoelasticity. Society of Rheology, v. 64, n. 4, p. 799–816, jul 2020.

52 SAAD, S. M.; NEUMANN, A. W. Axisymmetric drop shape analysis (ADSA): An outline. Elsevier BV, v. 238, p. 62–87, dec 2016.

53 YANG, J. et al. Determining the surface dilational rheology of surfactant and protein films with a droplet waveform generator. Elsevier BV, v. 537, p. 547–553, mar 2019.

54   ERNI, P. et al. Interfacial viscoelasticity controls buckling, wrinkling and arrest in emulsion drops undergoing mass transfer. Royal Society of Chemistry (RSC), v. 8, n. 26, p. 6958, 2012.

55   ARIGA, K. et al. 25th anniversary article: What can be done with the langmuir-blodgett method? recent developments and its critical role in materials science. Wiley, v. 25, n. 45, p. 6477–6512, oct 2013.

56   KALE, S. K. et al. A miniaturized radial langmuir trough for simultaneous dilatational deformation and interfacial microscopy. Elsevier BV, v. 582, p. 1085–1098, jan 2021.

57   RODRIGUEZ, J. L. F. et al. Phase transition beyond the monolayer collapse – the case of stearic acid spread at the air/water interface. **Colloids and Surfaces A: Physicochemical and Engineering Aspects**, Elsevier BV, v. 623, p. 126781, aug 2021.

58   BLUME, A. Lipids at the air–water interface. **ChemTexts**, Springer Science and Business Media LLC, v. 4, n. 1, feb 2018.

59   PEPICELLI, M. et al. Characterization and modelling of langmuir interfaces with finite elasticity. **Soft Matter**, Royal Society of Chemistry (RSC), v. 13, n. 35, p. 5977–5990, 2017.

60   MIYANO, K.; MAEDA, T. Langmuir trough with four movable barriers. **Review of Scientific Instruments**, AIP Publishing, v. 58, n. 3, p. 428–435, mar 1987.

61   MATSUMOTO, M. et al. A trough with radial compression for studies of monolayers and fabrication of langmuir-blodgett films. **Thin Solid Films**, Elsevier BV, v. 280, n. 1-2, p. 238–243, jul 1996.

62   DAEAR, W.; MAHADEO, M.; PRENNER, E. J. Applications of brewster angle microscopy from biological materials to biological systems. **Biochimica et Biophysica Acta (BBA) - Biomembranes**, Elsevier BV, v. 1859, n. 10, p. 1749–1766, oct 2017.

63   SPIECKER, P. M.; KILPATRICK, P. K. Interfacial rheology of petroleum asphaltenes at the oil-water interface. American Chemical Society (ACS), v. 20, n. 10, p. 4022–4032, apr 2004.

64   WANG, Z. et al. The role of shearing energy and interfacial gibbs free energy in the emulsification mechanism of waxy crude oil. **Energies**, MDPI AG, v. 10, n. 5, p. 721, may 2017.

65   WILDE, P. et al. Proteins and emulsifiers at liquid interfaces. **Advances in Colloid and Interface Science**, Elsevier BV, v. 108-109, p. 63–71, may 2004.

66   KONDER, H.; DENNHARDT, R.; HABERICH, F. J. Die wirkung unkonjugierter gallensäuren auf die elektrolyt- und wasserabsorption im proximalen jejunum. **Research in Experimental Medicine**, Springer Science and Business Media LLC, v. 175, n. 1, p. 37–49, feb 1979.

67   SOLANS, C.; MORALES, D.; HOMS, M. Spontaneous emulsification. **Current Opinion in Colloid & Interface Science**, Elsevier BV, v. 22, p. 88–93, apr 2016.

68   LÓPEZ-MONTILLA, J. C. et al. Spontaneous emulsification: Mechanisms, physicochemical aspects, modeling, and applications. **Journal of Dispersion Science and Technology**, Informa UK Limited, v. 23, n. 1-3, p. 219–268, jan 2002.

69   MILLER, C. A. Spontaneous emulsification produced by diffusion — a review. **Colloids and Surfaces**, Elsevier BV, v. 29, n. 1, p. 89–102, jan 1988.

70   MILLER, C. A. **Spontaneous emulsification: Recent developments with emphasis on self-emulsification. Emulsions and Emulsion Stability.** [S.l.]: 127-146, 2005.

71   MILLER, C. A.; NEOGI, P. (Ed.). **Interfacial Phenomena**. [S.l.]: CRC Press, 2007.

72   DUBOUÉ, J. et al. Auto-emulsification of water at the crude oil/water interface: A mechanism driven by osmotic gradient. **Energy & Fuels**, v. 33, n. 8, p. 7020–7027, 2019.

73   MURPHY, C. L. **Thermodynamics of Low Tension and Highly Curved interfaces**. Tese (Doutorado) — University of Minnesota, 1996.

74   EMADI, A.; SOHRABI, M. Visual investigation of oil recovery by low salinity water injection: Formation of water micro-dispersions and wettability alteration. In: **Day 2 Tue, October 01, 2013**. [S.l.]: SPE, 2013.

75   FACANHA, J. M.; MAHZARI, P.; SOHRABI, M. Direct observation of low-salinity water effect: Relationship between micro-dispersion formation and wettability alteration. In: **Day 4 Thu, March 09, 2017**. [S.l.]: SPE, 2017.

76   MAHZARI, P.; SOHRABI, M. Impact of micro-dispersion formation on effectiveness of low salinity waterflooding. In: **IOR 2015 - 18th European Symposium on Improved Oil Recovery**. [S.l.]: EAGE Publications BV, 2015.

77   ARAUJO, S. B. de et al. Droplet coalescence and spontaneous emulsification in the presence of asphaltene adsorption. **Langmuir**, v. 33, n. 40, p. 10501–10510, 2017.

78   SHEU, E. Y. Petroleum AsphalteneProperties, characterization, and issues. **Energy & Fuels**, American Chemical Society (ACS), v. 16, n. 1, p. 74–82, nov 2001.

79   ZANGANEH, P. et al. Asphaltene deposition during CO2 injection and pressure depletion: A visual study. **Energy & Fuels**, American Chemical Society (ACS), v. 26, n. 2, p. 1412–1419, jan 2012.

80   AKBARZADEH, K. et al. Asphaltene deposition measurement and modeling for flow assurance of tubings and flow lines. **Energy & Fuels**, American Chemical Society (ACS), v. 26, n. 1, p. 495–510, dec 2011.

81 BARRÉ, L.; SIMON, S.; PALERMO, T. Solution properties of asphaltenes. **Langmuir**, American Chemical Society (ACS), v. 24, n. 8, p. 3709–3717, mar 2008.

82 TCHOUKOV, P. et al. Role of asphaltenes in stabilizing thin liquid emulsion films. **Langmuir**, American Chemical Society (ACS), v. 30, n. 11, p. 3024–3033, mar 2014.

83 FREER, E. M.; RADKE, C. J. RELAXATION OF ASPHALTENES AT THE TOLUENE/WATER INTERFACE: DIFFUSION EXCHANGE AND SURFACE REARRANGEMENT. **The Journal of Adhesion**, Informa UK Limited, v. 80, n. 6, p. 481–496, jun 2004.

84 JERIBI, M. et al. Adsorption kinetics of asphaltenes at liquid interfaces. **Journal of Colloid and Interface Science**, Elsevier BV, v. 256, n. 2, p. 268–272, dec 2002.

85 LIU, D. et al. Synergetic effect of resins and asphaltenes on water/oil interfacial properties and emulsion stability. **Fuel**, Elsevier BV, v. 252, p. 581–588, sep 2019.

86 ZHANG, L. Y. et al. Asphaltene films at a toluene/water interface. American Chemical Society (ACS), v. 21, n. 1, p. 274–285, dec 2006.

87 GAWRYS, K. L.; BLANKENSHIP, G. A.; KILPATRICK, P. K. Solvent entrainment in and flocculation of asphaltenic aggregates probed by small-angle neutron scattering. **Langmuir**, American Chemical Society (ACS), v. 22, n. 10, p. 4487–4497, apr 2006.

88 ZÚÑIGA-HINOJOSA, M. et al. Behavior comparison of films of mexican bitumen and its asphaltene and maltenes fractions at interfaces. **Fuel**, Elsevier BV, v. 307, p. 121852, jan 2022.

89 HEADEN, T. F.; BOEK, E. S.; SKIPPER, N. T. Evidence for asphaltene nanoaggregation in toluene and heptane from molecular dynamics simulations. **Energy & Fuels**, American Chemical Society (ACS), v. 23, n. 3, p. 1220–1229, feb 2009.

90 MIKAMI, Y. et al. Molecular dynamics simulations of asphaltenes at the oil–water interface: From nanoaggregation to thin-film formation. **Energy & Fuels**, American Chemical Society (ACS), v. 27, n. 4, p. 1838–1845, jan 2013.

91 PRACTICE for the Preparation of Substitute Ocean Water. [S.l.]: ASTM International.

92 LASHKARBOLOOKI, M. et al. Effect of salts and their interaction with ingenious surfactants on the interfacial tension of crude oil/ionic solution. **Chinese Journal of Chemical Engineering**, Elsevier BV, v. 28, n. 1, p. 224–235, jan 2020.

93 OLIVEIRA, M. C. K. de et al. Characterization of the solid residue and the liquid extract separated by propane-induced crude oil fractionation. **Energy & Fuels**, American Chemical Society (ACS), v. 31, n. 12, p. 13198–13214, nov 2017.

94 OLIVEIRA, E. C. da S. et al. Study of brazilian asphaltene aggregation by nuclear magnetic resonance spectroscopy. **Fuel**, Elsevier BV, v. 117, p. 146–151, jan 2014.

95 LAAL-DEHGHANI, N.; CHRISTOPHER, G. F. 2d stokesian simulation of particle aggregation at quiescent air/oil-water interfaces. **Journal of Colloid and Interface Science**, Elsevier BV, v. 553, p. 259–268, oct 2019.

96 BALESTRIN, L.; LOH, W. Recent developments on the elucidation of colloidal aspects of asphaltenes and their relevance to oilfield problems. **Journal of the Brazilian Chemical Society**, Sociedade Brasileira de Quimica (SBQ), 2020.

97 MARQUEZ, R. et al. The oscillatory spinning drop technique. an innovative method to measure dilational interfacial rheological properties of brine-crude oil systems in the presence of asphaltenes. **Colloids and Interfaces**, MDPI AG, v. 5, n. 3, p. 42, aug 2021.

98 MOUSAVI, M. et al. Alteration of intermolecular interactions between units of asphaltene dimers exposed to an amide-enriched modifier. **RSC Advances**, Royal Society of Chemistry (RSC), v. 6, n. 58, p. 53477–53492, 2016.

99 VATTI, A. K. et al. Asphaltene aggregation in aqueous solution using different water models: A classical molecular dynamics study. **ACS Omega**, American Chemical Society (ACS), v. 5, n. 27, p. 16530–16536, jun 2020.

100 CAGNA, A. et al. On the reversibility of asphaltene adsorption at oil-water interfaces. **Colloids and Surfaces A: Physicochemical and Engineering Aspects**, v. 548, p. 46–53, 2018.

101 SAMANIUK, J. R. et al. Soft-glassy rheology of asphaltenes at liquid interfaces. Informa UK Limited, v. 36, n. 10, p. 1444–1451, apr 2015.

102 HUNG, J.; CASTILLO, J.; REYES, A. Kinetics of asphaltene aggregation in toluene-heptane mixtures studied by confocal microscopy. American Chemical Society (ACS), v. 19, n. 3, p. 898–904, mar 2005.

103 AMERI, A.; ESMAEILZADEH, F.; MOWLA, D. Effect of low-salinity water on asphaltene precipitation. **Journal of Dispersion Science and Technology**, v. 39, n. 7, p. 1031–1039, 2017.

104 FRANCO, J. C. et al. Towards in situ fluorescence spectroscopy and microscopy investigations of asphaltene precipitation kinetics. The Optical Society, v. 21, n. 25, p. 30874, dec 2013.

105 ROUX, J.-N.; BROSETA, D.; DEMÉ, B. SANS study of asphaltene aggregation: concentration and solvent quality effects. American Chemical Society (ACS), v. 17, n. 16, p. 5085–5092, jul 2001.

106 FENISTEIN, D. et al. Viscosimetric and neutron scattering study of asphaltene aggregates in mixed toluene/heptane solvents. American Chemical Society (ACS), v. 14, n. 5, p. 1013–1020, feb 1998.

107   VERRUTO, V. J.; KILPATRICK, P. K. Water-in-model oil emulsions studied by small-angle neutron scattering: Interfacial film thickness and composition. **Langmuir**, American Chemical Society (ACS), v. 24, n. 22, p. 12807–12822, oct 2008.

108   ALVAREZ, G. et al. Small-angle neutron scattering study of crude oil emulsions: Structure of the oil-water interfaces. **Langmuir**, American Chemical Society (ACS), v. 25, n. 7, p. 3985–3990, feb 2009.

109   HARBOTTLE, D. et al. Problematic stabilizing films in petroleum emulsions: Shear rheological response of viscoelastic asphaltene films and the effect on drop coalescence. **Langmuir**, American Chemical Society (ACS), v. 30, n. 23, p. 6730–6738, jun 2014.

110   HUTIN, A.; ARGILLIER, J.-F.; LANGEVIN, D. Influence of pH on oil-water interfacial tension and mass transfer for asphaltenes model oils. comparison with crude oil behavior. **Oil & Gas Science and Technology – Revue d'IFP Energies nouvelles**, EDP Sciences, v. 71, n. 4, p. 58, jul 2016.

111   HATTA, E. Sequential collapse transitions in a langmuir monolayer. **Langmuir**, American Chemical Society (ACS), v. 20, n. 10, p. 4059–4063, apr 2004.

112   PRZYKAZA, K. et al. Properties of the langmuir and langmuir–blodgett monolayers of cholesterol-cyclosporine a on water and polymer support. **Adsorption**, Springer Science and Business Media LLC, v. 25, n. 4, p. 923–936, may 2019.

113   RIES, H. E. Stable ridges in a collapsing monolayer. **Nature**, Springer Science and Business Media LLC, v. 281, n. 5729, p. 287–289, sep 1979.

114   RIES, H. E.; SWIFT, H. Twisted double-layer ribbons and the mechanism for monolayer collapse. **Langmuir**, American Chemical Society (ACS), v. 3, n. 5, p. 853–855, sep 1987.

115   SUN, X. et al. Probing the effect of salt on asphaltene aggregation in aqueous solutions using molecular dynamics simulations. **Energy & Fuels**, American Chemical Society (ACS), v. 32, n. 8, p. 8090–8097, jun 2018.

116   GMIRA, A.; ENEZI, S. M. A.; YOUSEF, A. A. Ions dependent stability of stearic acid langmuir monolayers: An insight of oil/water interface in SmartWater flood. In: **Day 2 Tue, March 07, 2017**. [S.l.]: SPE, 2017.

117   QIAO, J. et al. Probing the effect of NaCl concentrations on a model asphaltene adsorption onto water droplets of different sizes. **Energy & Fuels**, American Chemical Society (ACS), v. 33, n. 5, p. 3881–3890, apr 2019.

118   XU, Y. et al. DESTABILIZATION OF WATER IN BITUMEN EMULSION BY WASHING WITH WATER. **Petroleum Science and Technology**, Informa UK Limited, v. 17, n. 9-10, p. 1051–1070, oct 1999.

119   SCHWARTZ, D. K. et al. Surface order and stability of langmuir-blodgett films. **Science**, American Association for the Advancement of Science (AAAS), v. 257, n. 5069, p. 508–511, jul 1992.

120   SILVA, L. F. L. et al. Understanding the effect of solvent polarity on the polymorphism of octadecanoic acid through spectroscopic techniques and DFT calculations. **CrystEngComm**, Royal Society of Chemistry (RSC), v. 21, n. 2, p. 297–309, 2019.

121   ISRAELACHVILI, J.; PASHLEY, R. The hydrophobic interaction is long range, decaying exponentially with distance. **Nature**, Springer Science and Business Media LLC, v. 300, n. 5890, p. 341–342, nov 1982.

A
Appendix

The description of each assignment/comment for the ^{1}H NMR and ^{13}C NMR are detailed in the following itens:

- A1: Total aromatic hydrogens.
- A2: Total aliphatic hydrogens.
- A3: Hydrogen in terminal or isolated CH_3 and CH_3 in position γ or more to aromatic ring.
- A4: Naphthenic CH and CH_2 hydrogens + CH and CH_2 in paraffinic chains + hydrogens β to aromatic rings and CH_2 γ or more to aromatic rings.
- A5: Hydrogens α to aromatic rings.
- A6: Total aliphatic carbon.
- A7: Total aromatic carbon.
- A8: Aromatic carbon bonded to alkyl group (except methyl).

- C1: Total aliphatic carbon.
- C2: Total aromatic carbon.
- C3: Aromatic bonded to alkyl (except methyl).
- C4: Methyl-substituted aromatic carbon.
- C5: H-substituted aromatic carbon.
- C6: Peripheral carbon.
- C7: Bridgehead carbon.

Table A.1: ^{1}H NMR results for Brazilian asphaltenes.

Experiment	Assignment	Chemical shifts (ppm)	BR Asph. (mol %)
^{1}H NMR	A1	6.0-9.0	8,0
^{1}H NMR	A2	0.0-4.0	92.0
^{1}H NMR	A3	0.5-1.0	16.1
^{1}H NMR	A4	1.0-2.0	58.7
^{1}H NMR	A5	2.0-4.0	17.2

Table A.2: ^{13}C NMR results for Brazilian asphaltenes.

Experiment	Comment	Chemical shifts (ppm)	BR Asph. (mol %)
% $C_{aliphatic}$	C1	0-70	39.2 %
% $C_{aromatic}$	C2	110-160	60.8 %
% $C_{aromatic-alkyl}$	C3	137.5-160	7.4 %
% $C_{aromatic-Me}$	C4	-	1.1 %
% $C_{aromatic-H}$	C5	-	8.4 %
% $C_{aromatic-J}$	C6	-	16.9 %
% $C_{aromatic-bridgehead}$	C7	-	43.8 %

Table A.3: ¹H NMR results for Asphaltene A.

Experiment	Assignment	Chemical shifts (ppm)	Asph. A (mol %)
¹H NMR	A1	6.0-9.0	4,6
¹H NMR	A2	0.0-4.0	95.4
¹H NMR	A3	0.5-1.0	12.4
¹H NMR	A4	1.0-2.0	66.8
¹H NMR	A5	2.0-4.0	16.1

Table A.4: ¹H NMR results for Asphaltene B.

Experiment	Assignment	Chemical shifts (ppm)	Asph. B (mol %)
¹H NMR	A1	6.0-9.0	4,2
¹H NMR	A2	0.0-4.0	95.8
¹H NMR	A3	0.5-1.0	14.1
¹H NMR	A4	1.0-2.0	62.9
¹H NMR	A5	2.0-4.0	18.8

Table A.5: ^{13}C NMR results for Asphaltene A.

Experiment	Comment	Chemical shifts (ppm)	Asph. A (mol %)
% $C_{aliphatic}$	C1	0-70	36.3 %
% $C_{aromatic}$	C2	110-160	63.8 %
% $C_{aromatic-alkyl}$	C3	137.5-160	17.8 %
% $C_{aromatic-Me}$	C4	-	0.5 %
% $C_{aromatic-H}$	C5	-	5.5 %
% $C_{aromatic-J}$	C6	-	23.7 %
% $C_{aromatic-bridgehead}$	C7	-	40.0 %

Table A.6: ^{13}C NMR results for Asphaltene B.

Experiment	Comment	Chemical shifts (ppm)	Asph. B (mol %)
% $C_{aliphatic}$	C1	0-70	35.8 %
% $C_{aromatic}$	C2	110-160	64.2 %
% $C_{aromatic-alkyl}$	C3	137.5-160	4.3 %
% $C_{aromatic-Me}$	C4	-	4.5 %
% $C_{aromatic-H}$	C5	-	4.9 %
% $C_{aromatic-J}$	C6	-	13.7 %
% $C_{aromatic-bridgehead}$	C7	-	50.5 %